^{18}F-FDG PET imaging of atherosclerotic carotid stenosis

KJERSTI JOHNSRUD, MD

DIVISION OF RADIOLOGY AND NUCLEAR MEDICINE

OSLO UNIVERSITY HOSPITAL

INSTITUTE OF CLINICAL MEDICINE

FACULTY OF MEDICINE

UNIVERSITY OF OSLO

Oslo University Hospital

Series of dissertations submitted to the
Faculty of Medicine, University of Oslo

ISBN 978-82-8377-741-3

Cover: Hanne Baadsgaard Utigard.
Print production: Reprosentralen, University of Oslo.

ACKNOWLEDGEMENTS

The work presented in this thesis was carried out at Oslo University Hospital. The research grant received from The South-Eastern Norway Regional Health Authority grant number: 2009006, is gratefully acknowledged.
I thank the University of Oslo for admitting me to their PhD program and for having a thorough PhD education with great and dedicated lecturers doing everything they can to prepare us for all the hard work, pitfalls, dilemmas, temptations, obstacles and joy we will meet in the world of science.

I would like to express my appreciation to my supervisors,

to David Russell for making this project possible by very early seeing the potential of PET as a useful tool in stroke prevention, for endless support, for trusting my abilities and giving me the opportunity to become a member of the 'The unstable carotid artery research group'.

to Jan Gunnar Fjeld for hiring me, for supporting and following me through the search for and finalization of a suitable PhD project, and for giving me the opportunity to combine clinical work and research.

to Mona-Elisabeth Rootwelt-Revheim, for everything, for PET and research experience, for having confidence in me, for giving me hope in the darkest hours, for endless pushing and pulling. I had not done this without you.

In memory of Arne Skretting, his contributions as an inventive and experienced physicist were crucial in this project's early days and still remain so. I am thankful for the time I had with him and his endless energy in making nuclear medicine physics a little understandable for the rest of us.

A special thanks to Therese Seierstad at the Department for Research and Development, for teaching me everything I really needed to know to be able to finish this thesis. To always give help, never a detail too small or a dilemma too big, only solutions. I was lucky you were there.

I want to thank Karolina Skagen and Mona Skjelland at the Department of Neurology. To Karolina for making it possible to include PET imaging as part of a project with short time limits, for very good analytical and writing skills, and for being patient in the trying and failing when searching for a PET method suitable for carotid imaging. To Mona for being enthusiastic, calm, and giving important and constructive reviews.

I also want to thank my co-authors Helge Scott at the Department of Pathology for the meticulous work of linking PET imaging findings with what is actually seen through a microscope, and Kirsten Krohg-Sørensen at the Department of Thoracic Surgery for making it possible to plan and do research in the short time available before urgent surgery.

I want to thank to the patients in this study for being willing to give of their time and energy in a vulnerable phase of life.

Thanks to all my best colleagues at the Department of Nuclear Medicine and Department of Diagnostic Physics, for years with curiosity, team work, good spirits, support and endless energy in the understanding and optimization of how use our wonder PET machine to its uttermost for diagnosis of diseases and patient care.

Thank you to my closest family and friends, for believing in me and always being there for help and support.

My warmest thanks to Øyvind and Eva, for enduring the long road to finalization of this thesis, and for giving me the most precious in life, a family and a home filled with love.

I am grateful,
Kjersti

TABLE OF CONTENTS

ABBREVIATIONS

Bq/mL	becquerel per millilitre
BGL	blood glucose level
BMT	best medical therapy
^{14}C	carbon-14
CAS	carotid artery stenting
CD68	cluster of differentiation 68
CEA	carotid endarterectomy
CCA	common carotid artery
CM	contrast media
cSUV	corrected standardized uptake value
CVD	cardiovascular disease
CT	computer tomography
CTA	computer tomography angiography
DG	2-deoxy-D-glucose
DG-6-P	2-deoxy-D-glucose-6-phosphate
DUS	Duplex ultrasound
EANM	European Association of Nuclear
ECST	Medicine European Carotid Surgery Trial
ESUS	embolic stroke of undetermined source
^{18}F	fluorine-18
^{18}F-FDG	fluorine-18 labelled 2-deoxy-D-glucose
^{18}F-NaF	fluorine-18 labelled sodium fluoride
FOV	field of view
FWHM	full width at half maximum
^{68}Ga	gallium-68
GBD	The Global Burden of Disease study
GLUT	glucose transporter
GSM	grey scale median
ICA	internal carotid artery
ICC	intraclass correlation coefficients

i.v.	intravenous
kV	kilovoltage
LOR	line of response
mAs	milliampere second
MES	microembolic signals
MDS	most diseased segment
MIP	maximum intensity projections
MRI	magnetic resonance imaging
MRA	magnetic resonance angiography
NASCET	North American Symptomatic Carotid Endarterectomy Trial
OSEM	ordered subset expectation maximization
PCR	polymerase chain reaction
PD	power Doppler
PET	positron emission tomography
PET/CT	combined (hybrid) PET and CT
PMT	photo-multiplier tube
PSF	point spread function
ROI	region of interest
SMC	smooth muscle cell
SUV	standardized uptake value
SUV_{max}	maximum standardized uptake value
SUV_{mean}	mean standardized uptake value
TBR	target to background ratio
TCD	transcranial Doppler
TIA	transitory ischemic attack
TOF	time of flight
US	ultrasound
VOI	volume of interest
WHO	World Health Organization

LIST OF PAPERS

I. Karolina Skagen, **Kjersti Johnsrud**, Kristin Evensen, Helge Scott, Kirsten Krohg-Sørensen, Frode Reier-Nilsen, Mona-Elisabeth Revheim, Jan Gunnar Fjeld, Mona Skjelland, and David Russell. Carotid plaque inflammation assessed with ^{18}F-FDG PET/CT is higher in symptomatic compared with asymptomatic patients.
International Journal of Stroke. 2015;10:730-6.

II. **Kjersti Johnsrud**, Karolina Skagen, Therese Seierstad, Mona Skjelland, David Russell, and Mona-Elisabeth Revheim. ^{18}F-FDG PET/CT for the quantification of inflammation in large carotid artery plaques.
Journal of Nuclear Cardiology. 2019;26(3):883-93.

III. **Kjersti Johnsrud**, Therese Seierstad, David Russell, and Mona-Elisabeth Revheim. Inter-reader agreement of ^{18}F-FDG PET/CT for the quantification of carotid artery plaque inflammation.
Accepted for publication in JRSM Cardiovascular Disease.

SAMMENDRAG

Avbilding av aterosklerotisk carotisstenose med ^{18}FDG-PET

Bakgrunn og mål: Aterosklerose er en av hovedårsakene til hjerte- og karsykdommer som forårsaker høy sykelighet og dødelighet globalt. Forekomsten av hjerte- og karsykdommer går ned i høyinntekstland som har igangsatt forebyggende tiltak, men øker i lav- og mellominntektsland. Beregninger har vist at risiko for iskemisk hjerneslag i løpet av livet er 18,3% for voksne (≥25 år). Aterosklerotisk carotisstenose er en viktig årsak til iskemisk hjerneslag. Forebyggende operativ behandling med endarterektomi er tilgjengelig. Den kliniske beslutningen om kirurgi baseres hovedsakelig på stenosegrad bedømt med ultralyd og angiografi. Dette fører til både over- og underbehandling. Ny kunnskap indikerer at ikke bare stenosegrad, men også andre egenskaper ved det aterosklerotiske plakket er viktige for dannelsen av embolier til hjernen. Inflammasjon, med aktivering av makrofager, er den sentrale prosessen som gjør plakket ustabilt og symptomgivende. Positron emisjon tomografi (PET) med fluor-18 merket 2-deoksy-D-glukose (^{18}F-FDG) kan avbilde og kvantifisere inflammatorisk aktivitet fordi inflammatoriske celler har økt opptak av glukose. Opptak av ^{18}F-FDG har vist seg å korrelere med mengde makrofager i det aterosklerotiske plakket, og pasienter med nylige symptomer på embolus fra plakket har vist å ha høyere opptak av ^{18}F-FDG enn de uten. Til tross for dette er metoden ikke implementert i klinisk praksis, og det finnes ingen standardisert metode for å gjennomføre og kvantifisere ^{18}F-FDG PET undersøkelser ved denne problemstillingen. Målet med denne studien var å undersøke om ^{18}F-FDG PET kan brukes til å finne de aterosklerotiske plakkene i carotisarterien som gir pasientene høy risiko for hjerneslag. Videre var målet å finne en reproduserbar kvantifiseringsmetode for opptak av ^{18}F-FDG i carotisplakk. Dette vil muliggjøre prospektive kliniske multisenterstudier av pasienters individuelle risiko for hjerneslag, måling av effekten av forebyggende tiltak samt at ^{18}F-FDG PET kan benyttes som endepunkt i kliniske behandlingsstudier.

Materiale og metode: Totalt 44 pasienter henvist til operasjon for høygradig carotisstenose (≥70 %) ble inkludert. Pasientene var henvist til endarterektomi enten fordi de hadde hatt nylige iskemiske symptomer, eller fordi de skulle til annen operasjon med stor risiko for embolier fra carotisstenosen peroperativt. Preoperativt ble det utført ^{18}F-FDG PET/computertomografi (CT) av halskar og ultralyd Doppler for vurdering av stenosegrad og plakkets ekkogenisitet. Etter operasjon ble de fjernede plakkene undersøkt histologisk, og grad av inflammasjon ble kvantifisert.

Inflammasjonsgraden ble angitt som andel av plakkets undersøkte areal som bestod av inflammatoriske celler (makrofager og lymfocytter). På PET/CT bildene ble maksimum standardisert opptaksverdi (SUV_{max}) av ^{18}F-FDG målt i hvert bildesnitt i hele plakkets utstrekning. Det ble også målt gjennomsnittlig standardisert opptaksverdi (SUV_{mean}) av ^{18}F-FDG i blodbakgrunn i vena jugularis. Med utgangspunkt i opptaksverdiene i plakket og blodbakgrunn ble ulike parametere for ^{18}F-FDG opptaket beregnet basert på inklusjon av ulikt antall snitt, lokalisasjon av disse snittene, og hvorvidt det ble utført korreksjon av bakgrunnsopptak. To uavhengige bildegranskere kvantifiserte opptaket i alle plakkene.

Resultater: Det var en signifikant korrelasjon mellom opptaket av ^{18}F-FDG og inflammasjonsgrad i de 30 plakkene som ble undersøkt histologisk. Det var signifikant høyere opptak av ^{18}F-FDG i plakk hos pasienter med symptomer innen de siste 30 dager før operasjon (median mean SUV_{max} 1,75 (1,26–2,04)) enn hos de som hadde symptomer tidligere enn dette eller var asymptomatiske (median mean SUV_{max} 1,43 (1,15–2,28). Opptaket av ^{18}F-FDG var også høyere i plakk som hadde lav ekkogenisitet sammenlignet med høy på ultralyd. Det var en sterk korrelasjon mellom alle de ulike ^{18}F-FDG-opptaksparameterene, og en moderat korrelasjon mellom alle opptaksparameterene og inflammasjon på histologi. Opptaksparametere med bakgrunnskorreksjon var ikke bedre enn de uten, og korrelasjon var ikke påvirket av antall inkluderte snitt fra plakket. Dette indikerer at inflammasjonen er relativt jevnt fordelt i plakket, og at det å måle den høyeste opptaksverdien (max SUV_{max}) vil være representativt for inflammasjonsgraden. Sammenligning av inntegningene for de to bildetyderne viste høy grad av samsvar selv om avgrenset området for plakkets utstrekning var ulikt. Samsvaret var høyest for opptaksverdier uten bakgrunnskorreksjon.

Konklusjon: ^{18}F-FDG PET/CT kan brukes til å måle grad av inflammasjon i aterosklerotisk carotisstenose. Det er høyere opptak hos pasienter med nylige symptomer enn de uten, men forskjellen er liten og det er stor grad av overlapp mellom opptaksverdiene. Videre prospektive kliniske studier må gjennomføres dersom ^{18}F-FDG PET/CT skal kunne brukes til å forutsi risiko for hjerneslag hos individer med aterosklerotisk carotisstenose. Bakgrunnskorrigering av opptaksverdiene gir ikke bedre samsvar med inflammasjonsgrad målt med histologi, og vi finner bedre inter-observatør reproduserbarhet ved bruk av opptaksverdier uten bakgrunnskorreksjon. Bruk av plakkets høyeste opptaksverdi, max SUV_{max}, som inflammasjonsparameter vil forenkle metodens anvendelse i klinikk og multisenterstudier.

1. INTRODUCTION

Atherosclerotic artery disease is a leading cause of cardiovascular diseases (CVDs) causing considerable morbidity and mortality worldwide. Even though the incidence rates are declining in regions where preventive measures have had population effects, they are increasing in low-and middle-income countries. Globally, the life-time risk of ischemic stroke for adults (≥25 years) has been calculated to be 18.3% (GBD 2016 Lifetime Risk of Stroke Collaborators, 2018). A substantial number of ischemic strokes is caused by atherosclerotic carotid artery disease. Treatment selection solely based on the degree of stenosis is unsatisfactory as it leads to both over- and undertreatment. Inflammation is an important cause of atherosclerotic plaque progression, plaque rupture and symptomatic events. Positron emission tomography (PET) with fluorine-18 labelled 2-deoxy-D-glucose (^{18}F-FDG) is established as a valuable imaging procedure for the diagnosis and follow-up of several inflammatory conditions because it detects and quantifies glucose hypermetabolism in inflammatory cells. ^{18}F-FDG PET of atherosclerosis has been extensively studied, but it is still not implemented in clinical practice. This can partly be explained by the lack of consensus and guidelines on the methodology for quantification. In this thesis, we examined patients with large atherosclerotic plaques in the carotid artery with ^{18}F-FDG PET. Our aim was to determine if ^{18}F-FDG PET can be established as a reliable imaging modality for the detection of atherosclerotic plaques which have a high risk of causing thromboembolic events. Furthermore, to explore if any quantification methods are more suitable than others for implementing ^{18}F-FDG PET assessments of atherosclerosis in multicentre studies and in clinical routine.

2. BACKGROUND

2.1 ATHEROSCLEROSIS

2.1.1 Definition and epidemiology

2.1.1.1 General

Atherosclerosis results in the progressive alteration of the arterial vessel wall with the accumulation of fatty and/or fibrous deposits leading to a local thrombosis or stenosis or distal embolization. These events are important underlying causes of morbidity and mortality worldwide. Atherosclerosis is a leading cause of CVDs (Libby, 2019a). Globally, CVDs caused 31% of all deaths in 2016 (17.9 million people) of which 85% were caused by heart attacks or strokes (World Health Organization, 2017). The World Health Organization (WHO) estimated that approximately 75% of deaths due to CVD occur in low- and middle-income countries (World Health Organization, 2017). In Norway, CVDs caused 13 052 (31%) of all deaths in 2012, declining to 10 950 (27%) in 2016 despite the aging population (Kvåle, 2018) .

2.1.1.2 Cerebrovascular disease

Cerebrovascular diseases are diseases of the blood vessels supplying the brain (World Health Organization, 2017). WHO defines stroke as a focal or global loss of neurological function with vascular origin lasting more than 24 hours or causing death within 24 hours. Transitory ischemic attacks (TIAs) are defined as the symptoms above but with a duration less than 24 hours (Aho, 1980). These definitions are being reviewed as imaging of the brain during ischemia is improving and knowledge regarding time limits and reversible brain damage evolves (Sacco, 2013).

Strokes are categorized as ischemic or hemorrhagic, with ischemic strokes being the largest group. The Global Burden of Disease study (GBD) found that in 2016, there were 13.7 million new stroke cases worldwide causing 5.5 million deaths (2nd most common cause of death after ischemic heart disease). Of these, 2.7 million were due to ischemic stroke. The total number of prevalent strokes globally in 2016 (80.1 million), 84.4% were ischemic and the number of disability-adjusted life-years (DALYs) due to ischemic stroke was 51.9 million. The age standardised death rates and prevalence of stroke have decreased over time, but the overall burden has

remained very high. This can be explained by an aging population and the fact that low- and middle-income countries have an increase in modifiable risk factors (GBD 2016 Stroke Collaborators, 2019).

In Norway in 2016, 10 915 patients were registered with their first acute stroke (no other registrations carried out in the previous four years). This was a decrease of 2.6% from 2012. Forty-six percent were women and 85% of the strokes were ischemic. Deaths caused by strokes were reduced from 2 426 in 2012 to 1 927 in 2016. In 2016, 5 695 patients were registered with their first TIA, this was a 8.2% decrease from 2012, 50% were women (Kvåle, 2018). In 2007, the stroke-related total annual public costs in Norway were estimated to be between seven and eight billion Norwegian kroner (approximately 900 million Euros). The annual stroke incidence in 2007 was 15 000 (both first and recurrent strokes) (Fjaertoft, 2007).

2.1.1.3 Etiology of ischemic strokes

The main mechanisms behind ischemic strokes are embolism and small vessel disease, and some patients have multiple possible causes. The dominating source is embolization with either a cardiogenic or an arteriogenic origin (Ntaios, 2017). An atherosclerotic plaque of the carotid artery is assessed as causative if there is a stenosis of at least 50% (Brott, 2011). A previously asymptomatic atherosclerotic stenosis >50% of the internal carotid artery (ICA) is considered to be the embolic source in about 10-15% of all strokes (Naylor, 2015). Large artery atherosclerotic stenosis is considered the cause of 25% of the ischemic strokes in North American and European studies (Hart, 2014). Even though better diagnostic imaging tools have been developed, the group of strokes with unknown origin (cryptogenic) is estimated to be 25% of ischemic strokes (in North American and European studies) (Hart, 2014). Most of these strokes are believed to be embolic (embolic stroke of undetermined source (ESUS)). The correct secondary preventive treatment for these patients is difficult and debated. Atherosclerotic plaques in the aorta and non-stenosing (<50% diameter stenosis) atherosclerotic plaques in the carotid artery are possible embolic sources in patients where a clear source of the embolus is absent (Hart, 2014). Siegler *et al.* found that non-stenosing carotid plaques with thickness ≥3 mm were more frequent ipsilateral than contralateral to the infarct in patients with ESUS and that plaque thickness was greater ipsilateral than in the contralateral

carotid (Siegler, 2019). There were no significant differences in ipsilateral and contralateral plaque characteristics in patients above 65 years or in patients with stroke caused by atrial fibrillation **Figure 1** gives an approximation of stroke aetiologies in a 'typically Western community' based on estimates by Naylor (Naylor, 2015).

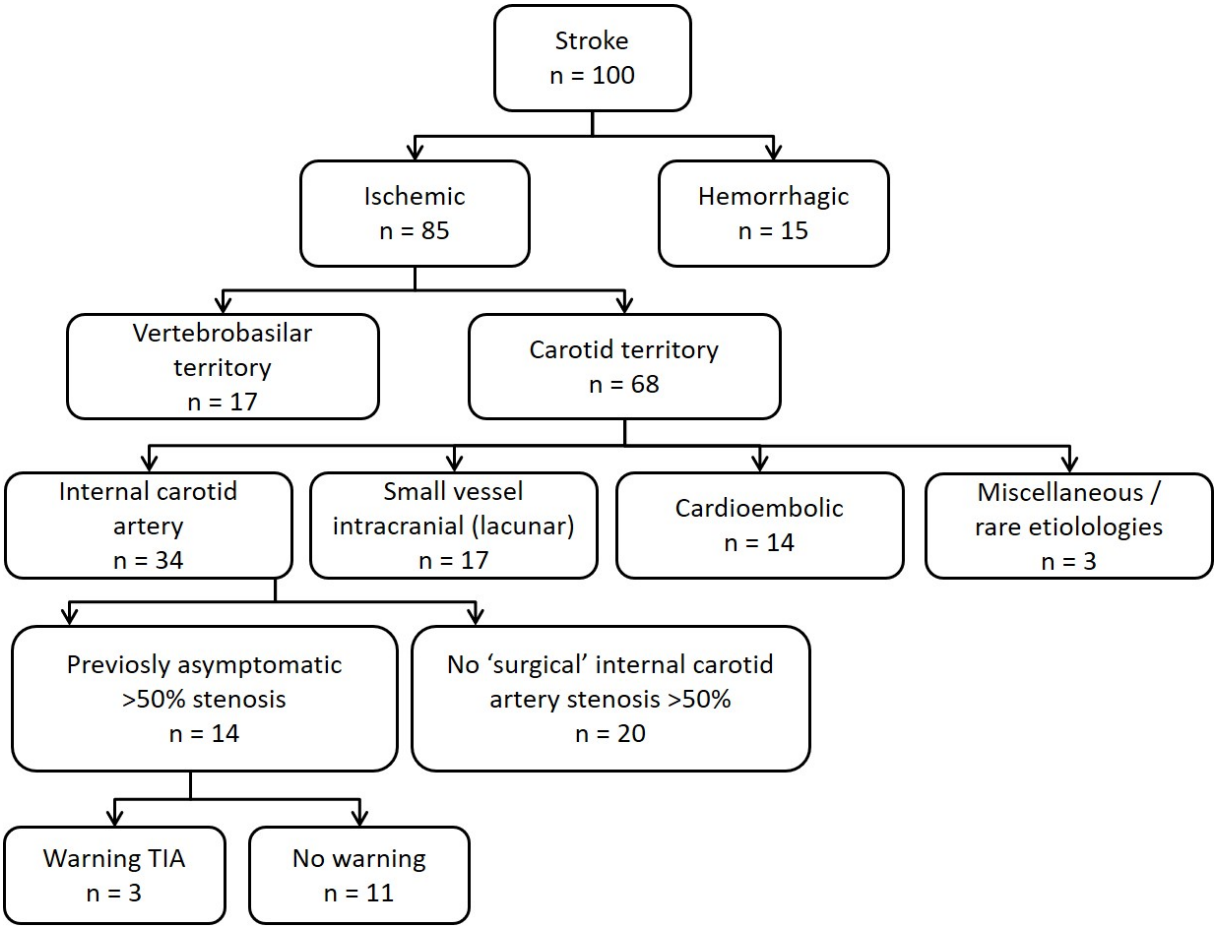

Figure 1: Stroke aetiologies in a 'typically Western community'. Cases per 100 (Naylor, 2015).

2.1.1.4 Risk factors

The decline in the number of patients with heart disease and stroke is believed to be a result of changes in the control of risk factors: tobacco use, unhealthy diet, obesity, physical inactivity, hyperlipidaemia, hypertension and high alcohol intake (Libby, 2019a). Despite this, the increasing epidemic of obesity in low- and middle-income

countries is seen as a threat to continued decline in CVDs (GBD 2015 Disease and Injury Incidence and Prevalence Collaborators, 2016).

2.1.2 Pathogenesis

2.1.2.1 From fatty streaks to plaque rupture - histology

Atherosclerosis as a lipid storage disease has been known since Windaus' and Anichkov's pioneering work with cholesterol in the 1910s (Buja, 2014; Nicholls, 2019). Low-density lipoprotein (LDL) cholesterol is crucial in the development of atherosclerosis (Libby, 2019a), but lipids alone could not explain plaque progression to stenosis and eventually the risk of a clinical event. Atherosclerosis is now understood to be a chronic disease with inflammation as the dynamic trigger to progression (Libby, 2002; Libby, 2019c). **Figure 2** shows the gradual progression of atherosclerosis.

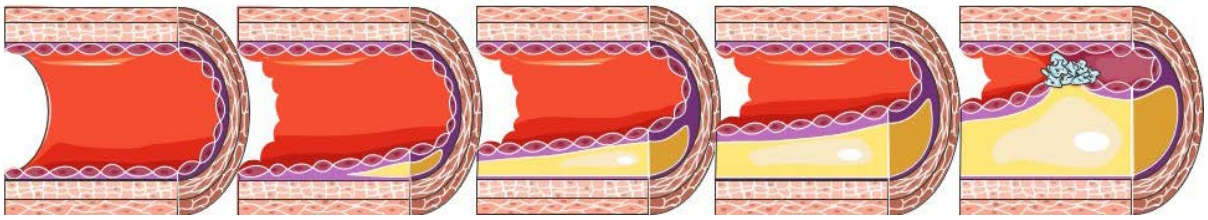

Figure 2: Atherosclerosis progress with a gradual build-up of fatty and necrotic material (yellow/white) in the innermost layer of the artery wall, the intima. In addition to the development of stenosis atherosclerosis can lead to the formation of a thrombus (far right).
The figure is retrieved from Servier Medical Art, by Servier and reused under a Creative Commons Attribution 3.0 Unported License.

Autopsy and histology studies in animals and humans have provided detailed information regarding the distribution, and the cellular and anatomical details, of atherosclerosis. The stages of atherosclerotic plaque progression have distinct features, from the early fatty streaks to the late stages characterized by a large necrotic core covered by a fibrous cap that is either thick, thin or ruptured, and the presence of inflammatory cells (Stary, 1992; Stary, 1994; Stary, 1995). When atherosclerosis progresses in coronary arteries with increasing amounts of lipids accumulating in fatty streaks, macrophages infiltrate toward the lipid deposits. When

the macrophages become lipid laden (foam cells), the lesion is defined as pathologic intimal thickening understood as an intermediate stage between early and advanced lesions (Nakashima, 2007). The evolution of the carotid atherosclerotic plaque goes from a pathologic intimal thickening with a lipid pool to a fibroatheroma. A necrotic core is covered with a thick fibrous cap which eventually may develop into a thin cap fibroatheroma where the fibrous cap is ruptured and a luminal thrombus may be present (Kolodgie, 2017).

In advanced carotid lesions, macrophages are the dominating inflammatory cell types, but other cells such as lymphocytes are also found in abundance (Jander, 1998; Redgrave, 2006). Inflammatory cells are found in the shoulder region/periphery of the necrotic core (Jander, 1998). The localization of the macrophages in fibroatheroma and thin-cap fibroatheroma in the carotid artery are shown in **Figures 3 and 4.** The macrophages are visualized as red areas in **Figure 3** part B and **in Figure 4** part C (Kolodgie, 2007).

The findings of a thrombus together with a rupture or fissures in coronary plaques causing ischemic events led to an understanding of an acute thrombus as the cause of acute ischemia (Davies, 1985). The characterization of plaques in patients with clinical events has been important for our understanding of the atherosclerotic process leading to the formation of a thrombus/embolus. Histological studies have revealed significant difference in the presence of infiltration of the fibrous cap with foam cells between asymptomatic (44%) and symptomatic (84%) carotid plaques (Carr, 1996). This was quantified in more detail by Jander *et al.* who found that both plaque areas with macrophages and number of T cells were more abundant in plaques (≥70% ICA stenosis) from patients with symptoms ≤120 days before enlistment than in those without (Jander, 1998). These cells are therefore strongly suspected to be contributors in plaque destabilization. Their role and presence in carotid plaques related to the time course of symptoms were documented in the Oxford plaque study where 526 plaques with ICA stenosis ≥70% were examined (Redgrave, 2006). Plaque inflammation and especially the presence of macrophages was strongly associated with cap rupture and a short time interval since the stroke.

They found that dense infiltration with macrophages was more strongly associated with plaque rupture than the presence of lymphocytes (Redgrave, 2006).

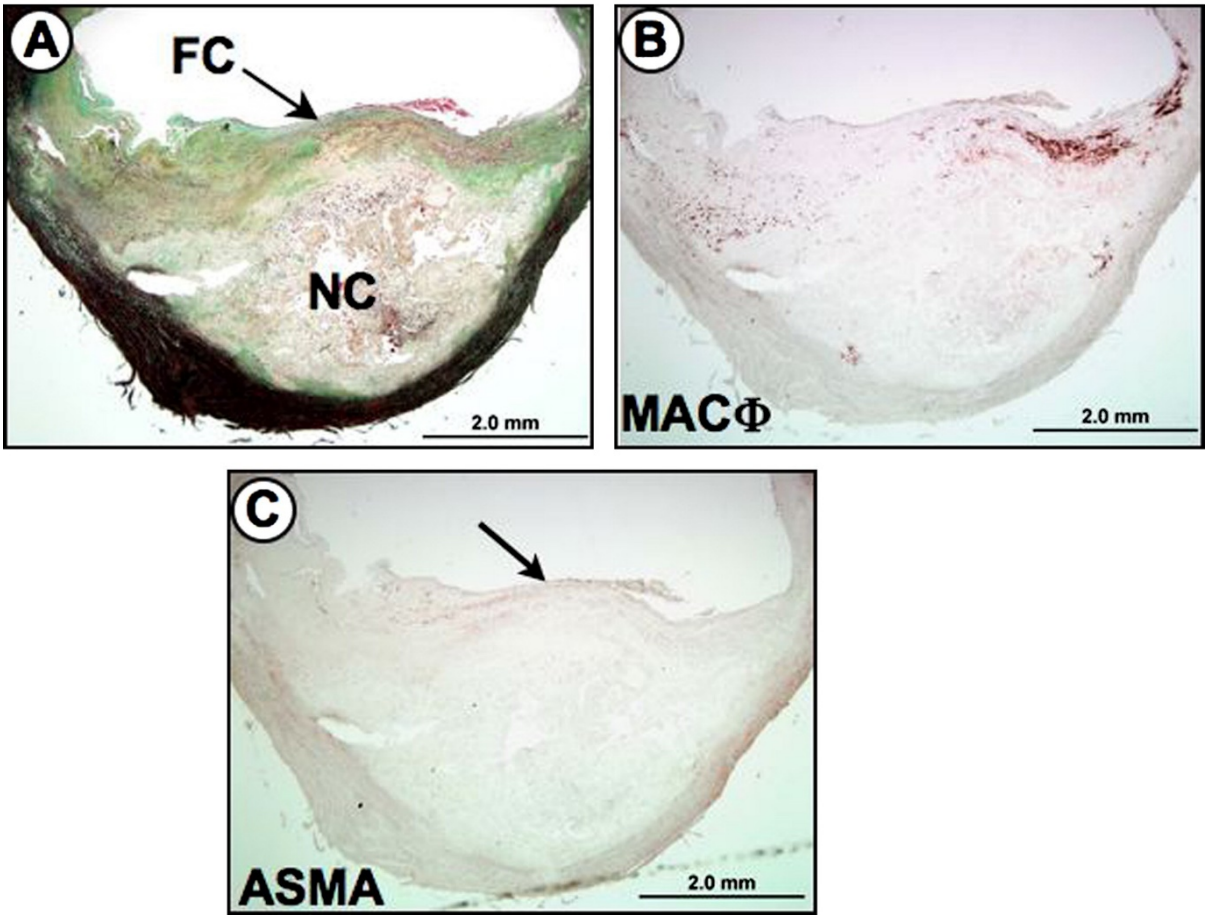

Figure 3: Serial sections of a carotid artery fibroatheroma.
(*A*) Movat pentachrome stain, showing an eccentric plaque with a relatively large necrotic core (NC) covered by a thick fibrous cap (FC). (*B*) A dense region of CD68-positive macrophages (MACΦ) in the shoulder region of the plaque. (*C*) Anti-α-smooth muscle cell actin (ASMA) immunostaining revealing a paucity of smooth muscle cells within the fibrous cap (*arrow*).
Figure is reprinted with permission from Elsevier (Kolodgie, 2007).

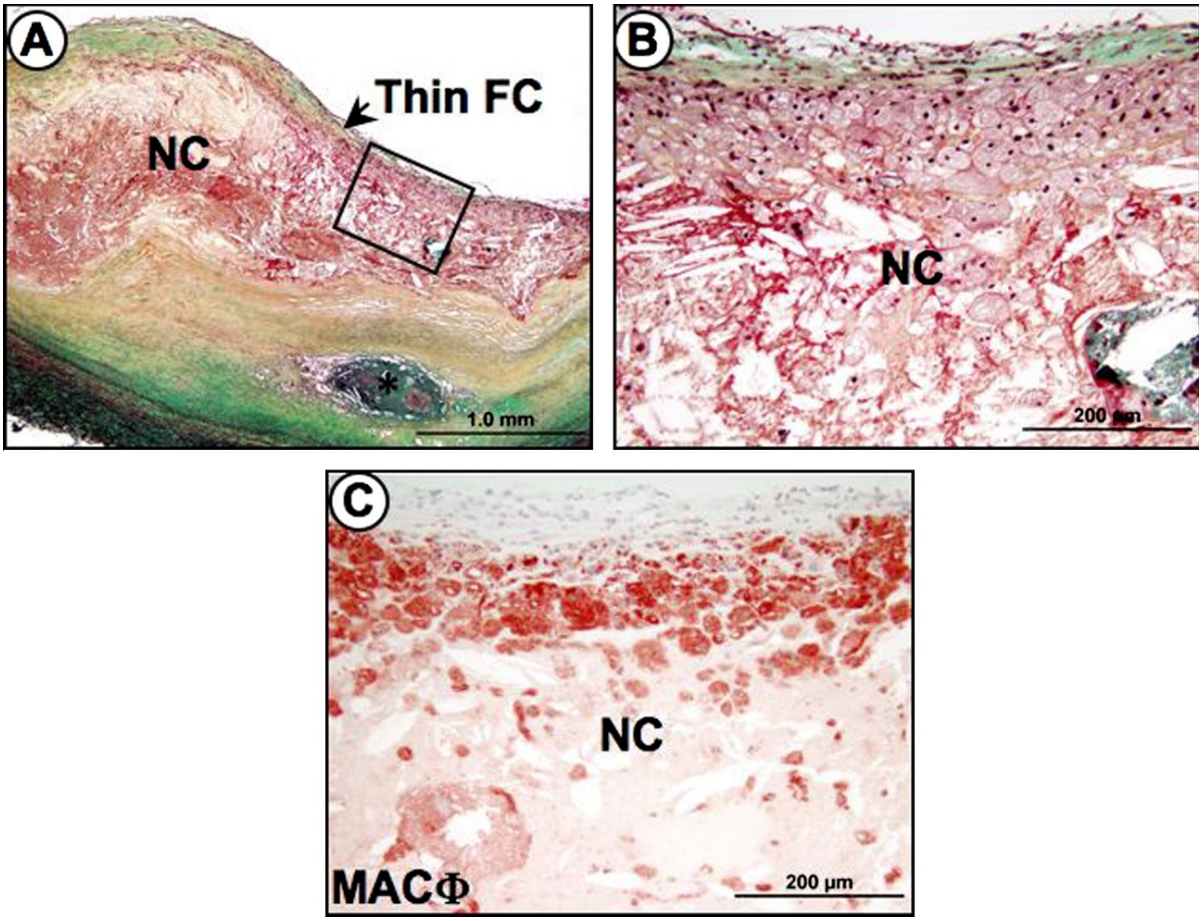

Figure 4: Thin-cap fibroatheroma "vulnerable" plaque in a carotid endarterectomy specimen. (*A*) Low-power image, showing a carotid plaque with a relatively larger necrotic core (NC) covered by a thin fibrous cap (FC). An area of calcified necrotic core (∗) is seen in the deeper intimal layers. (*B*) Higher-power image of an area represented by the black box in *A*, showing the necrotic core and thin fibrous cap infiltrated by foam cells. (*C*) Numerous CD-68 positive macrophages (MACΦ) seen infiltrating the fibrous cap. (*A* and *B*, Movat pentachrome staining.)
Figure is reprinted with permission from Elsevier (Kolodgie, 2007).

2.1.2.2 Bifurcations as atherosclerotic site and arterial remodelling

Artery bifurcations/branch points are prone to the build-up of atherosclerosis. The altered pattern of blood flow in the bifurcations (in particular the outer walls) with low shear stress is thought to be the cause. There is evidence that laminar flow with normal shear stress induces atheroprotection, and that the lower shear stress caused by increased tubular flow decreases the amount of local atheroprotection and increase local inflammation (Malek, 1999; Libby, 2002). The difference in turbulent flow and shear stress upstream (proximal) and downstream (distal) of the maximal stenosis is also thought to explain why a significantly higher number of macrophages were found in the upstream part of the plaque compared to the downstream part, and vice versa for the smooth muscle cells. In the same study six of nine ruptured plaques were in the upstream part (Dirksen, 1998).

Glagov *et al*. found that human coronary arteries responded to atherosclerosis by enlarging in relation to the plaque area (Glagov, 1987). The lumen cross-sectional area was preserved, and stenosis delayed until the atherosclerotic plaque occupied 40% of the area inside the internal elastic lamina area. For patients with carotid artery stenosis ≥50% expansive positive remodelling measured with computed tomography (CT) has been found to be significantly greater in patients with cerebral ischemic symptoms compared to asymptomatic patients (Hardie, 2007). Studies of patients with ESUS have shown more and thicker non-stenosing carotid plaques ipsilateral than contralateral to the ESUS site (Komatsu, 2018; Siegler, 2019). This suggests that the severity of the atherosclerotic burden is not necessarily sufficiently reflected by a measurement of the degree of luminal stenosis.

2.1.2.3 Mechanism to progression including inflammation

The initial step in the development of atherosclerosis requires a susceptible (inflammatory activated) endothelium in addition to cholesterol/lipoproteins. In a rabbit model of atherosclerosis the vascular cell adhesion molecule-1 (VCAM-1) was expressed by endothelial cells in response to cholesterol feeding in areas with early foam cell lesions (Cybulsky, 1991). VCAM-1 binds particularly to monocytes and T-lymphocytes, and its induction is thought to depend on inflammation caused by intimal lipoprotein accumulation in response to hyperlipidaemia (Libby, 2002). Once the leukocytes adhere to the endothelium, they can migrate into the intima layer of the vessel wall. When inside the intima, the monocytes develop macrophage

characteristics, phagocytose lipoproteins and eventually end as foam cells **(Figure 5)** (name after intracellular fatty material) and thereafter undergo necrosis. At the same time as the necrotic material builds up the smooth muscle, cells proliferate and form a fibrous cap which stabilizes the vessel wall and covers the necrotic core. The dynamics of the fibrous cap formation and destabilization resulting in plaque rupture is essential for the clinical consequences of an atherosclerotic plaque. Inflammation is a key mechanism in plaque rupture. An interplay between lymphocytes, macrophages/foam cells and lipoproteins is central in the process with many cellular mechanisms and pathways involved **(Figure 5)** (Libby, 2002; Libby, 2019a).

Studies of serological markers of inflammation have further supported the understanding of inflammation as an important factor in the progression of atherosclerosis. High-sensitivity C-reactive protein (hs-CRP) has been found to be a predictor of cardiovascular events in women (Ridker, 2000). Schillinger *et al.* found that hs-CRP and serum amyloid A predicted short-term progression of atherosclerotic lesions in the carotid arteries (Schillinger, 2005).

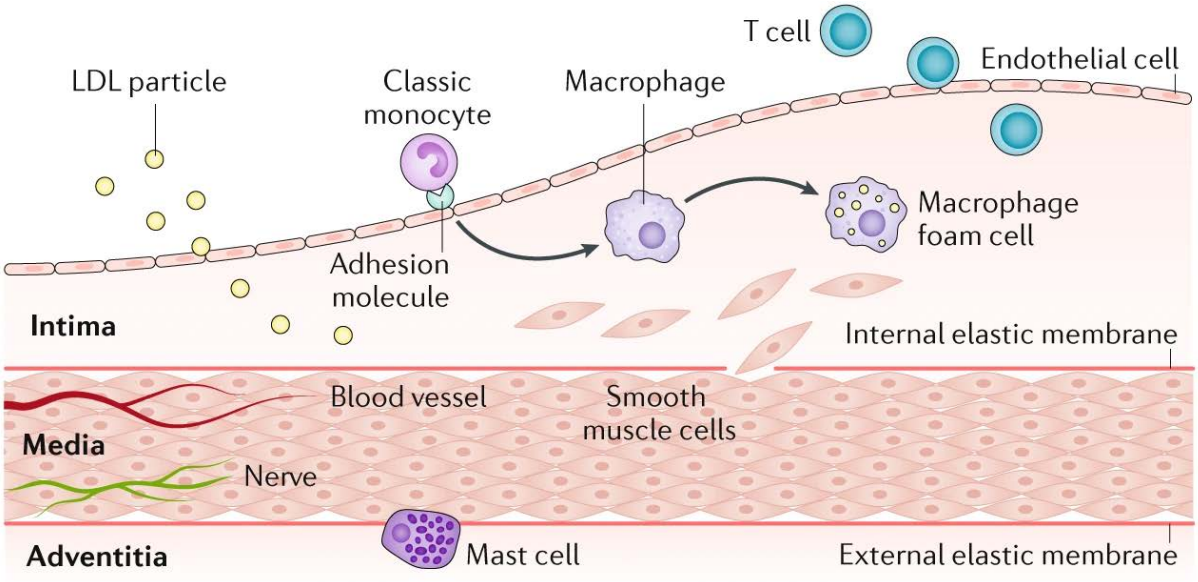

Figure 5: Inflammatory cells in atherosclerosis

In the early stage of atherosclerotic lesion initiation, low-density lipoprotein (LDL) particles accumulate in the intima, where protected from plasma antioxidants, they can undergo oxidative and other modifications that can render them pro-inflammatory and immunogenic. Classic monocytes that exhibit a pro-inflammatory palette of functions then enter the intima. Monocytes circulate in the bloodstream and can bind to adhesion molecules expressed by activated endothelial cells. Chemoattractant cytokines, known as chemokines, can promote the migration of the bound monocytes into the artery wall. Once in the intima, monocytes can mature into macrophages, and attain characteristics associated with the reparative or less pro-inflammatory monocyte/macrophage population. These cells express scavenger receptors that permit them to bind lipoprotein particles and become foam cells. T lymphocytes, although numerically less abundant than monocytes, also enter the intima, and regulate functions of the innate immune cells as well as the endothelial and smooth muscle cells. Smooth muscle cells in the tunica media can migrate into the intima in response to mediators elaborated by the accumulating leukocytes. The smooth muscle cell chemoattractant platelet-derived growth factor arising from macrophages and deposited by activated platelets at sites of endothelial breaches or intraplaque haemorrhage probably participates in this directed migration of medial smooth muscle cells into the intima.

Figure is reprinted with permission from Springer Nature (Libby, 2019a).

2.1.3 Treatment for atherosclerotic carotid artery disease

'*On the basis of anecdotal evidence, about 1 million endarterectomies were performed worldwide between 1974 and 1985'* (North American Symptomatic Carotid Endarterectomy Trial Collaborators, 1998).

Following this, large randomized, controlled clinical trials on the effect of surgical removal of carotid artery plaques (carotid endarterectomy (CEA)) versus best medical treatment in the prevention of strokes were performed. The presence of symptoms and the degree of stenosis caused by the plaque were the primary variables. The North American Symptomatic Carotid Endarterectomy Trial (NASCET) and The European Carotid Surgery Trial (ECST) found that for symptomatic patients with substantial stenosis (above 70–80% depending on method for stenosis measurement), CEA was superior to medical treatment (European Carotid Surgery Trialists' Collaborative Group, 1998; North American Symptomatic Carotid Endarterectomy Trial Collaborators, 1998). A later analysis of pooled data (total 6092 patients, uniform measurement of stenosis degree) found that CEA increased the five-year risk of ipsilateral ischaemic stroke in patients with less than 30% stenosis. It had no effect in patients with 30–49% stenosis, had marginal benefit in 50–69% stenosis and was highly beneficial in those with ≥70% stenosis without near-occlusion (absolute risk reduction 16%) (Rothwell, 2003). The benefit from surgery was greatest in men, in patients ≥75 years, when performed within two weeks after the last ischemic event and fell rapidly with increasing delays. Compared to men, the benefit from CEA in patients with 50–69% stenosis was significantly less in women. Women also had a lower risk of ipsilateral ischemic stroke on medical treatment and a higher operative risk. The benefit of surgery tended to be greatest in patients with stroke and to progressively decline in individuals with cerebral TIA and retinal events (Rothwell, 2004).

The annual risk of stroke caused by an asymptomatic carotid stenosis has been declining in the same period as an observed decline in the rate of myocardial infarction. The five year rate of ipsilateral stroke on best medical therapy was 11% in 1995 and 3.6% in 2010 (Naylor, 2009; Naylor, 2015). For asymptomatic patients, the stenosis degree predicts the risk of stroke to a lesser degree than in symptomatic patients. A meta-analysis which included 41 studies found no significant difference in stroke risk between patients with 50–70% stenosis (risk 1.9/100 person years) and

those with 70–99% stenosis (risk 2.1/100 person years) (Hadar, 2014). Because of the risk of serious complications (death and stroke) with surgery and lower incidence of strokes in patients with lower grades or asymptomatic stenosis, treatment selection for these patients has been challenging. The prognosis on best medical therapy (BMT) has also improved, and results from on-going studies are expected to give better recommendations on the choice of treatment (Hadar, 2014; Aboyans, 2018; Naylor, 2018; Silverman, 2019).

The on-going discussion and difficult clinical decisions being made for asymptomatic patients was highlighted in a study that found large variations between 12 countries in the number of CEAs performed on asymptomatic patients (Venermo, 2017). Recent guidelines recommend considering CEA in asymptomatic patients who have a stenosis of 60–99% with a life expectancy >5 years and clinical or plaque imaging feature suggesting a higher stroke risk. The imaging features mentioned include silent cerebral infarction on CT/MRI (magnetic resonance imaging), stenosis progression, large plaque area, a large juxta-luminal black area on computerized plaque analysis, plaque echolucency, intra-plaque haemorrhage on MRI, impaired cerebral vascular reserve, and spontaneous embolization on transcranial Doppler (TCD) monitoring (Naylor, 2018) (imaging described later in chapter 2.2).
The risk of serious complications associated with CEA has been an important consideration in finding better treatments. Carotid artery stenting (CAS), which is an endovascular procedure, is an alternative to CEA. CAS and CEA have similar long-term outcomes, but CAS is more strongly associated with peri-procedural stroke than CEA which is more strongly associated with myocardial infarction (Lamanna, 2019). The use of CAS to treat carotid stenosis varies considerably between countries (from 0-26% for asymptomatic patients and from 0-19% for symptomatic patients (Venermo, 2017)). CAS is an important alternative when the risk of complications with CEA are too high in symptomatic stenosis >70%. **Figure 6** shows current recommendations for treatment of atherosclerotic carotid artery disease (Aboyans, 2018; Naylor, 2018).

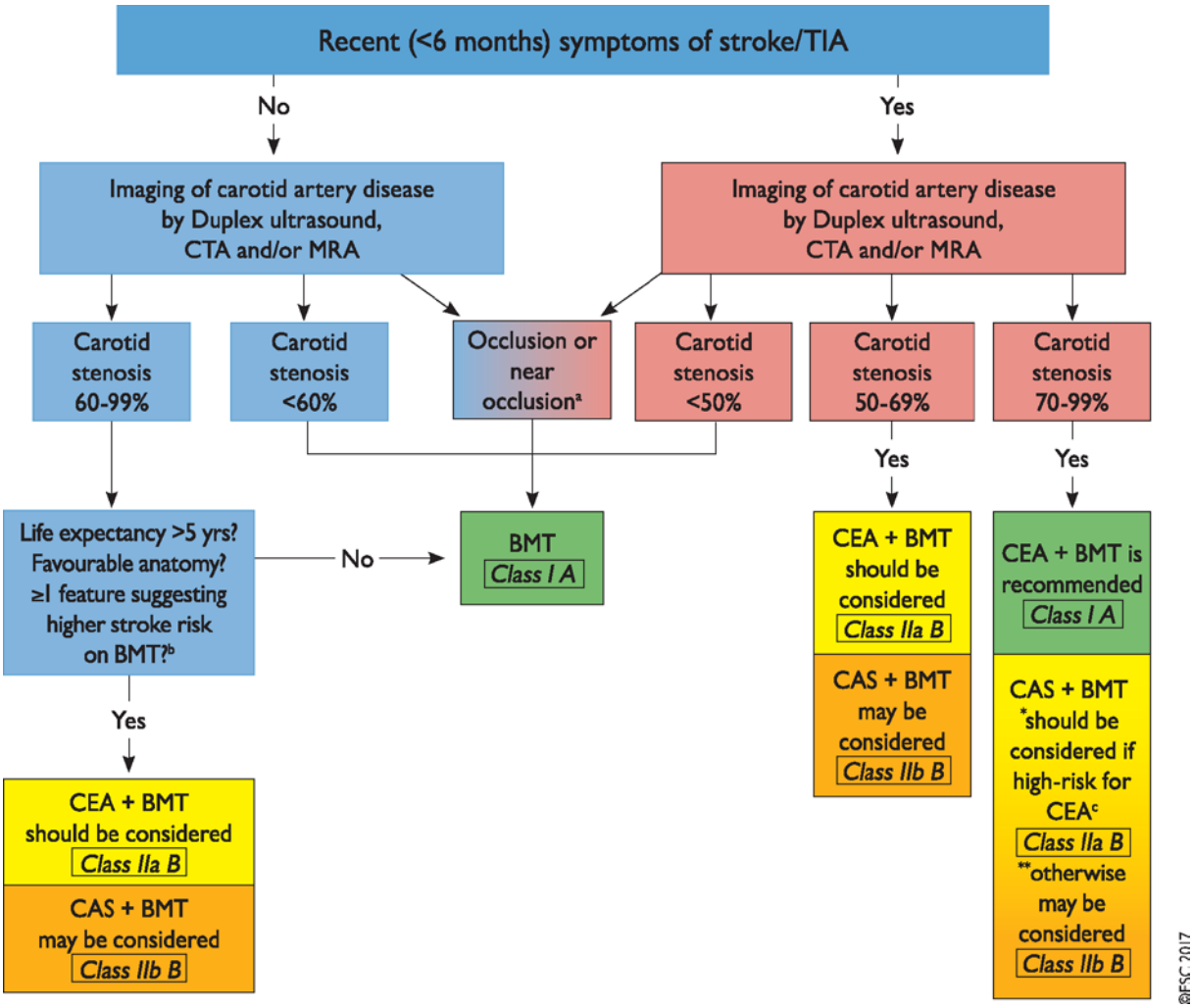

Figure 6: Management of extracranial carotid artery disease. BMT = best medical therapy; CAS = carotid artery stenting; CEA = carotid endarterectomy; CTA = computed tomography angiography; MRA = magnetic resonance angiography; TIA = transient ischaemic attack.

[a]With post-stenotic internal carotid artery narrowed to the point of near occlusion.

[b]See Table 4 (in original publication, clinical and imaging features suggesting higher stroke risk (Aboyans, 2018)).

[c]Age > 80 years, clinically significant cardiac disease, severe pulmonary disease, contralateral internal carotid artery occlusion, contralateral recurrent laryngeal nerve palsy, previous radical neck surgery or radiotherapy and recurrent stenosis after CEA.

Figure reproduced with permission from Oxford University Press on behalf of the European Society of Cardiology (www.escardio.org) (Aboyans, 2018).

Timing

The definition of a symptomatic plaque with respect to time since an event was within 6 months for ECST and NASCET (European Carotid Surgery Trialists' Collaborative Group, 1998; North American Symptomatic Carotid Endarterectomy Trial

Collaborators, 1998). When following the symptomatic group with BMT, but without a surgical intervention, it was shown that the risk for a new stroke declines with time, which suggests that acute destabilization is reversible. If the prophylactic effect of CEA is to have a positive effect, the intervention must be carried out early after the first symptoms (Rothwell, 2004). Guidelines state that the majority of recently symptomatic patients will gain maximum benefit when carotid interventions are performed within 14 days of symptom onset. The goal is to treat the patient as fast as possible, and latest within two weeks (Aboyans, 2018; Naylor, 2018).

Recent trends in surgical treatment

The number of CEAs performed in England declined between 2011 and 2017 (Johal, 2019). This has not been the case in Norway where 486 surgical interventions on the carotid artery were performed in 2016 and the number of operations has been stable since 2008 (Kvåle, 2018).

Medical treatments

Risk factor control, management of hypertension, antiplatelet therapy and lipid lowering therapy are essential in patients with carotid artery stenosis ≥50% (Naylor, 2018). The BMT strategies have evolved since the first endarterectomy trials and prevents more strokes now than earlier. This may alter treatment strategies in the future. Beside the established treatment strategies, the additional effect of other medical treatments have been explored (Libby, 2019b). The recent Canakinumab Anti-inflammatory Thrombosis Outcome Study (CANTOS) described the stand-alone effect of anti-inflammatory treatment on new vascular events for patients that already had suffered one (myocardial infarction). In this study patients with hCRP>2 were treated with Canakinumab (a selective monoclonal antibody that binds to and blocks the effect of interleukin 1 beta), but the price of fewer vascular events was an increase in serious infections (Ridker, 2017).

2.2 IMAGING OF ATHEROSCLEROSIS

Imaging of carotid artery stenosis can be divided into two categories, focusing either on lumen diameter/degree of stenosis or on plaque composition. Some imaging modalities depict both, others only one. At the time of study inclusion, the clinical focus was to measure the degree of stenosis. During the past 10–15 years there has been an extensive focus on the development of imaging techniques that are able to characterize the plaque causing the lumen stenosis.

2.2.1 Duplex ultrasound

Ultrasound uses sound waves to create images or measure velocities. Duplex ultrasound (DUS), the combination of brightness mode (B-mode) and Doppler ultrasound, is the workhorse in the diagnostic work-up of patients with carotid atherosclerosis. In B-mode ultrasound the signal intensity arises due to different reflective properties between tissues. These two-dimensional images characterize structures according to their echogenicity (reflective capacities). Doppler is the use of ultrasound to quantify blood velocity exploiting the fact that moving blood cells will produce reflected ultrasound waves with different frequency shifts depending on their speed and direction. The advantages of ultrasound are high spatial resolution, no ionizing radiation, low cost, and high availability.

A multicentre study of 270 patients undergoing CEA found that plaque echogenicity was inversely related to the plaque content of soft tissue (primarily haemorrhage and lipids) whereas increasing amounts of calcification in plaque correlated with increasing echogenicity (European Carotid Plaque Study Group, 1995). Plaque echogenicity was evaluated on a scale from one (strong echo) to three (low echogenicity/echolucency). Patients with recent symptoms had more soft tissue at histology than patients with earlier symptoms. Another study further linked echolucency to inflammation by finding that echolucent plaques were associated with increased presence of plaque macrophages at histology, independent of the degree of artery stenosis (Gronholdt, 2002).

Low ultrasound echo has been found to predict future strokes in patients with symptomatic (not asymptomatic) ≥50% carotid artery stenosis (Gronholdt, 2001). Mathiesen *et al.* graded plaque echogenicity from one to four (1, echolucent; 2,

predominantly echolucent; 3, predominantly echogenic, 4, echogenic) and found that echolucent plaques were associated with an increased risk of ipsilateral cerebrovascular events independent of the degree of artery stenosis and cardiovascular risk factors during a follow up of three years (Mathiesen, 2001). A meta-analysis and systematic review of asymptomatic patients confirmed the significant positive relationship between predominantly echolucent plaques and the risk of stroke irrespective of the degree of stenosis (Gupta, 2015). In addition to a visual evaluation of echolucency, a method quantifying the amount of grey (grey scale median (GSM)), in two-dimensional screen saves of the plaque, is available (Elatrozy, 1998).

Consensus criteria from the Society of Radiologists in Ultrasound describes how blood velocities measured by Doppler should be used to define the degree of carotid stenosis (Grant, 2003). Doppler can also be used to detect arterial emboli (Russell, 1991). Microembolic signals (MES) detected by TCD predict stroke risk in symptomatic carotid stenosis (King, 2009). A multicentre study of 467 patients with asymptomatic carotid stenosis ≥70% (77 had embolic signals at baseline) found that the hazard ratio for ipsilateral stroke and TIA within two years in patients with embolic signals compared to those without was 2.54. The absolute annual risk of ipsilateral stroke within two years was 3.6% in patients with embolic signals and 0.7% in those without (Markus, 2010).

2.2.2 Angiography

Digital subtraction angiography is a fluoroscopic technique that uses intravenous (*i.v.*) administration of contrast media (CM) with iodine in an arterial catheter to visualize blood vessels. Subtracting the post-contrast images from the images acquired prior to contrast administration eliminates structures with high density such as bones which allows an accurate depiction of the blood vessels. Digital subtraction angiography was the gold standard for stenosis evaluation until other methods with fewer complications (stroke being one complication) became available (Naylor, 2018).

Angiography with CT (CTA) or MRI (MRA) of the extra- and intracranial vessels are often included in the evaluation of carotid artery stenosis. CT uses photons from an x-ray tube and a ring of detectors to create a three-dimensional image of structures based on differences in photon attenuation. Blood vessels are evaluated with the

administration of high attenuating iodinated CM. MRI exploits the magnetic properties of protons placed in a strong magnetic field to produce images. Signal intensity in a MR image arises as protons in different tissues have different ability for energy exchange with its surroundings (T1-relaxation) and between protons (T2-relaxation). MRA can be performed with or without contrast media.

A study with 170 patients comparing the diagnostic accuracy of Duplex ultrasound (DUS), CTA and blood-pool-enhanced MRA compared with DSA in assessing carotid stenosis found an accuracy of 76% for DUS, 97% for CTA and 95% for steady-state contrast-enhanced MRA. Blood-pool contrast-enhanced steady-state MRA sequences offer improved evaluation accuracy which is identical to CTA (Anzidei, 2012). DUS was found to have a sensitivity of 94% and a specificity of 92% for diagnosing 60-99% carotid stenoses (Naylor, 2018). A health technology assessment report found DUS, CTA and MRA equivalent for the detecting of significant ICA stenosis (Wardlaw, 2006). When CEA is being considered, a DUS stenosis estimation is recommended in addition to a CTA or MRA. A CTA or MRA is recommended before CAS to provide additional information on the aortic arch and the extra- and intracranial circulation (Naylor, 2018).

Characterization of the plaque and its components is possible with CT and MRI (Saba, 2018). Plaque characteristics associated with an increased risk of late stroke in patients with asymptomatic 50-99% stenoses treated medically is mentioned in a recent practice guidelines as one of the criteria for selection of asymptomatic candidates for intervention (chapter 2.1.4) (Naylor, 2018).

2.2.3 Positron emission tomography (PET)

2.2.3.1 PET principles

The tracer principle introduced by the chemist George C. de Hevesy, stating that radioactive and nonradioactive isotopes of the same element have the same chemical properties, is the basis for the imaging and quantification techniques used in nuclear medicine (Myers, 1979). Biological processes can be followed and quantified by labelling molecules that are parts of these processes with radionuclides that emit radiation that can be detected. Opposed to radiologic imaging techniques where photons or waves are sent through the patients from the outside (transmission), the radiolabelled molecules are distributed in the body and radiation emitted from the inside of the patients are used for generating images. The radiolabelled molecules must not interact with or alter the processes they are going to characterize. The number of molecules developed for targeting various aspects of pathological processes is constantly increasing, but the number of radionuclides suitable as label is scarcer as they must exhibit distinct chemical properties to be incorporated in molecules and distinct physical properties to be suitable for imaging.

Radioactive or unstable nuclei gain stability by radioactive decay that release their excess energy. Radionuclides for use in imaging can be positron- or single photon emitters. The positron emitters are characterized by their emission of two identical gamma ray photons simultaneously, with energy of 511keV, almost 180 degrees (±0.2) to each other when the positron combines with an electron and annihilation occurs **(Figure 7)**. The principle of detection in positron emission tomography (PET) is that these two photons can be detected by dual photon coincidence counting.

Positron emitters used in medical imaging are mainly short-lived isotopes such as carbon-11 (^{11}C), nitrogen-13 (^{13}N), oxygen-15 (^{15}O), ^{18}F, gallium-68 (^{68}Ga) and rubidium-82 (^{82}Rb). ^{18}F has favourable characteristics for both image quality (relatively short positron range, 0.6 mm) and practical logistics (relatively long half-life, 110 min) (Basu, 2014).

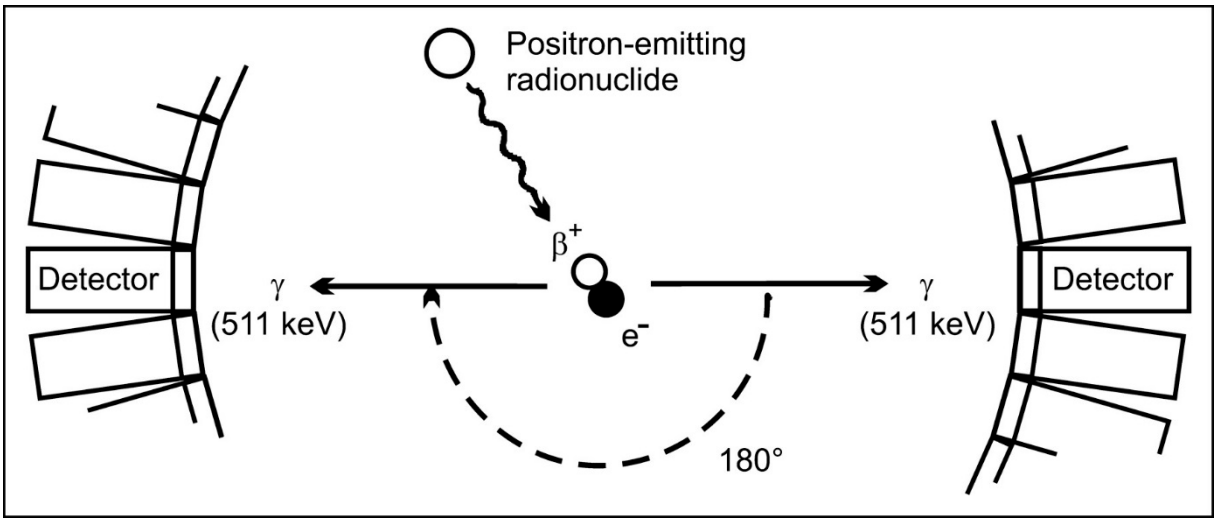

Figure 7: A positron emitted from a radionuclide that decays will travel a short distance before it combines with an electron. The positron and the electron annihilate, converting their masses into two 511-keV photons emitted in opposite directions. The two annihilation photons are electronically detected as a coincidence event if they strike two opposing detectors simultaneously (detector ring schematically depicted).
Figure adapted from original publication in JNM. © SNMMI. (Verel, 2005).

Modern PET scanners contain many small detectors placed in rings around the patient. A PET detector has a scintillator crystal that converts the photon energy into light and a device, most often a photo multiplier tube (PMT), that converts the light into an electric signal. Only pairs of photons that hit the PET detector within a predefined time and energy window will be accepted as originating from the same positron, the others are rejected. The line between two opposite hits is called line of response (LOR) (Basu, 2014). PET images are reconstructed from millions of LOR registrations providing a picture of the radiotracer's distribution in the imaged volume.
The raw data acquired is corrected for several factors to give correct and quantitative images of the tracer distribution (Dahlbom, 2017), e.g. correction algorithms for scatter photons and correction for photon attenuation in tissue with a CT scan that produces an attenuation map.
PET data is a collection of image projections at different angles around the patient. These projections contain the necessary information to reconstruct the three-dimensional activity distribution using different approaches for image reconstruction (Dahlbom, 2017). Iterative reconstruction techniques such as ordered subsets expectation maximization (OSEM) have replaced the filtered back projection method

because of better image quality and improved signal to noise ratio (Lonneux, 1999; Dahlbom, 2017).

Noise is present in all images, giving the image a mottled, grainy, textured, or snowy appearance. Image noise is caused by a variety of modality-specific factors such as scanner type, image reconstruction algorithm, etc. In PET and CT the major sources of image noise is quantum noise (the random variation in photon counts due to the statistical nature of these X-rays and related to the number of photons detected) and electronic noise (noise inherent to the detector and unrelated to number of detected photons) (Razifar, 2005). PET images contain relatively high levels of quantum noise due to limited counting statistics. A post reconstruction smoothing filter attenuates the high frequency noise (Dahlbom, 2017). The amount of noise is reduced with increasing full width at half maximum (FWHM) of the reconstruction filter. The resolution in OSEM reconstructions can be increased with increasing number of iterations but at the cost of increased noise. The use of a post-reconstruction smoothing filter reduces noise but also reduces the maximum signal of the measurements (Soret, 2007; Skretting, 2009).

After several corrections have been made to the raw data, the voxel values in the PET images represent the actual activity concentration (amount of radioactivity per unit volume), in Becquerel per millilitre (Bq/mL). Dynamic imaging is one way to quantify lesion or organ metabolism with PET, but the methods are complex and labour-intensive. The metric most used to quantify the uptake in lesions or organs is the standardized uptake value (SUV). SUV is the ratio of the average activity concentration in a specific region of an image (voxel, region of interest (ROI) or volume of interest (VOI), or organ system) to the average activity concentration in the entire patient or phantom being imaged. When weight is used as a surrogate for volume, with the assumption that the density of a person is approximately 1.0 g/mL, the SUV is calculated as follows:

$$SUV = \frac{Measured\ activity\ Concentration\ (Bq/mL)}{Injected\ activity\ (Bq)/\ Weight\ (kg)}$$

Calculation of SUV requires the amount of injected activity, time of injection, body weight (BW) and time between injection and imaging (circulation time) (Dahlbom, 2017; Surti, 2017). For the PET tracer ^{18}F-FDG, uptake in fat tissue is very low. The uptake of ^{18}F-FDG in lesions can therefore be overestimated in heavier compared to lighter individuals. To compensate for this, normalising the SUV to lean body mass (LBM), correcting for the presumed amount of fat tissue (Zasadny, 1993) (also requires height and sex of the subject) instead of pure body weight, is recommended, in particular for response assessment studies (Boellaard, 2015). Different formulas for LBM are proposed (Tahari, 2014), the Hybrid Viewer 2.0 software (Hermes Medical Solutions AB, Stockholm, Sweden) uses:

$$\text{Women:} \quad \text{LBM} = 1.07 \text{ x } \text{BW} - 148 \text{ x } \left(\frac{\text{BW}}{\text{Height}}\right)^2$$

$$\text{Men:} \quad \text{LBM} = 1.1 \text{ x } \text{BW} - 120 \text{ x } \left(\frac{\text{BW}}{\text{Height}}\right)^2$$

In addition to body mass and fat content, the SUV for imaging with ^{18}F-FDG is known to be sensitive to circulation time, glucose levels, spatial resolution and image noise (Keyes, 1995).

The spatial resolution of a PET scanner is the limiting distance needed to discriminate between two point or line sources. Spatial resolution in PET is characterized by the width of an image profile of a small object, e.g. point source giving a point spread function (PSF). The resolution is expressed as the FWHM of this profile (Bailey, 2003). The spatial resolution depends mainly on the width of the detector elements. Fundamental factors that limit the spatial resolution include positron range before annihilation and acollinearity of the direction of the annihilation photons. The influence of non-fundamental factors that can be reduced are penetration into the detector ring, sampling errors and decoding errors in the detector modules. Statistical noise and the reconstruction algorithm also affect the spatial resolution. The fundamental limit for spatial resolution for a clinical PET camera is 1.83 mm FWHM. A resolutions of 2.36 mm FWHM is achievable by using a detector width that compromises between spatial resolution and practical manufacturing purposes (Moses, 2011). The effective spatial resolution for the PET/CT scanner used in our study, (Siemens Biograph 64, images reconstructed with OSEM, 4

iterations, 8 subsets, 256x256 voxels giving pixel size 2.67 mm and slice thickness 2.03 mm) was 6.4 mm FWHM with post-reconstruction Gaussian smoothing filter with FWHM 5 mm, and 4.5 mm with post-reconstruction Gaussian smoothing filter with FWHM 2 mm (Skretting, 2010a).

Accurate uptake measurement with PET depends heavily on the size of the lesion or structure. For lesions with a size less than three times the FWHM of the reconstructed image resolution, the measured maximum value will be lower than the actual maximum value. This phenomenon is called partial volume effect (PVE) or intensity diffusion and is caused by two factors (Soret, 2007; Skretting, 2009). Firstly, the limited spatial resolution of the scanner makes the imaged structures appear larger than they are. The maximum activity concentration measured is lower than actual because it is smeared out, but the total activity is intact in a larger volume. This is illustrated in **Figure 8** (Soret, 2007).

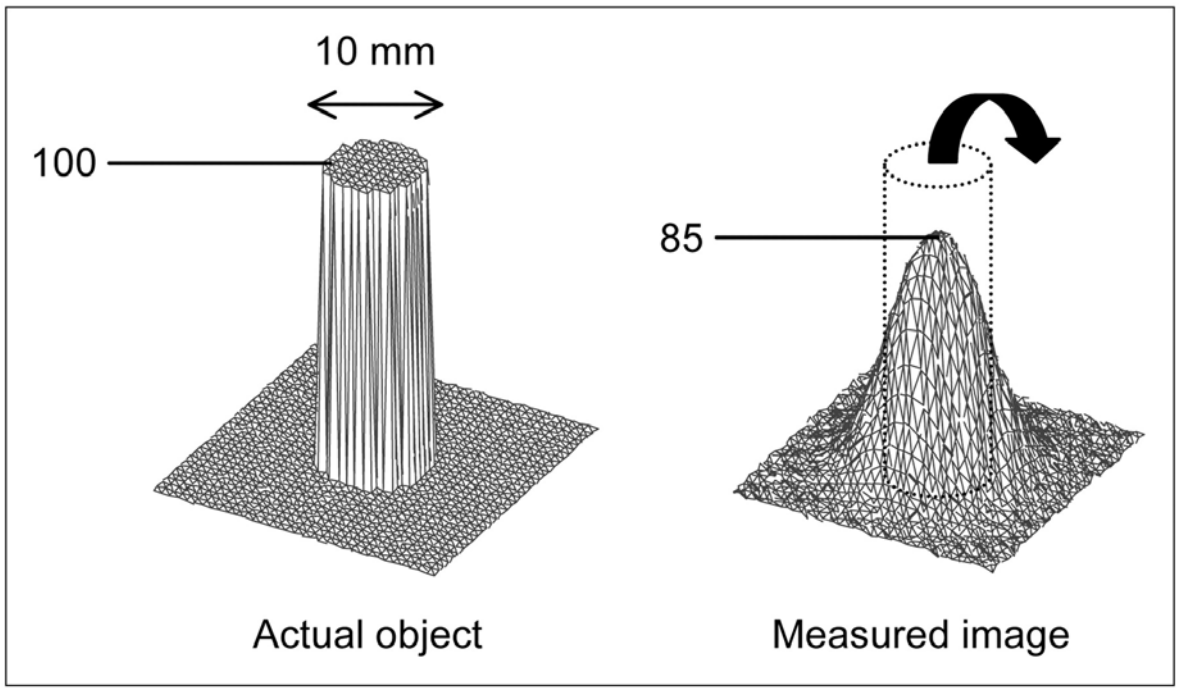

Figure 8: Circular source (diameter of 10 mm) of uniform activity (100 arbitrary units) in non-radioactive background yields measured image in which part of signal emanating from source is seen outside actual source. Maximum activity in measured image is reduced to 85.
This figure was originally published in JNM. © SNMMI. (Soret, 2007).

The second factor causing underestimation of uptake in small structures is the image sampling, meaning the size of each image element (voxel) with one unique activity concentration/uptake value. Since PET images are sampled on a voxel grid, the size and shape of the structure of interest decides how much of the voxel volume it will fill, and how much of the voxel that represents other tissue (background or neighbouring structures). **Figure 9** shows what happens with the voxel values in the edge of a tumour depending on the surrounding voxel values. If the lesion of interest is not able to 'fill' the entire voxel, the voxel uptake value will be influenced by the uptake of nearby voxels. Spill-out refers to the activity contribution in the edge voxels (not covered entirely by the lesion) by the lesion uptake, spill-in refers to the activity contribution in the edge voxels from the background (or neighbour structure) (Soret, 2007; Skretting, 2009).

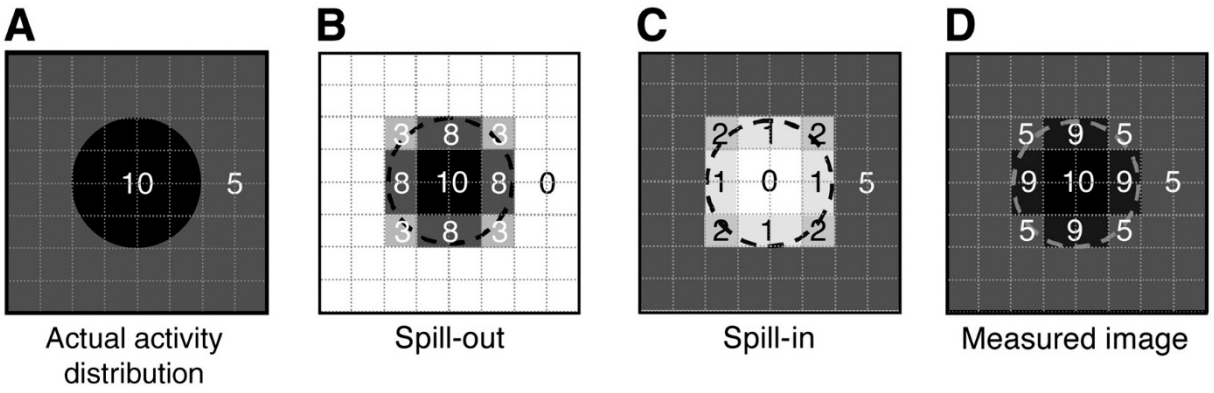

Figure 9: The measured image (D) of the activity distribution (A) results from mixture of spilling out (B) and spilling in (C). Image sampling affects background activity, creating spilling in within tumor (C). Resulting image is sum of spilling in and spilling out (D).
This figure was originally published in JNM. © SNMMI (Soret, 2007).

A phantom experiment at our department using gel spheres with ^{18}F-FDG (method described by Skretting *et al.* (Skretting, 2010b)) illustrated how the uptake in small lesions is underestimated **(Figure 10)**. The spheres had identical activity concentrations and diameters of 3, 5, 8, 10 and 12 mm. The study showed that the recovery coefficients (the ratio between the detected and the real activity concentration) decreases from 1 (100% detected) for spheres below 15-16 mm. The underestimation for spheres below 5 mm was profound with recovery coefficients below 0.2.

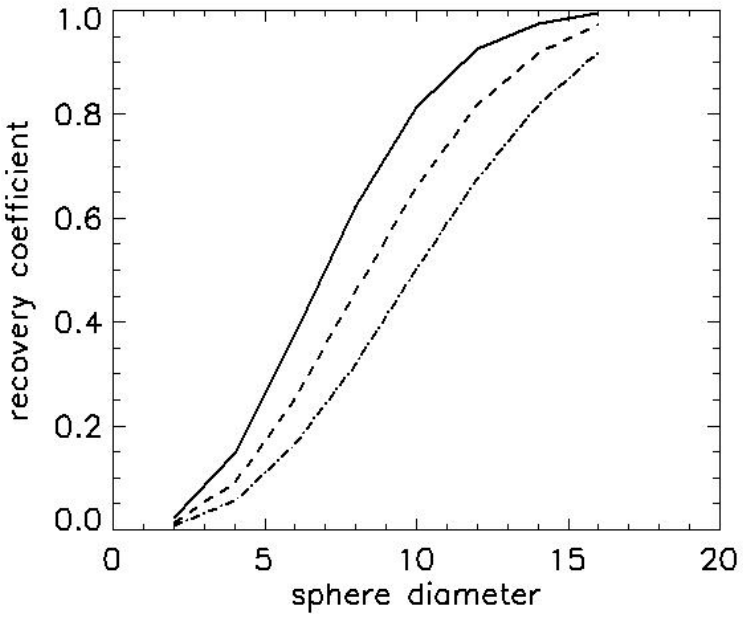

Figure 10: Recovery coefficients for spheres filled with ^{18}F-FDG imaged on Siemens Biograph 64 (Siemens Medical Systems, Erlangen, Germany). Smoothing filter FWHM = 2 (solid line), 3.5 (dashed), 5.0 (dot-dashed).
Figure courtesy of Arne Skretting, Oslo University Hospital.

A simulation study of a source that mimics the uptake in a plaque or vessel wall further illustrates how the images are smeared out/blurred and how the measured activity concentration is grossly underestimated **(Figure 11)**. The simulations were performed on the specifications from a scanner both with and without time of flight (TOF) capabilities.

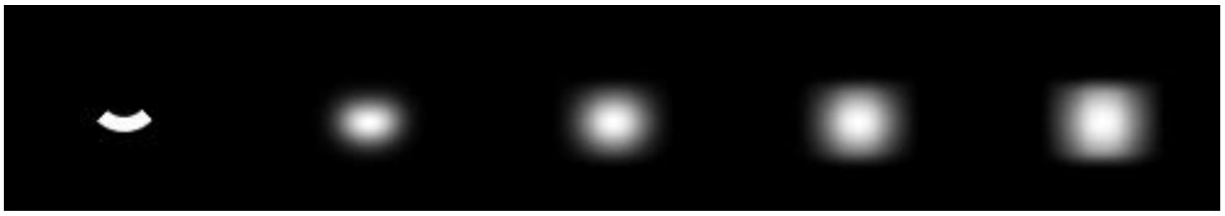

Source	TOF	FWHM 2	FWHM 3,5	FWHM 5
	0.206	0.103	0.077	0.061

Figure 11: Recovery coefficients for simulated images of ^{18}F-FDG plaques from two different scanners; Siemens mCT (TOF) and Siemens Biograph 64 PET/CT (Siemens Medical Systems, Erlangen, Germany) with postreconstruction filter FWHM 2, 3.5 or 5. *Figure courtesy of Arne Skretting, Oslo University Hospital.*

2.2.3.2 ^{18}F-FDG

Glucose uptake in cells can be quantified with radiolabelled 2-deoxy-D-glucose (DG) because the uptake mechanism for the two compounds is identical. Glucose is transported into living cells by cell membrane glucose transporters (GLUTs). Unlike glucose, the slightly altered DG (the 2-hydroxyl group is replaced by hydrogen) is not metabolized further after the initial intracellular phosphorylation to 2-deoxy-D-glucose-6-phosphate (DG-6-P) by hexokinase. DG-6-P is in that sense trapped intracellularly (Sols, 1954). Initial studies of the quantification of glucose metabolism with radiolabelled DG was done in rat brains with ^{14}C labelled DG, where the amount of ^{14}C DG accumulated in the whole brain was measured after removal with a scintillation counter (Hawkins, 1974), or regionally with autoradigraphy (Sokoloff, 1977). Metabolic trapping in brain and heart of mice was soon after achieved with DG labelled with ^{18}F (^{18}F-FDG) (Gallagher, 1978). Reivich *et al.* performed the first scan with ^{18}F-FDG for measurement of local cerebral glucose utilization in man (Reivich, 1979).

High level of glucose metabolism is a hallmark for several pathological processes. Most malignant cells have increased glucose metabolism. Warburg was first to describe that cancer tissue has accelerated glucose metabolism even when oxygen is present (aerobic glycolysis), thereby named the 'Warburg effect' (Warburg, 1956). ^{18}F-FDG was quickly recognized as suitable for imaging of oncologic diseases (Boellaard, 2010), after it was found that ^{18}F-FDG uptake was higher in high-grade than low-grade gliomas (Di Chiro, 1982). In oncological ^{18}F-FDG scans, an increased uptake of ^{18}F-FDG was also found in several types of infectious and inflammatory diseases (Shreve, 1999). This was a serious pitfall in the diagnosis of oncologic diseases, but ^{18}F-FDG has later gained an independent stronghold in the diagnosis and follow-up of a wide spectre of inflammatory and infectious diseases. Fever of unknown origin, sarcoidosis, vasculitis, peripheral bone osteomyelitis, suspected spinal infection, evaluation of metastatic infection and of high-risk patients with bacteraemia were of the first well-established indications for imaging with ^{18}F-FDG PET (Jamar, 2013).

The increased rate of glycolysis and its association with upregulation of GLUTs (Yamamoto, 1990) and intracellular hexokinase expression is a known mechanism of

high uptake of ^{18}F-FDG in malignant tissue. Similar mechanisms have also been documented for inflammatory conditions. Following injection of tumour cells in mice Kubota *et al*. found that, in addition to tumour cells, associated granulation tissue and macrophages also had high accumulation of ^{18}F-FDG (Kubota, 1992). Other animal models have shown that bacterial endotoxin induce enhancement of glucose influx into macrophages via GLUT-1 (Fukuzumi, 1996) and that glucose uptake and GLUT-1 in macrophages are increased following thermal injury and sepsis in mice (Gamelli, 1996). Uptake of ^{14}C-FDG and high expression of GLUT-1 and GLUT-3 were seen at site of inoculation with staphylococcus aureus (Mochizuki, 2001). ^{18}F-FDG was particularly found in areas with neutrophils and macrophages in a study where turpentine was used to induce inflammation (Yamada, 1995). ^{18}F-FDG's ability to identify sites of inflammation and infection seems to be related to the increased glycolytic activity of the cells involved in the inflammatory response and many types of cells are involved (Jamar, 2013).

In the normally functioning body facilitative glucose transport is mediated by members of the GLUT protein family. Several GLUTs have been described. They are expressed in a tissue- and cell-specific manner and exhibit distinct properties that reflect their specific functional roles. GLUT-1 is expressed widely in various tissues, up-regulated by several growth-factors and provides many cells with their basal glucose requirement. GLUT-2 expression is regulated by glucose concentration and it is mainly expressed in intestine, kidney, liver, pancreatic islets and brain. GLUT-3 is in neurons and ensures a glucose supply in the brain even in hypoglycemic conditions. GLUT-4 is stimulated by insulin and expressed in skeletal and cardiac muscle, brown and yellow fat (Mueckler, 1994; Finessi, 2019).

Based on the knowledge of the different GLUTs and since ^{18}F-FDG is treated like glucose until it accumulates intracellularly, patient preparations that ensures high uptake in the lesion or organ of interest and minimal uptake elsewhere are crucial. A long enough fasting period (4-6 hours) is essential to ensure low level of glucose and insulin. If not accomplished, hyperglycemia may reduce the binding sites available for ^{18}F-FDG because of competition with plasma glucose, and hyperinsulinemia causes up-regulation of GLUT-4 and thereby high uptake in skeletal and myocardial muscle. Other precautions within the 24 hours before examination are to avoid strenuous

physical activity to ensure low muscle uptake of ^{18}F-FDG, and to avoid freezing not to stimulate ^{18}F-FDG uptake in brown adipose tissue. Hyperglycemia and diabetes require special attention with preparatory instructions to optimize the balance between the level of insulin and blood glucose (Boellaard, 2015; Finessi, 2019). The guidelines for patient preparations are slightly different depending on which organ system or diseases that are to be imaged with ^{18}F-FDG PET. Brain imaging for the detection of hypometabolic cortical areas seems to be more sensitive to light hyperglycemia than the detection of infectious and inflammatory conditions (Varrone, 2009; Jamar, 2013; Boellaard, 2015; Slart, 2018).

2.2.3.3 ^{18}F-FDG PET in atherosclerosis

Rudd *et al.* were the first to explore if ^{18}F-FDG could be used to quantify inflammatory metabolic active cells in atherosclerotic plaques in humans (Rudd, 2002). Autoradiographic imaging of atherosclerotic plaques from three patients with symptomatic carotid stenosis ≥70% incubated with tritiated DG showed uptake in the macrophage rich areas of the plaques, and little or no uptake in other areas. Macrophage rich areas were mainly located at the lipid core/fibrous cap border of the lesions. They also reported a higher accumulation rate of ^{18}F-FDG in symptomatic than in contralateral asymptomatic stenosis (35–75%) (Rudd, 2002). Later studies found a significant positive correlation between the degree of ^{18}F-FDG uptake in carotid stenosis and macrophage content in the removed plaques (Tawakol, 2006; Graebe, 2009). A recent meta-analysis including 14 studies (539 patients) found a significantly higher tracer uptake in symptomatic than asymptomatic atherosclerotic carotid disease (Chowdhury, 2018). The Dublin Carotid atherosclerosis Stroke Study showed that carotid plaque uptake of ^{18}F-FDG was associated with a high risk of early stroke recurrence, independent of the degree of stenosis (Marnane, 2012). A multicentre study by Kelly *et al*. including 109 patients confirmed the results from Marnane *et al.* regarding the prediction of a new stroke after the first clinical event, recurrent stroke risk increased across SUV_{max} quartiles (Kelly, 2019).

Other factors associated with plaque vulnerability that correlate with uptake of ^{18}F-FDG are matrix metalloproteinase-1 (Wu, 2007), plaque CD68 gene expression (Graebe, 2009) and MES on TCD (Moustafa, 2010; Muller, 2014).

^{18}F-FDG PET is also promising for patients with ESUS. A PET/MRI study of 18 patients found that the prevalence of complicated atherosclerotic plaques (American Heart Association lesion type VI with intraplaque haemorrhage, fibrous plaque rupture or luminal thrombus on MRI) was significantly higher in the carotid artery ipsilateral to the ischaemic stroke than contralateral. Furthermore, they found that complicated plaques were associated with higher ^{18}F-FDG uptake than less complicated lesions (Hyafil, 2016).

Uptake of ^{18}F-FDG in entire vascular beds has been used in several studies as a marker of generalized vascular inflammation in atherosclerosis. One of these studies followed 513 patients without symptomatic CVD at inclusion for 4.2 years, ^{18}F-FDG uptake in ascending aorta was an independent predictor of future CVD events (Figueroa, 2013). ^{18}F-FDG PET has also been used in several intervention studies to measure the treatment effect on vascular inflammation (Fayad, 2011; Elkhawad, 2012; Tawakol, 2014).

2.2.3.4 Methods for atherosclerosis imaging

Standardization of imaging procedure and analysis is a challenge in vascular atherosclerosis imaging with ^{18}F-FDG PET. The imaging of lesions with relatively low uptake and unclear boundaries are much more challenging than measuring uptake in a lung tumour or screening for metastatic hot spots in oncology.

Several methods for the quantification of ^{18}F-FDG uptake in atherosclerosis have been suggested. A literature search by Huet *et al* identified 53 different acquisition protocols, 51 different reconstruction protocols and 46 different quantification methods used in 49 studies (Huet, 2015). A position paper in 2016 by the Cardiovascular Committee of the European Association of Nuclear Medicine (EANM) (Bucerius, 2016) proposed optimized and standardized protocols for imaging and interpretations of PET scans in atherosclerosis. They also addressed the absence of conclusive evidence. A recent systematic review and meta-analysis evaluating the association between carotid artery ^{18}F-FDG or ^{18}F-labelled sodium fluoride (^{18}F-NaF) uptake in recent or future cerebral ischemic events described in detail the obstacles in trying to pool results from several studies (Chaker, 2019).

^{18}F-FDG PET studies of inflammation in atherosclerosis can be divided in two main groups:

Group1. Studies of localized atherosclerosis in the carotid artery bifurcation and ICA.

Group 2. Studies of one or more vessel segments e.g. common carotid artery, aorta (divided in segments), iliac and femoral arteries in subclinical atherosclerosis.

Studies of the coronary arteries have also been carried out (Rogers, 2010; Tarkin, 2017), but these vessels have other methodological challenges and are not included in the current thesis.

In Group 1 the definition of area of interest or localization of the plaque in known carotid artery disease is carried out in different ways. All methods need a CTA (or MRA) for the correct localization of the stenosis (the CCA can be localized without CM). Graebe *et al.* (Graebe, 2010a) defined the plaque as the vessel segment where axial CTA showed a luminal filling defect. Figueroa *et al.* (Figueroa, 2012) included an artery segment from 2 cm below to 3 cm above (in the ICA) the bifurcation; Marnane *et al.* (Marnane, 2012) and Kelly *et al.* (Kelly, 2019) included 10 axial slices with centre on the maximum stenosis. In Group 2 the whole vessel segment is defined as the area of interest, but the definite borders can be a little different depending on the length of the axial coverage on the scan. In almost all the published studies, the region of interest (ROI) is drawn around the whole vessel wall including the plaque and lumen on all the axial slices covering the plaque or the vessel segment. This is because the spatial resolution of the image is not good enough to delineate details around the plaque. The uptake value from the ROI is either the mean of the pixel values, $SUV_{mean,}$ or the highest pixel value, SUV_{max}. The metric most commonly used is the mean of all the maximum SUVs (mean SUV_{max}) of the ROIs from individual image slices. The ROIs include the entire plaque (in localized stenosis), or one or more vessel segments (in subclinical/generalized disease). Sub-analysis looking for the most metabolically active areas of a vessel segment, either as the mean of neighbouring slices (most diseased segment MDS) or as the mean of slices above a preset threshold have also been used (**Figure 12)** (Maki-Petaja, 2012; Tawakol, 2013). Bural *et al.* calculated the atherosclerotic burden of the aorta by multiplying the mean uptake values for each aorta segment with the vessel wall volume (Bural, 2006).

The limited spatial resolution of the PET images does not permit the activity in the blood background to be excluded from the quantification of the uptake in the vessel wall plaque. To overcome possible quantification errors due to this, correction for the blood background (most often the mean of SUV_{mean} from several venous ROIs) has been suggested but implemented differently. The uptake values have either been normalized to the blood background activity (Tawakol, 2006; Rudd, 2007; Rudd, 2008; Fayad, 2011), corrected for the background activity with subtraction (Blomberg, 2014) or not corrected for background activity (Graebe, 2010a; Graebe, 2010b; Marnane, 2012). Some studies report both corrected and uncorrected values (Vesey, 2017; Kelly, 2019; Kelly, 2020). The rationale for background correction has been strongly criticized by some authors (Chen, 2015; Huet, 2015). **Figure 12** summarizes the different quantification methods and the use of background correction.

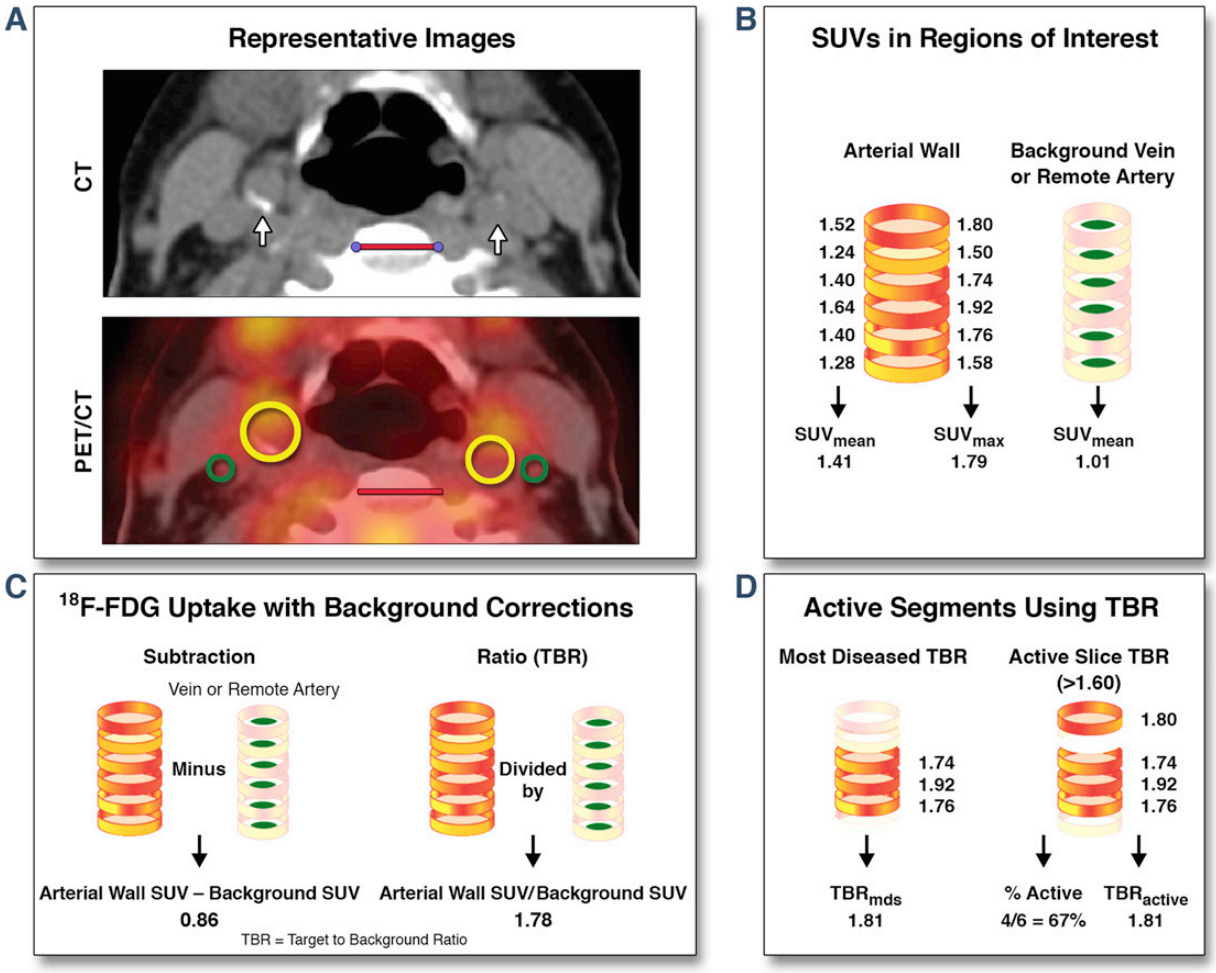

Figure 12: Arterial PET/CT images and analysis methods.
(A) Representative CT and ^{18}F-FDG PET/CT images of the carotid arteries (white arrow, yellow ROIs) and jugular veins (green ROIs) in a patient with cardiovascular disease. Red scale bars indicate 2 cm. Schematics showing (B) standardized uptake values (SUVs) in the entire artery and the background, (C) background corrections, and (D) active segment analysis with corresponding imaging parameters. MDS = most diseased segment; ROI = regions of interest; SUV_{max} = maximum standardized uptake value; SUV_{mean} = mean standardized uptake value; TBR = target to background ratio.
Figure is reprinted from van der Valk et al. (van der Valk, 2016).

3. THESIS AIMS

The aim of this thesis was to explore the value and optimal method of ^{18}F-FDG PET measurements for the detection of inflammation and instability in atherosclerotic plaques causing severe stenosis in the carotid artery.
Secondary, to expand biological knowledge regarding inflammation in atherosclerosis.

The following specific aims were addressed:

1. To evaluate the different methods for quantification of uptake of ^{18}F-FDG in atherosclerotic carotid plaques.
2. To develop a quantification method with high accuracy and applicability in clinical practice and for multicentre studies.
3. To explore if ^{18}F-FDG-PET can discriminate between patients with recent symptoms and those with more distant or without symptoms.
4. To explore the inter-reader reproducibility of the different quantification methods, and thereby their robustness in a clinical setting.

4. MATERIAL AND METHODS

An overview of the material and methods used in the three papers included in this thesis is presented in **Figure 13.** In paper I, patients operated for high-grade carotid artery stenosis were preoperatively examined with ultrasound and ^{18}F-FDG PET. Histological analyses of inflammation in the resected plaques were compared with the presence of symptoms due to the stenosis, plaque characteristics on ultrasound and uptake of ^{18}F-FDG. In papers II and III, patients not operated were also included. In paper II different approaches for quantification of the uptake of ^{18}F-FDG in the plaques were compared and correlated to inflammation on histology. Paper III assessed inter-reader performance for the different quantification methods that were explored in Paper II.

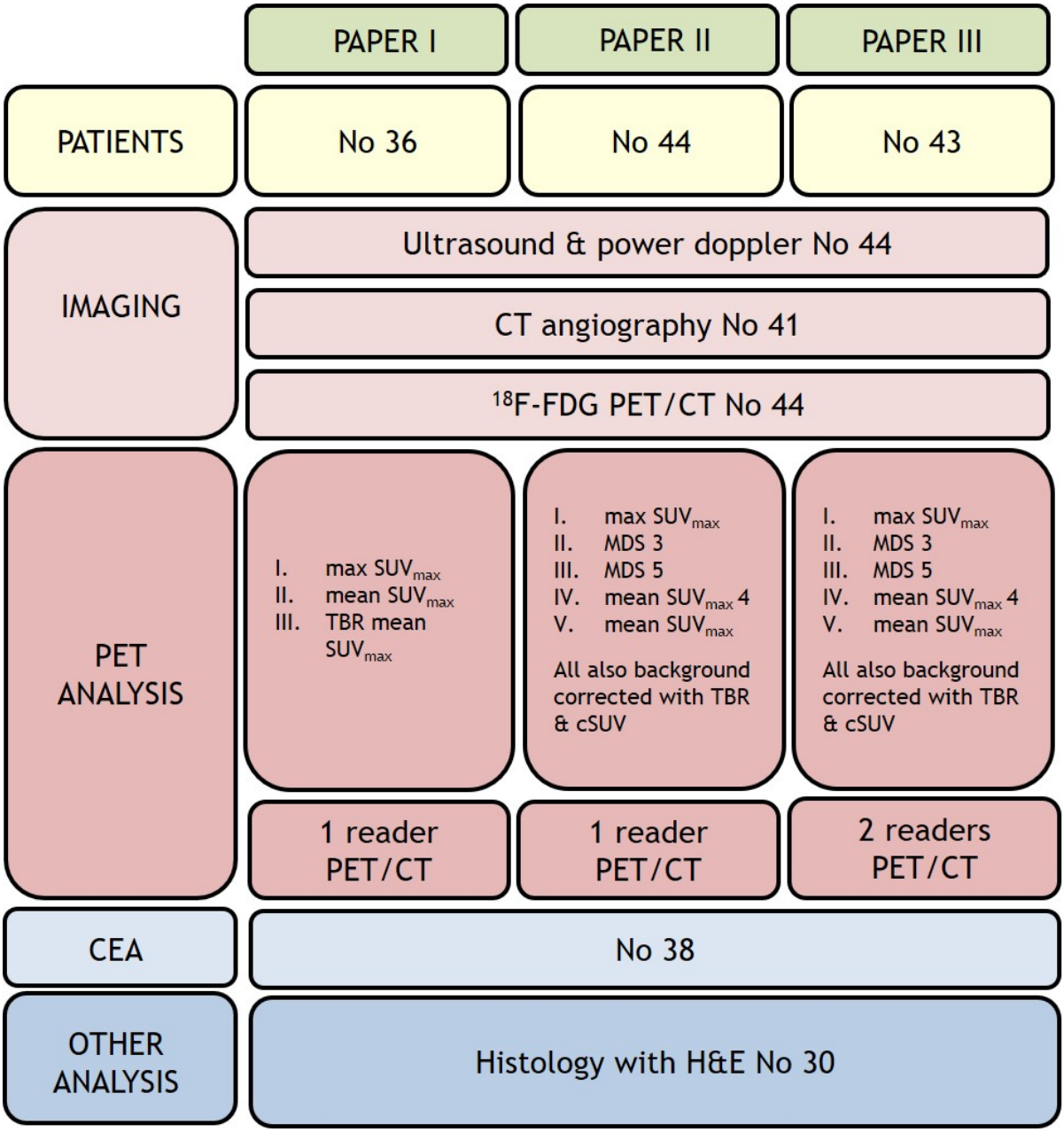

Figure 13: Overview of papers.

4.1 STUDY POPULATION

The patients included in this thesis are a subpopulation of 'The Unstable Carotid Artery Plaque Study' headed by the Department of Neurology, Rikshospitalet, Oslo University Hospital. Both symptomatic and asymptomatic patients referred to surgical treatment for severe atherosclerotic carotid stenosis (≥70 %) were included. Plaques were defined as symptomatic if the patient had experienced an ipsilateral minor stroke, TIA or amaurosis fugax (transient visual loss) within the past 30 days. Exclusion criteria were carotid occlusion, prior interventions in the carotid artery (CEA or CAS), prior radiation therapy to the neck, vasculitis and treatment with immunomodulating drugs or oncological disease.

Included patients underwent a clinical examination, registration of cardiovascular risk factors (hypercholesterolemia, hypertension, coronary artery disease, diabetes, smoking history and weight) and venous blood samples were collected. Duplex ultrasound was performed to grade the stenosis and visually classify plaque echogenicity. The patients were referred to CEA due to recent symptoms, or as a prophylactic treatment before heart surgery. Because of the short time window between symptoms and surgery (optimally two weeks) we had reserved timeslots for PET which allowed the examination of patients at short notice.

CEA was performed in 38 of the 44 included patients. Plaques for histological analyses were collected from 30. The rest of the operated plaques were not delivered for histology after CEA due to practical reasons and were lost from the histology analysis. The patients included in paper I were those who had CEA, but two patients were wrongly coded as non-surgical in the project database and not included. (However, the relationship between symptoms and ^{18}F-FDG uptake did not change when we retrospectively included these two in the analysis). For one patient an incorrect SUV calculation had been done due to incorrect registration of body height, which significantly influences the uptake value since we use a SUV related to lean body mass. This dataset was removed from the analyses in paper III.

4.2 IMAGING AND HISTOLOGY

4.2.1 PET protocol

After a minimum of six hours fasting the patients were injected with 5 MBq/kg ^{18}F-FDG and blood glucose, weight and height were recorded. After approximately 90 minutes a two-bed position PET/CT from the base of the skull to the aortic arch was performed with 15 minutes per bed position using a hybrid PET/CT scanner (Siemens Biograph 64, Siemens Medical Systems, Erlangen, Germany). The PET images were acquired with a 256 x 256 matrix and the images were reconstructed to two-millimetre-thick slices, with four iterations/eight subsets OSEM algorithm and Gaussian post-reconstruction filter with 3.5 mm FWHM.

All patients were informed face to face or on the telephone on how to prepare for the PET examination. All known diabetics were instructed on how to prepare for the PET study regarding fasting and timing of medication. Despite this, the mean of the blood glucose levels measured at time of injection for the patients presented in paper II was 6.8 mmol/ L (SD 2.2, range 4.9–14.9). Ten patients had blood glucose >7.0 mmol/L, four of them >11 mmol/L (**Table 1**). We did not exclude any patients from our study due to high blood glucose.

4.2.2 CT protocol

A CT without CM for attenuation correction was performed in all patients. The scanner settings varied from 100–120 kilovoltage (kV) and 15–250 milliampere second (mAs). CT with *i.v*. administration of iodinated CM was acquired immediately after the PET examination when the patient was still lying on the scanner table (scanner settings varied between 100–120 kV and 120–250 mAs). A minimum of 40 mL Iomeron (iodine concentration 350 mg/mL; Bracco Imaging S.P.A, Milan, Italy) or Visipaque (iodine concentration 320 mg/mL); GE Healthcare, Chicago, USA) was administered to ensure contrast filling of the carotid arteries. For 24 patients CTA was performed at other radiologic departments. We did not want to replicate a recent CTA to comply with the radiation protection principle ALARA (as low as reasonably achievable) and to minimize possible kidney stress from iodinated CM. For three patients no CTA was available when the PET images were analysed, one patient

could not undergo CTA due to high creatinine value, one had an external MRA and for one the images were not successfully imported from referring hospital.

Table 1: Blood glucose level per patient (n = 44)

Blood glucose (mmol/L)	Number	Cumulative Percent
4.9	1	2.3
5.0	2	6.8
5.1	1	9.1
5.3	3	15.9
5.4	1	18.2
5.5	1	20.5
5.6	4	29.5
5.7	5	40.9
5.8	2	45.5
5.9	1	47.7
6.1	3	54.5
6.2	3	61.4
6.4	2	65.9
6.5	2	70.5
6.6	1	72.7
6.9	2	77.3
7.1	1	79.5
7.2	2	84.1
8.0	1	86.4
8.8	1	88.6
10.0	1	90.9
11.6	1	93.2
11.8	1	95.5
13.2	1	97.7
14.9	1	100.0

4.2.3 ^{18}F-FDG uptake quantification

The Hybrid Viewer 2.0 software (Hermes Medical Solutions AB, Stockholm, Sweden) was used for image fusion and ^{18}F-FDG uptake quantification. CTA findings were used to guide drawing of the ROIs on the fused slices (PET and non-contrast CT). A plaque was defined as vessel wall thickening and a lumen contrast-filling defect on CTA. For patients without an available CTA, the plaque was defined as vessel wall with calcification and fat deposits at the level of the carotid bifurcation. ROIs were drawn around the entire vessel wall and lumen on all plaque-containing axial PET slices. ROIs were carefully placed to exclude the influence from ^{18}F-FDG uptake in structures close to the plaque (e.g. lymph nodes, paravertebral muscles or salivary glands). Blood background activity was obtained from four ROIs placed in the lumen of the jugular vein away from other structures with ^{18}F-FDG uptake but in the same cranio-caudal level as the plaque. The number of plaque-containing slices and plaque localization in relation to the carotid bifurcation were recorded. The most cranial slice of the common carotid artery before the division was defined as the bifurcation. The pixel values in the PET images were converted into SUV normalized to lean body mass.

For all plaque ROIs, SUV_{max} was obtained and the ^{18}F-FDG uptake was quantified using the following approaches:

1. Max SUV_{max} = the single highest SUV
2. Mean SUV_{max} = the mean of all plaque SUV_{max}
3. Most Diseased Segment (MDS)3 = the mean SUV_{max} of the three contiguous slices centred on the slice with the highest SUV_{max}
4. MDS5 = the mean SUV_{max} of the five contiguous slices centred on the slice with the highest SUV_{max}
5. Mean SUV_{max}4 = the mean SUV_{max} of the four slices with highest SUV_{max}

Blood background ROIs were obtained from four venous regions, the blood background activity was expressed as the mean of the SUV_{mean} from these ROIs. Blood background corrected values for all SUV measurements were calculated by division and subtraction:

- Target-to-background ratio (TBR): SUV divided by the blood background activity

- Blood pool corrected SUV (cSUV): subtraction of the blood background activity from SUV.

A second independent experienced nuclear medicine physician drew ROIs on the 43 patients included in Paper III to assess inter-observer variability of the different quantification methods.

4.2.4 Duplex ultrasound

The plaque echogenicity was visually classified into four categories on high-resolution B-mode grey-scale pictures:

- Echolucent (vessel lumen)
- Predominantly echolucent, >50 % of plaque area is echolucent
- Predominantly echogenic, >50% of plaque area is echogenic
- Echogenic (as the bright echo zone produced by the media-adventitia interface).

The plaque was classified as echolucent or echogenic if >80% was homogenously low or high in echolucency, respectively.

The degree of stenosis was decided by adding a Doppler examination of the stenosis' effect on blood velocities (Grant, 2003).

4.2.5 Histological analysis

Immediately after removal at CEA, the plaques were fixed in 4% formaldehyde, decalcified in ethylenediaminetetraacetic acid and cut into 2–3 mm slices. After dehydration, the slices were embedded in paraffin and a 5 µm histological section from each slice was cut and stained with hematoxylin and eosin. For the quantification of plaque inflammation, the sections were evaluated with 120x magnification. For every field of view from the section, the total area was measured in square millimetres. The inflammatory area was calculated after the two co-readers in consensus had estimated a percentage of the field of view occupied by inflammatory cells (macrophages and leucocytes) by 'eye-balling'. The amount of inflammation per plaque was defined as the sum of all calculated areas with inflammatory cells divided by the total area of all the sections.

4.3 STATISTICAL METHODS

All the statistical analyses were conducted using the IBM Statistical Package for the Social Sciences (SPSS) version 18.0, 21.0 and 25 (IBM Corp., Armonk, USA).

Papers I and II: Groups of unpaired data were compared using Student's *t* test for normally distributed variables or Mann-Whitney U test for non-normal distributions. The Chi-square test was used for analysing contingency data. Coefficients of correlation were calculated by the Pearson correlation for normally distributed variables and Spearman correlation for non-normal distributions.

Paper III: Groups of paired data were compared using the Wilcoxon signed rank test for non-normally distributed variables. Inter-reader agreement was calculated using intraclass correlation coefficients (ICC's; model two-way random, type absolute agreement).

All statistical results were considered significant when $p < 0.05$.

4.4 APPROVALS

The study was approved by the Regional Committee for Medical and Health Research Ethics South-East A in Norway, REC ID:S-09233a THE UNSTABLE PLAQUE. All patients gave informed written consent prior to study participation. This study received funding from the South-Eastern Norway Regional Health Authority, grant number: 2009006.

5. SUMMARY OF THE PAPERS

PAPER I: Carotid plaque inflammation assessed with ^{18}F-FDG PET/CT is higher in symptomatic compared with asymptomatic patients.

Clinical observations have shown that the risk of a new stroke after a symptomatic event due to carotid stenosis is highest shortly after the first event, and that preventive treatment must be initiated quickly. Histological analyses of removed plaques have confirmed that the inflammatory characteristics are most prominent close to an event. ^{18}F-FDG PET studies of carotid artery plaques have not been uniform with respect to time since symptoms and time to endarterectomy and histology.

In paper I we wanted to investigate the correlation, within a short time-frame, between ^{18}F-FDG uptake, clinical symptoms, and both histological and ultrasound markers for inflammation.

The quantification methods used for ^{18}F-FDG uptake were max SUV_{max}, mean SUV_{max} and TBR mean SUV_{max}. We found that all three quantification methods correlated significantly with inflammation assessed at histology. Furthermore, max SUV_{max} and mean SUV_{max} showed a significant difference between symptomatic and asymptomatic patients. The relationship between ultrasound findings of instability and ^{18}F-FDG PET was confirmed as the plaque mean SUV_{max} was significantly higher in echolucent compared to echogenic plaques.

The impact of paper I is that we have proven a correlation between ^{18}F-FDG uptake, clinical symptoms, and histological and ultrasound markers for plaque instability. This increases the evidence that ^{18}F-FDG PET can be used as a marker for inflammation and clinical instability of large carotid artery plaques.

PAPER II: ^{18}F-FDG PET/CT for the quantification of inflammation in large carotid artery plaques

The procedure and quantification methods for atherosclerosis imaging with ^{18}F-FDG PET has not been standardized. Patient populations and the reference standards have been highly variable. In paper II we explored five of the most common uptake metrics used in vascular ^{18}F-FDG PET studies (max SUV_{max}, mean SUV_{max}, MDS3, MDS5 and mean SUV_{max}4) together with two different methods for background

correction, i.e. by division (TBR) and by subtraction (cSUV). Amount of inflammation assessed on histology was used as reference standard.

We found a moderate correlation between all uptake quantification measures and inflammation on histology. We did not find a superiority of measures with background correction. The other important finding was that there was a high correlation between the different uptake methods independent of number of plaque ROIs/slices included in the assessment. This indicates that the inflammation as measured by ^{18}F-FDG PET is uniform throughout the plaque and that max SUV_{max} might have value in the characterization of carotid plaques.

<u>PAPER III:</u> Inter-reader agreement of ^{18}F-FDG PET/CT for the quantification of carotid artery plaque inflammation.

The value of a diagnostic method in clinical use is dependent on its feasibility and that readers in different centres will obtain the same results. In paper III we wanted to assess the inter-reader variability of the most commonly used quantification methods for ^{18}F-FDG uptake in atherosclerosis.

How to define the plaque or vessel segment of interest was also of great interest as several ways have been described in the literature. To the best of our knowledge, there has been no specific inter-reader analysis of these definitions.

Two experienced nuclear medicine physicians (reader 1 and reader 2) individually performed the delineations of plaques and calculated the corresponding uptake measures. Our results showed that the two readers included a significantly different number of slices in their plaque regions. However, the median values and ranges were very similar. Reader 1 identified a median of 9 slices (range 3-18) and reader 2 a median of 10 slices (range 4-23). The uncorrected uptake values had the highest ICC (0.97-0.98), followed by values with background corrected by subtraction (0.89-0.94) and finally, values with background corrected by division (0.74-0.79). These latter two results are closely linked to the low ICC for the measurement of the background region between the two readers (0.77) with the division used in TBR causing a relatively larger spread of the results than the subtraction used in cSUV.

Our main conclusion from this paper was that the two readers, despite including different number of slices, found the same uptake values when using the uncorrected uptake values. A more surprising result was that the highest uptake value in the plaque (max SUV_{max}) had as high ICC as mean SUV_{max}. Max SUV_{max} is an easier

parameter to obtain because the reader can search for the highest uptake in the plaque area without delineating the ROIs slice by slice.

Impact of papers II and III:

Paper II studied the different quantitative PET parameters and paper III the inter-reader agreement of the different methods suggested in the literature. These papers have highlighted well-known shortcomings and possibilities regarding the selection of uptake metrics and their reproducibility. This might counteract the delay of the use of this method in clinical practice. The impact of our findings in these papers is that for the quantification of inflammatory activity in carotid plaques causing severe stenosis, uptake parameters without background correction show no inferiority. The results also suggest that uptake parameters without background correction are easier to reproduce between readers.

6. METHODOLOGICAL CONSIDERATIONS AND DISCUSSION

6.1 ^{18}F-FDG UPTAKE VERSUS CLINICAL SYMPTOMS

Our study shows a significantly higher uptake of ^{18}F-FDG in carotid plaques that have caused symptoms within the last month compared to those with earlier or without symptoms (median SUV_{max} 1.75 (range 1.26–2.04) in symptomatic versus in asymptomatic patients 1.43 (1.15–2.28). Our findings are in agreement with similar studies (Chowdhury, 2018; Chaker, 2019), but due to the numerically small difference in SUV and the high degree of overlap between the two groups the method has limited value in clinical practice.

6.1.1 Are asymptomatic stenoses really asymptomatic?

All included patients had severe atherosclerosis in their carotid artery, which caused a stenosis ≥70%. Although a carotid stenosis is asymptomatic at inclusion, it has been estimated that about 11% of strokes are due to thromboembolism from a previously asymptomatic stenosis >50% (Naylor, 2015). The implication for our study is that even though asymptomatic, it is possible that some of the plaques from these patients had a high inflammatory activity that could cause an ischemic event. The presence of unstable plaques among asymptomatic patients was investigated in a study of cerebral MES, symptoms and ^{18}F-FDG uptake findings. Sixty symptomatic and 63 asymptomatic stenoses (50–99%) in 110 patients were examined. MES were found in 25% of the symptomatic, and in 9% of the asymptomatic stenoses. TBR was higher for symptomatic versus asymptomatic (median 2.07 versus 1.78) and for MES positive versus MES negative plaques (median 2.14 versus 1.86). Furthermore, the TBRs were also significantly higher in asymptomatic MES positive compared with asymptomatic MES negative plaques (median 1.97 versus 1.76) (Muller, 2014). This suggests that asymptomatic stenosis can have a relatively high inflammatory activity as some of them produce MES which is a measure of instability and increased risk of stroke and TIA (Markus, 2010). One of the patients in our study clearly illustrates the challenge with the clinical definition of symptomatic versus asymptomatic. The patient with the highest mean SUV_{max} was not asymptomatic as initially described. MRI

showed a small silent infarct. An anamnestic report of symptoms can be insufficient for correct classification.

6.1.2 Type of symptoms

The patients in our study were classified as symptomatic irrespective of the symptoms being cerebral or retinal, stroke or TIA. Plaques causing TIAs have lower inflammation on histology in the first weeks after an event than plaques leading to strokes (Redgrave, 2006). Howard *et al.* found that patients with previous ocular ischemic events had fever plaque characteristics of vulnerability on histology than those with cerebral events. Patients with cerebral events had greater macrophage staining, and lymphocyte infiltration was significantly associated with cerebral events (Howard, 2013). In agreement with this, pooled analysis of the indications for CEA in symptomatic patients showed that the benefit of CEA tended to be greatest in patients with stroke, and progressively declined in individuals with cerebral TIA and retinal events (Rothwell, 2004). Our inclusion of all types of symptomatic events in one group in paper I may be part of the explanation for the wide range of ^{18}F-FDG uptake values. However, our study was not planned for a subdivision of the symptomatic group, and the subgrouping would have given very few patients in each group.

6.1.3 Time from symptoms

Clinical and histological studies have demonstrated that the risk of a thromboembolic event caused by an atherosclerotic plaque in the carotid artery is not static. The plaque is 'dangerous' or unstable in a certain period (Rothwell, 2004; Redgrave, 2006). This fact has had great implications on the treatment guidelines. For preventive treatments after the first cerebral ischemic event, the period for those who are candidates for carotid revascularization (CEA or CAS) is now set to two weeks. After two weeks, the positive effect of intervention is lower, and the complication rate unchanged. Surgery may therefore not be the most appropriate treatment after two weeks (Naylor, 2018).

A study of 526 excised plaques where different inflammatory characteristics were compared with type and timing of symptoms showed that the inflammation was at its highest at the time of the event and thereafter decreased. For stroke plaques the

proportion of plaques with marked overall inflammation or marked macrophage infiltration had the greatest decrease in the first two to three months after the event. This study also found that the macrophage infiltration (and overall inflammation) was more stable during the period after a TIA than after a stroke. TIA plaques may therefore preserve plaque inflammation for a longer period compared to stroke plaques. Moreover, the prevalence of features of instability in patients with stroke operated >180 days after the event were similar to those that underwent surgery for asymptomatic stenosis (Redgrave, 2006).

There has not been a coherent definition of what is considered a symptomatic plaque regarding time between last event and the PET study. Some studies do not report or define a time limit (Kwee, 2011; Chowdhury, 2018), others define the plaque symptomatic if the event was within one (Muller, 2014) or three months (Moustafa, 2010). We chose a cut-off of 30 days. It is likely that the choice of time window has had impact on the inflammatory activity detected by ^{18}F-FDG PET. If the time from event had been longer, the maximum inflammatory activity could have been missed, at least in patients with stroke. In a PET imaging perspective, it is unlikely that there is a clear cut-off point in days between high and low uptake in the plaques reflecting inflammatory status. A gradual increase to maximum and then a gradual decrease to a more stable phase seems more likely and this is in accordance with histology studies. However, since the period for endovascular treatment is so short, there is a large interest from the clinical community to explore if this short time window of instability can be confirmed/supported by imaging. Our understanding of the dynamics in the inflammatory process is essential when trying to find imaging markers for clinical important atherosclerosis.

In our study we did not find any difference between the amount of inflammation on histology in symptomatic versus asymptomatic patients. This can be explained by the factors addressed above including short time frame for the symptomatic group, heterogeneous symptomatic group with inherently different levels of inflammation and limited sample size. The different levels of inflammation that can be expected in symptomatic plaques is supported by Marnane *et al.* They studied plaques from 44 patients with symptomatic (within 28 days) carotid stenosis ≥50% and the risk of stroke recurrence (Marnane, 2014). They found that 27.3% of the cohort had stroke

recurrence before CEA and that 91.7% of those plaques had extensive macrophage infiltration compared to only 37.5% of those without recurrence. In those with stroke recurrence the index event was stroke in 25% (3/12), TIA in 41.7% (5/12), and retinal artery embolism in 33.3% (4/12).

6.2 ^{18}F-FDG UPTAKE AND HISTOLOGY

The strength of our study was the close timing between ^{18}F-FDG PET examination and CEA. This is essential if we want the inflammatory/metabolic status to be comparable between our imaging studies and histology (Redgrave, 2006). The mean time between PET/CT and endarterectomy for the 30 plaques that were available for histological assessment was 2.7 days, and only 3 patients were operated ≥8 days after the ^{18}F-FDG PET scan. Our method for histological quantification of inflammation was a manual delineation of areas with macrophages and leukocytes. The area containing inflammatory cells was divided by the total plaque area evaluated. The quantification was done by consensus by an experienced pathologist and a research physician. They re-examined 11 slices from three plaques more than two months apart and found high agreement (Kappa = 0.73) with the area of inflammatory cells being within the same 5% category at both assessments for eight of 11 slices.

In other ^{18}F-FDG PET studies of carotid plaques the histological quantification of inflammatory activity have focused on CD68 as a macrophage marker, either by counting the macrophages (with computer aid) after labelling them with CD68 antibodies (Tawakol, 2006), or polymerase chain reaction (PCR) analysis of CD68 gene up-regulation (Graebe, 2010b).

Even though macrophages might be the most prominent inflammatory cells in the unstable plaques, histological studies have linked other leukocytes, in particular T lymphocytes, to the destabilization process together with the macrophages (Jander, 1998). Histological analyses of removed plaques from 37 (21 classified as symptomatic, symptoms less than 121 days before inclusion) patients with ICA

stenosis ≥70% showed larger percentage of macrophage rich areas and number of T-cells in symptomatic than asymptomatic patients. The amount of macrophages and T-cells covaried, and they were mainly located in the fibrous cap directly overlaying the atheromatous core (Jander, 1998). The uptake of ^{18}F-FDG is not restricted to macrophages, but a wide range of inflammatory cells show uptake (Jamar, 2013).

In our study, we compared ^{18}F-FDG uptake with the concentration of inflammatory cells on histology. Due to manual reading, we had the opportunity to include lymphocytes. We believe that including lymphocytes made the comparison between inflammatory cell concentration and uptake of ^{18}F-FDG more correct. **Figure 14** illustrates how macrophages and lymphocytes coexist in the plaques.

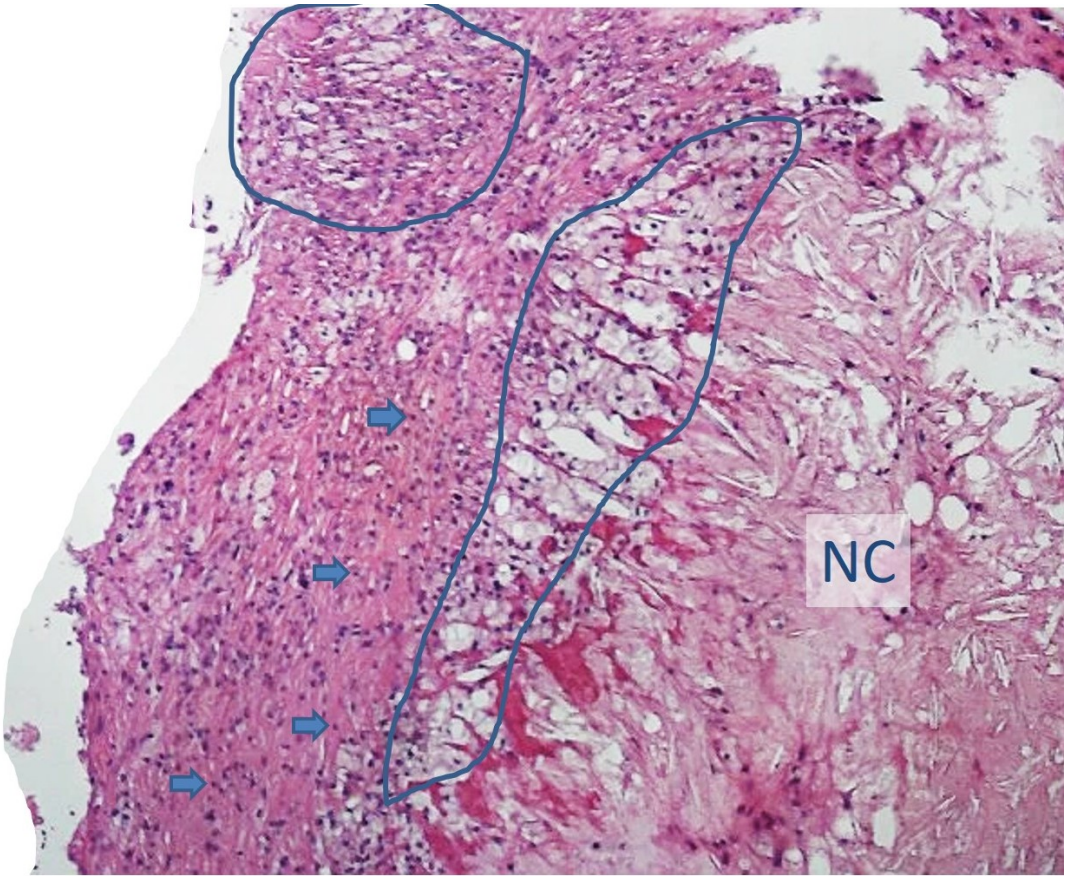

Figure 14: Macrophages and lymphocytes co-exist in inflammatory areas of the plaque. Leukocytes surrounding a necrotic core (NC). Large cells with white content (fat) are macrophages, areas are delineated with blue. Lymphocytes have smaller nuclei that are not surrounded by light halo (blue arrows).
Photo courtesy of Helge Scott, Oslo University Hospital.

The quantification of inflammatory activity is problematic because the inflammatory cells partly are grouped and concentrated, and partly scattered and intermixed with other cells within the plaques. The distribution and small size of foci is demonstrated previously in **Figures 3 and 4**. To overcome the issues concerning distribution and size, we chose to measure all areas in the plaque in square mm, thereafter, the two co-readers decided a percentage of each area containing leukocytes by 'eyeballing' (both concentrated and scattered). Finally, the percentage of the field areas in square mm were summed and divided by the whole plaque area to make the final inflammatory area per plaque.

The percentage inflammatory area per plaque versus uptake of ^{18}F-FDG correlated, with correlation coefficients between 0.44 and 0.59. This comparison of carotid plaque imaging *in vivo* with histology of excised specimen might be hampered by fragmentation of the plaque during surgery and that the removed plaque was from a shorter plaque segment than what was measured with PET. It is also a potential problem that the inflammatory content is measured only every 2-3 mm on histology, while ^{18}F-FDG PET uptake is measured from the whole volume.

6.3 ^{18}F-FDG UPTAKE AND ULTRASOUND ECHOGENICITY

We found a higher ^{18}F-FDG uptake in the echolucent plaques compared to the echogenic plaques, i.e. the two most extreme categories on a 4-point scale. Despite the uptake values were significantly higher in the echolucent plaques (category 1), the range of values was very wide with a high variation. On the contrary, the echogenic plaques (category 4) only had lower uptake values. Our method of quantifying the amount of fat versus amount of calcification by a visual score into four groups is a qualitative method. However, our results are in agreement with results from a quantitative GSM analysis of echolucency in plaques, presenting a negative correlation between plaque GSM and ^{18}F-FDG uptake (Graebe, 2010b). The echogenic plaques (high GSM) had low ^{18}F-FDG uptake, but the plaques with low GSM had a wide range of uptake values. This finding was also supported by CD68 expression that correlated with ^{18}F-FDG uptake but not with GSM (Graebe, 2010b).

Therefore, echogenicity on ultrasound can be used to rule out instability in the echo-rich plaques, but it is less accurate in finding the most unstable plaques in the echolucent category.

6.4 PET PROTOCOL

6.4.1 Time between ^{18}F-FDG injection and imaging

From the early days of vascular ^{18}F-FDG PET imaging there has been a concern about the methods ability to visualize and quantify the vessel wall uptake in the presence of a relatively high activity in the blood background. Rudd *et al.* addresses this in the first paper to present ^{18}F-FDG uptake in symptomatic carotid stenosis (Rudd, 2002). They concluded that imaging 190 min after ^{18}F-FDG injection yielded optimal contrast between ^{18}F-FDG uptake in the plaque and the blood background. However, the advantage of late imaging has been questioned because too much delay between injection and imaging raises concern regarding reduced count statistics in the images, a prolonged circulation time can be stressing for the patients and may also cause logistical problems. Finally, several studies have demonstrated inflammation in atherosclerosis on clinical oncological scans imaged after 60 min.

6.4.1.1 Effect on carotid plaque uptake

Graebe *et al.* scanned 11 symptomatic (within three months) patients with carotid artery stenosis above 50% after 60 and 180 min circulation time (Graebe, 2010a). Contralateral plaques with stenosis above 50% were also included in the study (total 19). They found that the SUV_{max} preserved the inter-individual relative uptake in plaques over time, even though the absolute values changed. Plaques with high uptake tended to further increase the uptake at the later scan, whereas low uptake plaques tended to be stable with time or slightly decrease their uptake. There was no significant difference in mean SUV_{max} between the two imaging time points. In contrast, for TBR the inter-individual relationship between plaques was not constant, and there was a significant difference in the group means between the two time points. Oh *et al.* imaged patients with recent (<six months) symptomatic plaques (stenosis ≥30%) in the carotid arteries either at 120 min (n=5) or 180 min (n=7). They

used data from 14 oncologic patients imaged after 60 min as control group for blood pool activity (Oh, 2010). Blood glucose was below 7.2 mmol/L and the carotid artery (from arcus aortae to ICA, 2 cm above the bifurcation) was imaged. They found that mean SUV_{max} and maximal TBR (carotid mean SUV_{max} / jugular vein mean SUV_{mean}) both increased from 120 to 180 min, but increase in mean SUV_{max} was not statistically significant. Moreover, a study looking at the areas with the highest uptake of ^{18}F-FDG in 17 patients with atherosclerotic aortic aneurism (Menezes, 2009) at four time points found no significant difference in SUV_{max} measured at 60 and 180 min post injection. These studies are small, but unique because they examine patients with localized plaques in the carotid artery or localized atherosclerosis in the aorta. They indicate that imaging between 60 and 180 minutes after injection will yield similar uptake values in plaques.

6.4.1.2 Effect on vessel wall uptake in generalized atherosclerosis

Bucerius *et al.* examined 195 patients with a diagnosis of CVD or multiple risk factors for CVD. They found no significant difference between carotid mean SUV_{max} on images acquired from 97 min to more than 178 min post injection. In contrast, there was a significantly higher aortic mean SUV_{max} for the earliest circulation time tertile (≥78 – ≤111 min) compared to the second tertile (>111–<145 min) (Bucerius, 2014).

6.4.1.3 Effect on vessel wall uptake in oncologic studies

Blomberg *et al.* scanned 15 patients (with suspected lung cancer) at 60, 120 and 180 min after injection of ^{18}F-FDG. Mean SUV_{max} was calculated for the entire common carotid artery and it decreased from 1.90 at 60 min to 1.74 at 120 min, and 1.73 at 180 min (Blomberg, 2013).

6.4.1.4 Effect on blood background

The literature is uniform on documenting that the blood pool activity of ^{18}F-FDG decreases with time after injection (Graebe, 2010a; Oh, 2010; Blomberg, 2013; Bucerius, 2014).

In summary, there is no clear evidence that uptake in large carotid plaques change significantly with time, while the blood background decreases. This means that uptake values without background correction are relative stable, whereas uptake

parameters with background correction will vary with time after injection of ^{18}F-FDG. This implies that our choice of 90 min between ^{18}F-FDG administration and imaging is enough for detecting the plaque uptake of ^{18}F-FDG. This also implies that uptake parameters using blood background correction are more dependent on the same time interval between injection and imaging than those without.

6.4.2 Blood glucose level

Normalized levels of blood glucose and insulin are important prerequisites for obtaining accurate measures of ^{18}F-FDG uptake (described in chapter 2.2.5.2). When including patients in this study there were no guidelines concerning blood glucose level (BGL) and ^{18}F-FDG PET imaging of inflammation. We therefore did not define a BGL limit as an exclusion criterion in our study. The position paper by EANM on ^{18}F-FDG PET imaging of atherosclerosis (Bucerius, 2016) states that the ideal BGL is less than 7.0–7.2 mmol/L. The fact that the inclusion of patients with elevated BGL possibly may have affected our results made it essential to examine this in detail.

6.4.2.1 Effect of BGL on uptake in tumours and in non-atherosclerotic inflammatory lesions

Preclinical studies have documented that elevated BGL, although, studied only for very high level (900 mg/dl), reduces the uptake of ^{18}F-FDG in malignant cells (Wahl, 1992). For inflammatory cells, the mechanism is not so clear. Zhuang *et al.* carried out an *in vitro* study where human mononuclear cells and mesothelioma cells were compared. They found that the ^{18}F-FDG uptake in mesothelioma cells significantly decreased when glucose level decreased from 50 to 200 mg/dL (2.8–11.1 mmol/L). However, the uptake in the mononuclear cells changed little between glucose concentrations of 50–250 mg/dL (2.8–13.9 mmol/L), but decreased when glucose levels exceeded 250 mg/dL (13.9 mmol/L) (Zhuang, 2001). A proposed explanatory mechanism from the authors was that inflammatory cells have the ability to mobilize stored glycogen to produce glucose during periods of low plasma glucose, in contrast to malignant cells that depend only on extracellular glucose (Zhuang, 2001). However, there are also preclinical studies that report opposite findings (Zhao, 2001; Zhao, 2002). When rats were exposed to moderate hyperglycemia (150–180 mg/dL, 8.3–11.1 mmol/L), the ^{18}F-FDG uptake in inflammatory lesions decreased

significantly, but no changes were found for the tumour cells. Insulin loading decreased the ^{18}F-FDG uptake in both tumour and inflammatory lesions (Zhao, 2001). They also found that glucose loading significantly decreased the expression level of GLUT-1 in the non-infectious inflammatory lesions and GLUT-3 in the infectious inflammatory lesions, but there were no changes in the GLUTs in the tumour cells (Zhao, 2002).

Clinical studies comparing pre-scan BGL between diagnoses have not been able to find a negative correlation between SUVs and the uptake in inflammatory and infectious lesions. In one of these studies scans of 71 patients with painful lower limb arthroplasty and 24 patients with known inflammatory/infectious condition were analysed. The average SUVs were higher for patients with glucose above than below 110 mg/dL (6.1 mmol/L). The average SUV was not higher in infectious compared to inflammatory lesions (Zhuang, 2001). A study assessing primarily pancreatic malignancies (Diederichs, 1998) found that in patients with chronic pancreatitis, the average SUV was slightly higher in hyper- than euglycemic patients (>130 mg/dL, 7.2 mmol/L). A clinical study including 123 patients with suspected infection found that hyperglycemia (BGL >180 mg/dL,10 mmol/L) did not have a significant impact on the false-negative rate at ^{18}F-FDG PET (Rabkin, 2010). Due to these findings that differed from the findings in oncology studies the EANM/SNMMI Guideline for ^{18}F-FDG Use in Inflammation and Infection (Jamar, 2013) stated: '*Although efforts should be made to decrease blood glucose to the lowest possible level, if the study is normally indicated in those with unstable ('brittle') or poorly controlled diabetes (often associated with infection), hyperglycemia should not represent an absolute contraindication for performing the study.*'

6.4.2.2 Effect of BGL on uptake in atherosclerosis

There are only a few clinical studies that have investigated the relationship between BGL and uptake of ^{18}F-FDG in atherosclerosis. A study referred to in procedural recommendations (Bucerius, 2016; Slart, 2018) included 195 patients with a diagnosis of, or multiple risk factors for CVD (Bucerius, 2014). They performed a dedicated scan of the ascending aorta and carotid arteries, and the scans were optimized for vascular imaging with at least 78 min between injection and imaging and an acquisition time of 15 min/bed position. Patients with BGL ≥11.1 mmol/L were

excluded. Uptake in the entire common carotid artery (one bed of 15.5 cm) was measured slice by slice and a mean SUV_{max} for both arteries was calculated. Analyses on BGL were done either with continuous values or divided in three groups with BGL <6.1, 6.2–6.9 or ≥7.0 mmol/L. For the carotids, both the continuous BGL and BGL ≥7.0mmol/L were weakly negatively correlated with the mean SUV_{max} and mean TBR_{max} in the multivariate regression models, however ANOVA failed to show any significant difference for either of the carotid ^{18}F-FDG uptake parameters in relation to the three groups of BGL (mean SUV_{max} 2.19; 2.24; 2.07). For the aorta, the continuous BGL as well as the BGL ≥7.0 mmol/l were negatively correlated with the mean $TBR_{max,}$ but there was no correlation between aorta mean SUV_{max} and BGL.

The implication for our study is that elevated BGL could falsify vessel wall uptake of ^{18}F-FDG. However we do not know to what extent their results are transferable to our population since their study (Bucerius, 2014) was not focusing on carotid plaques. They included a heterogeneous population and the uptake measurement from the carotids was only from the common carotid artery. A sub-group analysis of the patients with localized carotid artery disease and a further division of the BGLs between 7.0 and 11.1 mmol/L would have been of interest. To our knowledge, there are no published studies on the effect of hyperglycemia on ^{18}F-FDG uptake in localized atherosclerosis in the carotid artery.

6.4.2.3 Recent views on BGL in oncological imaging

A meta-analysis including 8380 patients from 29 studies of ^{18}F-FDG uptake in tumours and organ distribution of activity (not inflammatory indications) concluded that if the blood glucose is <200 mg/dL (11.1 mmol/L), there is no need to lower the blood glucose in tumour imaging studies, unless the liver is the target organ (Eskian, 2019). This is in accordance with the EANM Guidelines for clinical routine examinations (Boellaard, 2015).

6.4.2.4 Effect of BGL on blood background

Vascular studies with ^{18}F-FDG

Buceris *et al.* also studied blood background activity in detail (results concerning vessel wall uptake referred in the previous paragraph). They found that the continuous BGL correlated significantly with the ^{18}F-FDG activity in the blood of the superior vena cava, but not in the jugular vein. The mean SUV_{mean} from the three groups of patients with BGL <6.1 mmol/L, 6.2–6.9 mmol/L and 7.0–11.0 mmol/L was for the superior vena cava 1.21, 1.26 and 1.25, and for the jugular vein 1.12, 1.16 and 1.14 (Bucerius, 2014).

A study of noninsulin-dependent type 2 diabetes patients and vessel wall uptake found no difference in the blood background activity between the diabetic and nondiabetic groups. The mean circulation time was 136 and 138 min (Bucerius, 2012). The mean fasting BGL level was 6.8 mmol/L in the diabetic group and 44% of the patients had BGL ≥7 mmol/L (30% ≥7.8 mmol/L). In the nondiabetic group mean BGL was 5.4 mmol/L and 3% of the patients had BGL ≥7 mmol/L (0% ≥7.8 mmol/L).

Studies from oncology

A retrospective study of clinical PET examinations from 500 patients, acquired after approximately 60 min, found a very weak correlation (0.12) between BGL and mean SUV_{mean} in the mediastinal blood pool. Furthermore when the patients were paired with regard to age and gender, there was no significant difference between the group with BGL ≥7.0 mmol/L and the group with ≤6.0 mmol/L (Lindholm, 2013). A recent extensive meta-analysis focusing on tumour uptake in relation to blood glucose found a significant positive correlation between BGL and both SUV_{max} and SUV_{mean} in the blood background. Eskian *et al.* found significantly higher blood background SUV_{max} and SUV_{mean} for the hyperglycemic compared to the euglycemic groups. This did not include the mild hyperglycemic group (110–125 mg/dL, 6.1–6.9 mmol/L) that did not have a significantly higher SUV_{mean} (Eskian, 2019).

A systematic review (Sprinz, 2018) concluded that the effect of glycemia on mediastinal blood background appeared to be negligible, because only two of five studies showed a significant influence of glycemia and the impact was very small in both studies.

In summary, it is possible that inflammatory cells are less susceptible than tumour cells to elevated blood glucose. However, the findings from studies looking into this field are scarce, and the few clinical studies carried out lack confirmation of findings with e.g. tissue sample or other imaging and their relevance to inflammation in atherosclerosis is unknown. The vascular studies open the possibility that blood glucose might have a minor influence on vessel wall uptake, but these studies did not include the effect on confirmed carotid plaques. The studies on blood background are also inconclusive and there is a possibility that elevated BGL leads to a slightly increased blood background. To elaborate more on this question, we need either to scan the same patients at two time points with different BGLs or compare the imaging results with other aspects of the inflammatory activity, e.g. histology.

The EANMs Position paper on PET imaging of atherosclerosis (Bucerius, 2016) recommends a cautious approach until more data are available. The recommendations for patients that have blood glucose level above 7.0–7.2 mmol/L is to lower the patient blood glucose (Bucerius, 2016), or if not successful consider applying a correction of the vascular ^{18}F-FDG uptake as proposed in the EANM Guidelines for oncologic imaging (Boellaard, 2015). However, the latter is not sufficiently validated for studies of the vascular wall (Bucerius, 2016).

IMPLICATIONS FOR OUR STUDY

Following the findings in the above-mentioned studies, it is possible that elevated BGL have reduced the amount of ^{18}F-FDG taken up by the macrophages in our study. This could lead to a lower correlation to inflammation on histology since as many as 10 out of 44 patients had BGL >7 mmol/L (7/30 with histology). The elevated BGL could also have influenced the results by leading to a higher blood background value even though we did not find a correlation between BGL and blood background SUV_{mean}.

A relationship between BGL and background $SUV_{mean,}$ and uptake in inflammatory lesions could make the background corrected values more susceptible to errors than non-corrected values, and most pronounced for the TBRs. We partly addressed this in paper II: '*When excluding the four patients with blood glucose >11mmol/L, we actually found a slightly higher correlation to histology. We did not exclude the*

patients with elevated blood glucose from the analysis on the relationship between the individual uptake parameters' (Johnsrud, 2019).

Since the existing recommendations on BGL in ^{18}F-FDG imaging of atherosclerosis (Bucerius, 2016) were published after publication of our first paper, we have later reanalysed the data set after the exclusion of patients with BGL >7 mmol/L. This had little effect on the correlation between inflammation on histology and the ^{18}F-FDG metrics **(Table 2)** and indicates that our previously published results were minimally influenced by patients with high BGL.

Table 2: Effect of BGL on correlation between ^{18}F-FDG PET uptake values and histology

^{18}F-FDG uptake parameter	**Spearman correlation coefficient All patients n = 30**	**Spearman correlation coefficient Patients with BGL ≤7 mmol/L n = 23**	**Numeric change in correlation coefficient**
Max SUV_{max}	0.48 (0.008)	0.51 (0.013)	+0.03
Mean SUV_{max}	0.54 (0.002)	0.61 (0.002)	+0.07
MDS3	0.48 (0.007)	0.53 (0.009)	+0.05
MDS5	0.49 (0.006)	0.52 (0.010)	+0.03
Mean SUV_{max}4	0.52 (0.003)	0.57 (0.005)	+0.05
TBR max SUV_{max}	0.44 (0.016)	0.45 (0.030)	+0.01
TBR mean SUV_{max}	0.58 (0.001)	0.55 (0.007)	-0.03
TBR MDS3	0.47 (0.009)	0.48 (0.021)	+0.01
TBR MDS5	0.48 (0.008)	0.50 (0.021)	+0.02
TBR mean SUV_{max} 4	0.48 (0.007)	0.50 (0.016)	+0.02
cSUV max SUV_{max}	0.47 (0.009)	0.51 (0.013)	+0.04
cSUV mean SUV_{max}	0.59 (0.001)	0.63 (0.001)	+0.04
cSUV MDS3	0.52 (0.004)	0.55 (0.007)	+0.03
cSUV MDS5	0.52 (0.003)	0.55 (0.006)	+0.03
cSUVmean SUV_{max}4	0.54 (0.002)	0.58 (0.004)	+0.04

Data given as correlation coefficient (*p*-value).

6.4.3 Minutes per bed position

We scanned our patients with a long acquisition time of 15 min per bed position. Quantification of ^{18}F-FDG uptake in small lesions is prone to image noise. In a study of 19 carotid plaques with stenosis ≥50% increasing time per bed position from two to 15 min significantly decreased SUV_{max}, interpreted as a decrease in noise (Graebe, 2010a). There was no difference between the uptake values for 8 and 15 min per bed position. Studies quantifying atherosclerotic inflammation retrospectively in ^{18}F-FDG PET scans from patients scanned with oncologic protocols (whole body, 2–3 min per bed position) should be interpreted with the possibility of elevated noise levels in mind.

6.5 OTHER PATIENT FACTORS

High uptake of ^{18}F-FDG in neck muscles located next to the carotid arteries can lead to a spill-in partial volume effect with too high uptake values measured in the ROIs around the plaque. **Figure 15** illustrates how high uptake in the prevertebral muscles can contaminate the plaque ROI. To overcome this, we had to exclude parts of the ROI measuring plaque uptake, and this might have underestimated uptake values when delineating the plaque in some patients. We did not take any precautions on how to minimize muscular uptake in the neck muscles. Several of the patients had a long ultrasound examination of the neck arteries the day before the PET scan. This could have led to abnormal tensions and static muscle work leading to higher ^{18}F-FDG uptake the following day.

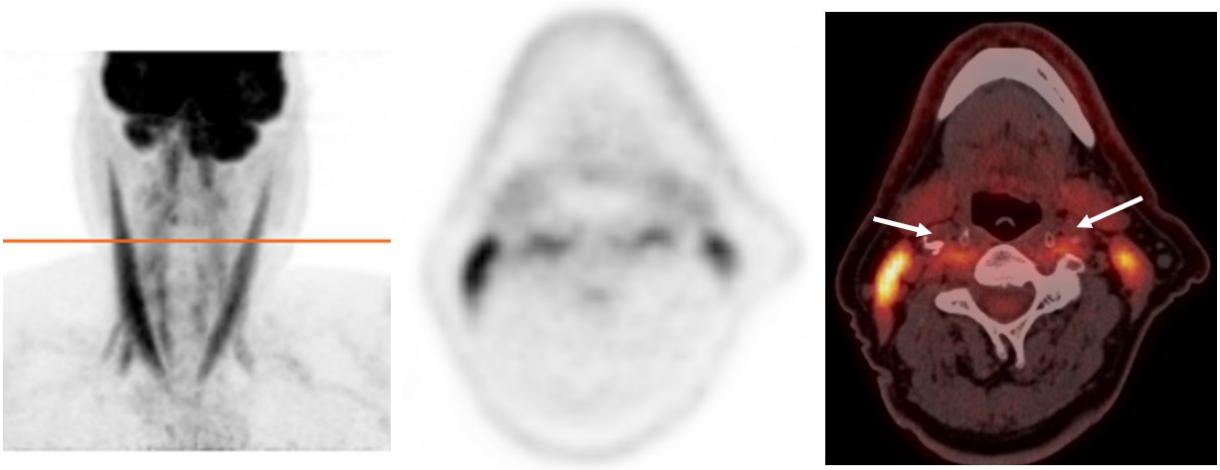

Figure 15: High uptake of ^{18}F-FDG in neck muscles close to the plaques in the carotid arteries (white arrow points at the lumen in the common carotid arteries in the image to the right).

6.6 PET AND SMALL LESIONS

Inflammation in plaques in the vessel wall does not have the same geometrical distribution of ^{18}F-FDG uptake as we are used to from oncology. The foci of inflammatory cells are smaller, they are spread out in the plaque and their volumes are not uniform in shape (**Figures 3 and 4**). From phantom studies of spheres, it is usually stated that the quantification of an uptake is accurate if the lesion is 2-3 times the scanners spatial resolution. For lesions below this size, the uptake is underestimated (Soret, 2007). Due to the inaccuracy of using standard phantom sphere models to understand the underestimation of uptake in inflammatory lesions in the vessel wall Huet *et al.* performed a simulation study. They constructed two lesions, similar to one mm thick parts of cylinders along the vessel wall; 1) 10 mm long and covering 60 degrees of the cylinder circumference, 2) 30 mm long and covering 300 degrees (Huet, 2015). For the reconstruction parameters we used in our studies, the error in measured activity was ≥80%. With optimized reconstruction parameters with more iterations, smaller voxels and PSF, the measured bias remained with an underestimation of more than 60%.

For fourteen of our patients who underwent surgery the same day as the PET scan, the plaque specimens were imaged in a microPET scanner after removal (unpublished data)**. Figures 16 and 17** show examples of plaques with different amount of uptake. This can also be an illustration of underestimation and/or the information lost due to the lower spatial resolution of the human scanner compared to the microPET scanner (Focus 120 MicroPET, Siemens Medical Systems, Erlangen, Germany).

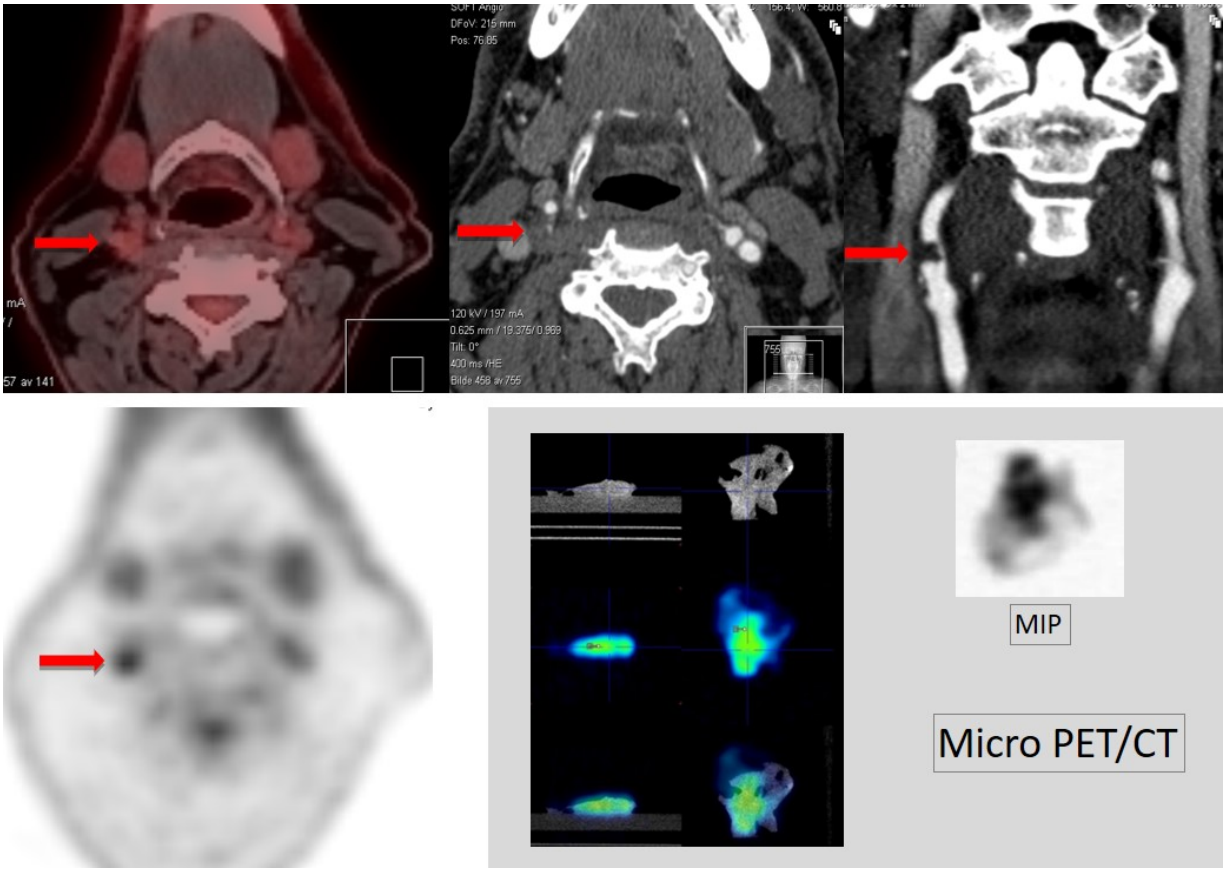

Figure 16: Patient with high uptake on clinical PET (upper panel and bottom panel left) (max SUV_{max} 2.24, mean SUV_{max} 1.97) and with microPET max SUV_{max} 35.9 (bottom panel right). The CTA shows a small homogeneous low-attenuating plaque (no calcification) with severe stenosis (upper panel middle and right). The patient had experienced symptoms two months earlier and the plaque was echolucent on ultrasound.
MicroPET/CT photo courtesy of Trine Hjørnevik, Oslo University Hospital.

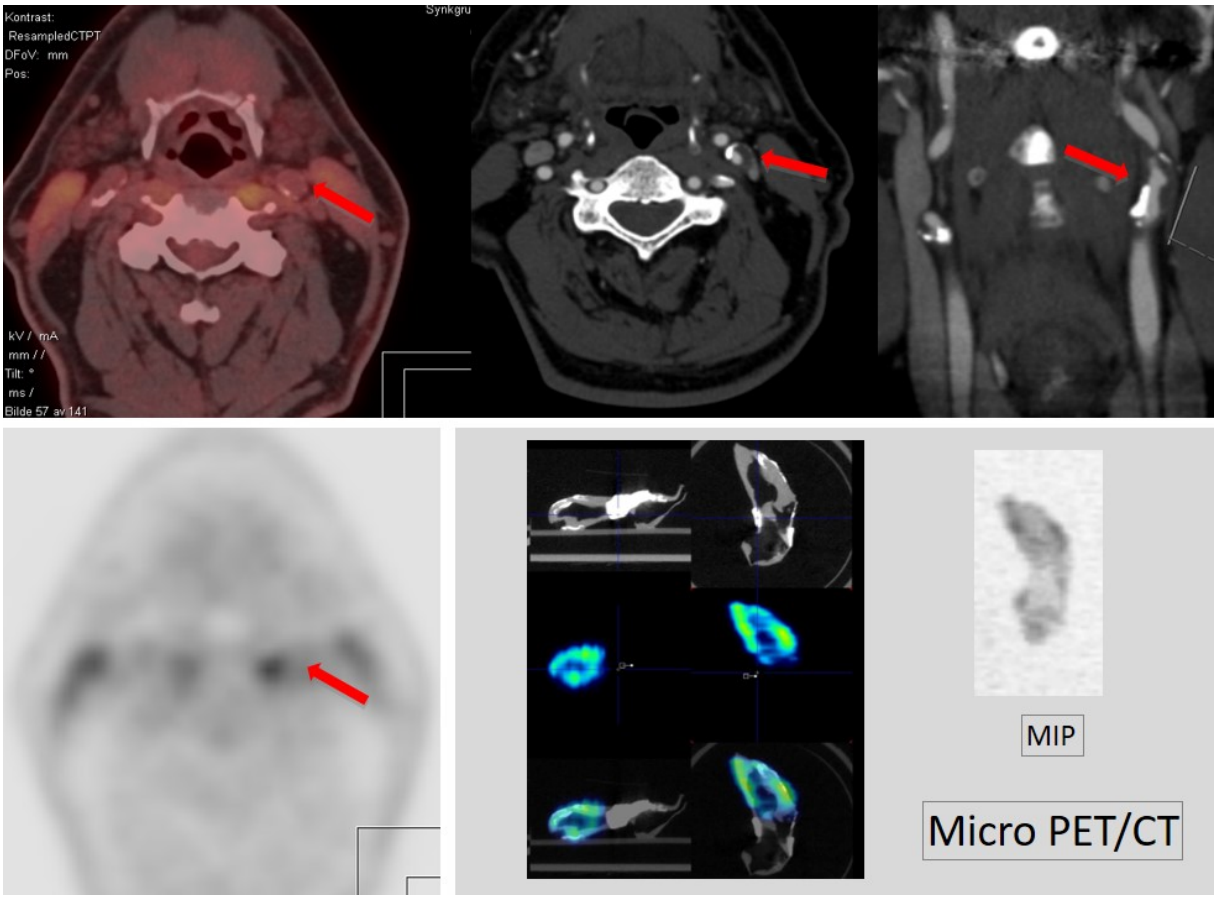

Figure 17: Patient with low/medium uptake on human PET (lower panel left) (max SUV_{max} 1.82, mean SUV_{max} 1.51) and with microPET max SUV_{max} 11.7. The CTA shows a mixed plaque containing calcifications and low-attenuating areas stretching 2.5 cm cranially with severe stenosis (upper panel middle and right). The patient had experienced symptoms nine months earlier and the plaque was echolucent on ultrasound examination.
MicroPET/CT photo courtesy of Trine Hjørnevik, Oslo University Hospital.

It is obvious that the underestimation of the real activity concentration in our study is considerable, and that this may partly explain the relatively small difference between uptake values in plaques with low and high inflammatory activity. However, even though this is an inherent limitation of all imaging modalities with limited pixel size we assume that different levels of ^{18}F-FDG uptake per cell and different concentrations of inflammatory cells will give different uptake values. To overcome the underestimation of uptake in vessel wall pathology, methods for partial volume correction of aorta wall uptake (Burg, 2013) and for aorta aneurysms (Reeps, 2013)

have been suggested. To our knowledge, no specific correction technique has so far been recommended in guidelines or used in clinical studies of carotid artery stenosis. Our uptake values were measured on images with post reconstruction filters with FWHM of 3.5 mm. A narrower FWHM might have given more accurate uptake values (**Figure 11**), but a narrower FWHM would also increase image noise. Thus, we will have a trade-off between noise and 'true' uptake values. We concluded that the noise was acceptable with a FWHM of 3.5 mm. Graebe *et al.* documented that lower FWHM lead to increased SUV_{max}, but the results were not compared to histology or symptoms. It was thereby difficult to conclude how an increase in noise affects the quantification in clinical studies (Graebe, 2010a).

6.7 PLAQUE DEFINITION/LOCALIZATION

Since the PET scan alone do not provide information on where the atherosclerosis is most severe, or where the plaque is localized, use of complimentary information from the CTA scan is important to define the areas to include in the quantitative analysis of plaque inflammation. We chose to define the plaque as all slices in relation to the stenosis where the vessel wall had pathological appearance on CTA (increased thickness and/or lumen contrast filling defect). The definition of plaque extension is not consistent in the literature and several methods are described: the whole region from 0.9 cm proximal (in CCA) to 3 cm distal to the carotid bifurcation (in ICA) (Evans, 2020), *'ROIs were delineated along the plaque'* without explaining more (Muller, 2014), plaque defined as *'luminal filling defect on contrast images'* (Graebe, 2010a) or plaque defined as 10 slices centred on the slice with maximum ICA stenosis (Marnane, 2012; Kelly, 2019). In the first and last approach, slices without plaque can be included, and in the last approach the slice with the highest SUV_{max} can be missed. In paper II we found that the slice with the highest uptake value can be in the plaque periphery, and an assumption of a symmetric extension of the plaque cranially and caudally from the maximum stenosis can therefore be an incorrect simplification. Furthermore, an autopsy study described asymmetry in plaque inflammation, macrophages and the thinnest part of the fibrous cap was predominantly located downstream from the site of maximal stenosis (Dirksen, 1998).

However, our findings of a high correlation between the plaque max SUV_{max} and the mean SUV_{max} are supported by Evans *et al.* who found diffuse uptake of ^{18}F-FDG along the length of the culprit artery (vessel segment from 0.9 cm below the bifurcation to 3 cm above in ICA) even though they used a newer scanner than ours with TOF and PSF capabilities (GE Discovery 690, GE Medical Systems Ltd, Hatfield, United Kingdom) (Evans, 2020). This implies that variations in the plaque definition do not necessarily affect the results. This can change in the future where we will see more studies using PET scanners with higher sensitivity. This might lead to detection of plaque variations in uptake values that we have missed in studies performed on older scanners.

6.8 QUANTIFICATION METHOD

A central aim of this thesis was to explore different methods for quantification of inflammation in atherosclerotic plaques. In paper I we found that both max $SUV_{max,}$ mean SUV_{max} and TBR mean SUV_{max} were significantly correlated with inflammation at histology. Moreover, max SUV_{max} and mean SUV_{max} were significantly higher in symptomatic compared to asymptomatic patients, whereas TBR was indifferent between these two groups. In papers II and III we included more parameters (max $SUV_{max,}$ mean SUV_{max}, MDS3, MDS5, mean SUV_{max} 4 highest: all with and without background correction by division and by subtraction) and more patients, without plaque histology, in the analysis. The parameters showed similar correlations to histology and they were all highly correlated. We concluded that background correction did not improve the correlation between ^{18}F-FDG uptake parameters and inflammatory status in high-grade carotid artery stenosis. In paper III we found a very high inter-reader correlation for all of the parameters, but slightly lower correlation if the parameters were background corrected by division. In conclusion, background correction is unnecessary and slightly more difficult to reproduce, the max SUV_{max} should be explored more.

Currently, the most frequently used parameter for assessment of plaque inflammation has been the mean SUV_{max} (Graebe, 2010b; Marnane, 2012). To our knowledge no

clinical studies had assessed the use of whole plaque max SUV_{max} until the recent multicentre study by Kelly *et al.* that found that the max SUV_{max} was an independent predictor of future recurrent stroke post-PET (Kelly, 2019). Max SUV_{max} is easily obtained, highly reproducible, and less influenced by partial-volume effects (Soret, 2007; Lodge, 2012) but prone to image noise (Soret, 2007). Although max SUV_{max} is a widely used uptake quantification method for oncological examinations (Boellaard, 2015) with ^{18}F-FDG PET, this is not the case for ^{18}F-FDG PET and atherosclerotic vascular inflammation. The first publication in the field highlighted the importance of achieving a favourable contrast between the uptake in the arterial vessel wall and the level of ^{18}F-FDG in arterial blood (Rudd, 2002). Since the size of and uptake in the vessel wall was relatively low compared to the larger and higher uptake in lesions seen in oncology, there was a concern that the spill-in effect from the ^{18}F-FDG blood concentration could influence on the measured uptake in the vessel wall. Delayed imaging, i.e. at least >60 min, was proposed to overcome this problem. It was easy to observe visually and quantitatively that the vessel lumen concentration of ^{18}F-FDG declined with time, while the wall uptake was preserved. To further overcome the possible spill-in effects from circulating ^{18}F-FDG the ratio between the vessel wall uptake and the intraluminal concentration as uptake parameter was proposed (Tawakol, 2006; Rudd, 2007; Rudd, 2008; Bucerius, 2016). The method of choice was to correct with blood background by division, even though some studies did not use any kind of correction for the quantification of uptake in localized plaques (Graebe, 2010b; Marnane, 2012). The logic behind this was not questioned until 2015 when Huet *et al.* (Huet, 2015) stated: '*Therefore, there is no legitimate rationale for using TBR instead of SUV. In addition, the use of TBR increases the variability of the measurements because of the biologic and measurement variability of the blood uptake, as actually underlined or suggested in a few articles. Furthermore, the variance of TBR is indeed the sum of the variance in OWA (observed wall activity) and of the variance of the estimated BA (background activity), making TBR less reproducible than SUV.'*

There is a polarized debate about which uptake parameter to use to interpret atherosclerosis imaging with ^{18}F-FDG PET. When Chen and Dilsizan were invited to comment on the methodological literature- and phantom study by Huet *et al.* (Chen, 2015; Huet, 2015) they strongly supported the problems with TBR as uptake

parameter in atherosclerosis concluding that: *'..., dividing the vascular wall SUV with the venous blood pool SUV may introduce more variability and confusion to the TBR measurement than confidence'*, and *'In the meantime, incorrect use of quantification parameters may lead to misinterpretation of study results'* (Chen, 2015)). Shortly after, Bucerius *et al.* published the Cardiovascular Committee of EANMs position paper on PET imaging of atherosclerosis (Bucerius, 2016) stating the superiority of TBR: '*TBR is robust with different scan settings (acquisition times and reconstruction filters) and tracer circulation times, while SUV might show significant differences with each of these settings…….For the quantification of FDG uptake in atherosclerotic plaques, we recommend using TBR instead of SUV as the use of a ratio between two measurements limits the effects on signal quantification of errors in patient weight and in the dose of radiotracer injected and of the imaging time-point'.*

In two recent meta-analysis of ^{18}F-FDG uptake in culprit carotid stenosis and CVD a slightly higher number of the included studies used uncorrected SUVs compared to TBRs (Chowdhury, 2018; Chaker, 2019). A multi-centre ^{18}F-FDG PET study of carotid stenosis ≥50% and risk of early recurrent stroke used three uptake parameters, max $SUV_{max,}$ MDS3 and TBR max SUV_{max}. The findings were concordant for all parameters, this further supports our findings that background correction is unnecessary in the evaluation of localized carotid stenosis (Kelly, 2019). Chaker *et al.* highlighted the lack of consensus on uptake reporting and recommend that studies report all available metrics so systematic analysis and validation can be performed (Chaker, 2019).

To be able to draw any conclusions, it would be preferable to gather and compare studies with a separation between at least two distinct patient populations studied with ^{18}F-FDG in atherosclerotic vessel wall inflammation;

1) studies on patients with diagnosed atherosclerotic carotid artery disease (often most severe in the ICA), where the ^{18}F-FDG uptake is anticipated to be correlated to symptoms, alternative imaging modalities, or to postoperative histology of the atherosclerotic plaque. In these studies, the uptake measurements are primarily performed in what is defined as the plaque/stenosis region (**Figure 18 B**).

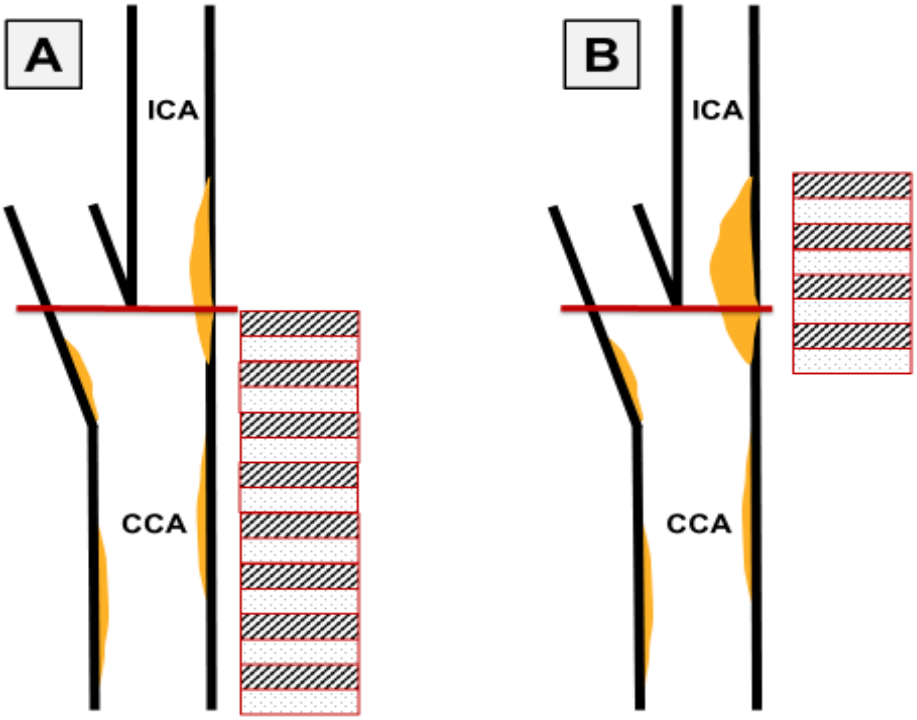

Figure 18: Vessel segments of interest used for quantification of ^{18}F-FDG uptake in the carotid artery differs between studies of general atherosclerosis (A) that mostly uses the whole common carotid artery (CCA) and localized stenosis in the bifurcation (red line) and internal carotid artery (ICA) that defines a plaque area (B).

2) Studies on patients with possible generalized vessel wall inflammation without a defined point of atherosclerotic disease in the examined vessel segments, defined as subclinical atherosclerosis. In these studies, the uptake measurements are done in whole vessel segments, e.g. the common carotid artery bilaterally (rarely including ICA) or the aorta thoracalis. In the data analysis the vessel segments are treated separately or grouped together (**Figure 18 A**). So far, methodological recommendations have not distinguished between these two very different patient populations.

Studies on patients diagnosed with localized atherosclerotic disease should have greater opportunities to define 'gold standards' for image-based quantification of ^{18}F-FDG uptake in plaques. There are direct comparable plaque evaluation methods available, e.g. histology, clinical events, MRI or ultrasound. With a mixture of these two patient groups with both different vessel segments of interest and different stages

in the atherosclerosis development, it will be challenging to decide on and optimize the most appropriate quantification method.

Generally, the TBR methodology is almost always used and supported by researchers studying general vascular inflammation. Those studying localized carotid atherosclerotic disease more often use one or both when publishing.

In conclusion, maybe the time is ripe to introduce separate methodological recommendations for imaging of ^{18}F-FDG PET in 1) localized atherosclerotic carotid artery disease, and 2) generalized vascular inflammation.

7. ETHICAL CONSIDERATIONS

A PET/CT examination involves the use of ionizing radiation from an intravenously administered positron-emitting isotope (^{18}F-FDG) and x-rays from a CT scanner. Our patients received 5 MBq/kg ^{18}F-FDG, this is an exposure burden of 7–8 millisieverts that equals the radiation burden of a CT scan of the abdomen. A CT scan without CM is a necessary part of a PET examination, in addition a CT angiography with CM necessary for plaque localization was performed in those patients in whom this was not already acquired. A CT of the neck arteries covers a small proportion of the body, and thereby has a low general radiation burden. The mean age in our patient population was 66 years. They therefore had a much lower risk to develop pathology induced by radiation compared to younger individuals. The potential of gaining new knowledge about stroke and stroke prevention justifies the very small risk of harmful effects from radiation and can be considered of minor ethical concern for this patient population.

An *i.v* injection carries a very low risk for infection. Injection of ^{18}F-FDG carries a negligible risk of a serious allergic reaction. Iodinated CM can induce kidney failure in patients with reduced kidney function and serious allergic reactions can happen, but rarely do (<1:10.000). In the present study CM was not administered to patients with reduced kidney function.

The physicians that recruited patients to our study were from the same hospital as the ones responsible for evaluating and treating the eligible patients. The patients could feel obliged to participate in research at the hospital responsible for their treatment even though it was highlighted that the participation was voluntarily.

Currently, ^{18}F-FDG PET is an expensive investigation with limited availability. All clinical projects involving PET must take this into consideration and the focus of developing a method that will become clinically cost-effective should be high. ^{18}F-FDG PET has very promising features in the characterization of carotid atherosclerotic disease, but the current availability can be too low and the cost to high to implement it for all potential patient groups. In this perspective, an important research focus of ^{18}F-FDG PET in atherosclerotic carotid disease should be to help develop more accessible and less costly diagnostic methods.

8. CONCLUSION

Our study confirms that ^{18}F-FDG PET/CT can detect inflammation and clinical vulnerability in large carotid atherosclerotic plaques.

The clinical question asked in paper I was whether ^{18}F-FDG PET can help to identify whom to treat with CEA. ^{18}F-FDG PET adds valuable information about the inflammatory status in plaques. In accordance with other studies, we found a significant, but small difference between symptomatic and asymptomatic patients. Understanding of plaque inflammation dynamics in time and its relation to different ischemic symptom categories must be included in clinical studies if ^{18}F-FDG PET is to become a useful tool in the management of patients with atherosclerotic carotid plaques.

The methodological question in paper II was if the quantification of ^{18}F-FDG uptake in atherosclerotic plaques could be done in the same way as for oncologic disease. Our findings support the use of mean SUV_{max} and max SUV_{max} as uptake parameters. We also found that blood background correction was not needed. In paper III we further supported these findings by showing that parameters without blood background correction had the highest inter-reader agreement, including max SUV_{max}.

The development of atherosclerotic carotid disease starts long before the plaque becomes unstable. ^{18}F-FDG PET has the potential to detect inflammatory activity early in the atherosclerotic process. Prospective clinical studies that measure inflammatory activity and monitor the development and progress of the atherosclerosis might give new information about risk factors in CVD. Early detection of risk factors opens the possibility for personalized preventive treatments of the atherosclerosis before the ischemic events occur.

9. FUTURE PERSPECTIVES

9.1 TECHNICAL IMPROVEMENTS IN PET QUANTIFICATION

During the past decades, PET imaging has improved substantially with respect to image quality, small lesion detectability and accuracy in quantification (van der Vos, 2017). Advances in scanner technology and image reconstruction have made this possible. The scanner used in our study was state-of-the-art when it was installed in 2006, and since then two or three new generations of scanners have been developed.

Time of flight (TOF) technology has been an important step for more accurate quantification (Walrand, 2018; Zaidi, 2018). TOF is based on a better time resolution in the detection of the annihilation photons. PET scanners with TOF are able to detect annihilation photons within an extremely short time window and they can calculate the time difference between the hits of a pair of annihilation photons within the coincidence window, termed TOFs (Karp, 2008). This possibility of measuring the time difference between the arrival of two photons at the detector and thereby the difference in flight distance makes the localization of the lesion along the LOR more precise. The result is improved image quality and consequently, more accurate quantification. The first PET scanner with TOF for commercial sale was produced by Philips in 2006 (Surti, 2007), the other vendors developed and offered their TOF scanners for sale in the following years.

Together with the TOF technology, there has also been a development of reconstruction algorithms with the same goal of better image quality, lesion detectability and more accurate quantification. The driving forces besides improved image quality has also been to lower the scan time and/or the amount of radioactivity needed for ‘sufficient’ image quality for clinical workflow. In general, the new reconstruction algorithms show higher SUVs (meaning more correct) in small lesions compared to OSEM reconstructions (van der Vos, 2017). Point spread function (PSF) is a reconstruction algorithm correcting for physical processes that degrade the resolution of PET, including detector crystal effects, positron range and annihilation

photons deviation from the anticipated 180° LOR (Munk, 2017). The quantitative performance of PSF for small lesions has not been unproblematic, and artefacts leading to overestimation of uptake values have been reported (Munk, 2017). In this phantom study of small gel spheres (diameter 3-12 mm) with ^{18}F-FDG the recovery coefficients did not fall monotonically together with sphere size but had the highest value for the spheres with diameter of 8 mm.

A method that has been shown to improve the detection of small lesions in TOF-PET systems is the reconstruction with larger matrices and thereby smaller voxels, e.g. 400 x 400 matrix giving 2 x 2 x 2 mm voxels (van der Vos, 2017). A phantom study by Koopman *et al.* found higher contrast-recovery coefficients and signal to noise ratios using small-voxel reconstructions for spheres from 4–13 mm (Koopman, 2015). The simulation study of uptake in carotid plaques by Huet *et al.* similarly found that the smallest voxel of 1 x 1 x 1 mm has the lowest degree of uptake underestimation (Huet, 2015).

The latest step in PET technology improvement is based on solid-state photodetectors, e.g. small silicon digital photomultipliers (SiPMs) replacing the conventional photomultipliers (PMTs) with digital readout. This leads to one-to-one correspondence between PMTs and detector elements in contrast to the older PMTs which were much larger than the individual detectors. SiPMs can improve the spatial resolution in PET because they can be made to couple with crystal elements smaller than 4 x 4 mm (Slomka, 2016). Based on phantom and patient studies that were recently performed on a digital PET system (van der Vos, 2017) it is expected that digital PET can provide a higher image quality, improved small lesion detection and allow for a lower radiopharmaceutical dose compared to an analogue PET system with PMTs. Together with the digital PET a maximum-a-posteriori based reconstruction has been introduced commercially, e.g. block sequential regularized expectation maximization. The aim is to give more accurate quantification at low noise levels (van der Vos, 2017). Lastly, scanners with increased axial coverage will increase photon detection sensitivity. The most extreme version developed is a whole-body scanner, meaning a two meter long scanner that simultaneously acquires annihilation photons from the whole body (Badawi, 2019).

In summary, the technical improvements hold promise for a more accurate quantification of the uptake of positron emitters, and in particular for the uptake in small lesions of interest, such as clusters of inflammatory cells in atherosclerotic plaques. This will hopefully reduce the underestimation and improve the methods ability to quantify the plaque activity. This can lead to a higher sensitivity for uptake activity alterations and maybe more distinct risk categories with less overlap than what has been achieved until now. How to optimize and standardize the new uptake and reconstruction parameters available will be an important task that should be done as fast as possible so that the results from studies can be compared. There are already many clinical studies using new equipment. If the study protocols are not harmonized, we lose both time and resources before the amount of evidence is good enough for clinical practice.

Improved quantification on one hand will inquire a need to look at what quantification parameters to use on the other hand (Boellaard, 2019). Ly *et al.* have documented how the visual scoring system (Deuville score – lesion uptake compared to mediastinal blood pool and liver uptake) used to stratify lymphoma patients is affected by the new Discovery MI scanner (GE Healthcare, Milwaukee, WI, USA) (Ly, 2019). Reconstructions using the newly proposed updating of the EANM/EARL recommendation (Kaalep, 2018) was compared to the current EANM/EARL harmonizing standard. They found that the use of the updated EARL recommendations will significantly change the Deuville score and fewer patients will be classified as responders. Small lesions will have a higher uptake value while the background uptake values in e.g. liver and blood background are changed to a lesser extent (Ly, 2019). We can probably expect that the uptake in atherosclerosis will be less underestimated with the new scanners. This will probably, as for the lymphomas, increase and alter the ratio between lesion or vessel wall uptake and background activity in blood. This must be addressed in meta-analyses and multi-centre studies.

9.2 OTHER PET TRACERS

^{18}F-FDG has gained a stronghold in atherosclerosis imaging because of its long history in PET imaging and wide availability, but probably most importantly, it targets and quantifies inflammation, regarded as the key process in atherosclerosis development and progression. On the downside, imaging with ^{18}F-FDG requires thorough patient preparations, in particular for patients with diabetes. ^{18}F-FDG also lacks specificity and other tracers might be more specific and easier to handle, as miscellaneous glucose avid structures are not depicted. However, newer PET scanners with increased spatial resolution are anticipated to reduce the problem with spill-in activity from neighbouring structures, at least for the carotid artery. For the imaging of atherosclerosis in the coronary and intracerebral arteries, a tracer without uptake in normal myocardium and normal neurons will greatly enhance the methods utility. In the search for better atherosclerosis tracers, the focus is both on experimental ones and on clinically available PET tracers used for other indications. **Figure 19** illustrates how PET tracers can target different steps of the atherosclerotic process.

Tracers that binds specifically to macrophages could be the optimal ones for atherosclerosis imaging. Somatostatin receptor imaging is a cornerstone in imaging of neuroendocrine tumours (Bombardieri, 2010; Virgolini, 2010). And the clinical availability of PET tracers targeting somatostatin receptors is increasing. Somatostatin receptor imaging has been positive in sarcoidosis and other granulomatous diseases (Kwekkeboom, 1997) and somatostatin receptor subtype-2 (SST2) is expressed on activated macrophages (Dalm, 2003). Tarkin *et al.* performed a clinical PET study with ^{68}Ga labelled [1,4,7,10-tetraazacyclododecane-*N,N',N'',N'''*-tetraacetic acid]-d-Phe^{1}, Tyr^{3}-octreotate (DOTATATE) that has a high specificity for SST2. They found that culprit lesions in both coronary and carotid arteries had higher uptake than non-culprit lesions. Further, *ex-vivo* autoradiography of removed carotid plaques showed binding of ^{68}Ga-DOTATATE in the plaques necrotic core and shoulder regions, and co-localization between SST2-staining and macrophages (Tarkin, 2017). Pedersen *et al.* found a higher uptake in culprit versus contralateral carotid plaques when labelling DOTATATE with copper-64 (Pedersen, 2015). These

findings indicate that DOTATATE can be used to characterize inflammatory activity, and thereby the instability in atherosclerotic lesions. The clinical safety and increasing availability of ^{68}Ga-DOTATATE is an advantage.

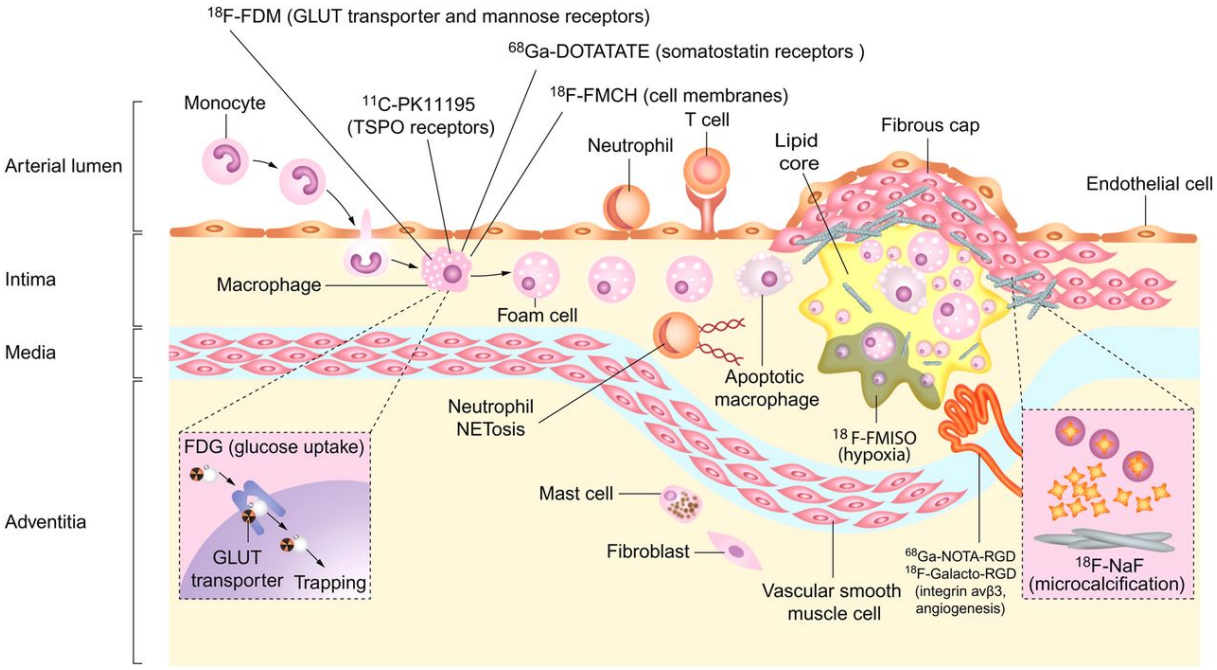

Figure 19: Molecular targets for PET atherosclerosis imaging. During atherosclerosis development macrophages avidly utilize glucose, and simultaneously take up ^{18}F-fluorodeoxyglucose. ^{18}F-fluorodeoxymannose is taken up by facilitative glucose transporters on macrophages and binds mannose receptors. Somatostatin receptors expressed on activated macrophages act as a target for the tracer ^{68}Ga-DOTATATE. Macrophage-mediated inflammation can be detected by novel tracers targeting translocator protein receptors (^{11}C-PK11195) and macrophage cell membranes (^{18}F-FMCH). Additional PET tracers targeting atherosclerosis can identify micro-calcification (^{18}F-sodium fluoride), neoangiogenesis (^{68}Ga-NOTA-RGD, ^{18}F-Galacto-RGD), and cellular hypoxia (^{18}F-FMISO). Adaptation reprinted by permission from Macmillan Publishers Ltd: Tarkin *et al*. (Tarkin, 2014), copyright (2014) (Joseph, 2016).
Unadapted figure is reprinted with permission from Oxford University Press (Joseph, 2016) and Springer Nature (Tarkin, 2014).

Other tracers further from clinical use, but chosen for their specificity for macrophages, are those binding to translocator protein (TSPO) (Joseph, 2016). ^{11}C-PK11195 has shown higher uptake in symptomatic carotid stenosis than asymptomatic (Gaemperli, 2012). Labelling with ^{18}F is easier to handle in clinical

practice than ^{11}C (half-life only 20 min). ^{18}F-labelling of PK11195 and other TSPO tracers have been investigated in other inflammatory conditions (Largeau, 2017), and they might have a potential for atherosclerosis imaging.

There has been great interest in PET imaging with ^{18}F-NaF in atherosclerosis. ^{18}F-NaF has been in clinical use as a bone-seeking tracer for a long time (Beheshti, 2015). Beside uptake in bone ^{18}F-NaF has no disturbing uptake for atherosclerosis imaging and calcification is a known process in atherosclerosis development. ^{18}F-NaF binds to bone after exchange of an hydroxyl ion and is tested for the identification of active and progressing calcifications in patients with aortic valve stenosis (Hyafil, 2019a). Irkle *et al.* found that ^{18}F-NaF co-localizes to areas of nascent calcification within vascular tissue (Irkle, 2015). ^{18}F-NaF is thereby established as an imaging marker of active microcalcification in atherosclerosis, but Hyafil and Vigne summarize the available evidence and conclude that it is not specific for microcalcifications as it also can bind to macrocalcifications (detectable using conventional imaging) (Hyafil, 2019b). Regarding the uptake of ^{18}F-NaF and instability and development of atherosclerosis in the coronary arteries Dweck *et al.* found that increased uptake corresponded with a higher clinical CVD risk profile (Dweck, 2012). A swine model of metabolic syndrome demonstrated that ^{18}F-NaF uptake preceded the emergence of macroscopic calcification on IVUS and CT scans (McKenney-Drake, 2018). Joshi *et al.* found higher uptake in culprit versus non-culprit plaques in patients with myocardial infarction and focal uptake of ^{18}F-NaF in coronary plaques were associated with more high-risk features on intravascular ultrasound than those without uptake in patients with stable angina (Joshi, 2014).

It has been unclear how ^{18}F-NaF performs in the assessment of instability in carotid artery plaques. A microPET study of excised carotid plaques incubated with ^{18}F-NaF did not find a difference in average uptake between culprit and non-culprit plaques (Hop, 2019). Clinical studies have compared the uptake of ^{18}F-NaF and ^{18}F-FDG in the same symptomatic carotid stenosis. Evans *et al.* imaged 26 individuals with acute ischemic stroke with ipsilateral carotid stenosis of ≥50% and found that culprit carotid plaque vessel segment showed higher uptake than the non-culprit (contralateral) segment with both tracers. Whereas ^{18}F-NaF was concentrated around the carotid bifurcations, ^{18}F-FDG was evenly distributed throughout the vessel segments (Evans,

2020). Vesey *et al.* found higher uptake in culprit carotid plaques than in contralateral or control vessels with ^{18}F-NaF, but not with ^{18}F-FDG (Vesey, 2017). Limitations of this study is that the time interval between symptoms and imaging were not given, and that both the contralateral and chosen control vessels could have had a high degree of inflammation. Quirce *et al.* examined nine patients and used contralateral plaque as controls. Both tracers showed a tendency to be highest in the symptomatic plaques, but the difference was not statistically significant (Quirce, 2016).

9.3 OTHER MODALITIES

The ability of other imaging modalities to characterize atherosclerotic lesions has been and is being explored. MRI is more available than PET, and can depict plaque components including the lipid rich necrotic core, the fibrous cap, intraplaque haemorrhage and more (Saba, 2019), but not the plaques characteristics on a molecular level. Intraplaque haemorrhage is the most promising plaque feature of plaque instability and the risk of future stroke on MRI. It is suggested adding MRI sequences covering the carotid plaque to a standard MRI examination of the brain for patients evaluated for carotid artery atherosclerosis and cerebrovascular disease. This will only add 4–6 min to the examination time (Saba, 2019).

A hybrid scanner with PET and MRI has been possible after the development of photomultipliers (SiPM) that are made of MR compatible materials and thereby can operate in a magnetic field. There have been several studies with PET and MRI of atherosclerotic plaques before the development of a hybrid scanner. One-stop-shop will make it much more accessible to scan with both modalities. It will also reduce the radiation dose and possibly lower the use of CM, depending on the MRI sequence used. A study documenting an advantage of a dual PET and MRI examination was carried out on 12 recently symptomatic (TIA) stenosis ≥65% in the carotid artery. High uptake of ^{18}F-FDG was found in the lesion targeted for endarterectomy in 7 of 12 patients. For 3 of the remaining patients other non-stenotic lesions in the same vascular territory identified on MRI had a high level of ^{18}F-FDG uptake (Davies, 2005).

Ultrasound is today widely available and used by neurologists as a part of their clinical evaluation of carotid artery stenosis. Ultrasound techniques evaluating features of instability such as neo-angiogenesis/microvessels are under development as well as techniques to measure of the plaque volume (Khan, 2017; Zamani, 2019).

10. REFERENCES

Aboyans, V., J. B. Ricco, M. E. L. Bartelink, M. Bjorck, M. Brodmann, T. Cohnert, J. P. Collet, M. Czerny, M. De Carlo, S. Debus, C. Espinola-Klein, T. Kahan, S. Kownator, L. Mazzolai, A. R. Naylor, M. Roffi, J. Rother, M. Sprynger, M. Tendera, G. Tepe, M. Venermo, C. Vlachopoulos, I. Desormais and E. S. C. S. D. Group (2018). 2017 ESC Guidelines on the Diagnosis and Treatment of Peripheral Arterial Diseases, in collaboration with the European Society for Vascular Surgery (ESVS): Document covering atherosclerotic disease of extracranial carotid and vertebral, mesenteric, renal, upper and lower extremity arteriesEndorsed by: the European Stroke Organization (ESO)The Task Force for the Diagnosis and Treatment of Peripheral Arterial Diseases of the European Society of Cardiology (ESC) and of the European Society for Vascular Surgery (ESVS). *Eur Heart J* 39(9): 763-816.

Aho, K., P. Harmsen, S. Hatano, J. Marquardsen, V. E. Smirnov and T. Strasser (1980). Cerebrovascular disease in the community: results of a WHO collaborative study. *Bull World Health Organ* 58(1): 113-130.

Anzidei, M., A. Napoli, F. Zaccagna, P. Di Paolo, L. Saba, B. Cavallo Marincola, C. Zini, G. Cartocci, L. Di Mare, C. Catalano and R. Passariello (2012). Diagnostic accuracy of colour Doppler ultrasonography, CT angiography and blood-pool-enhanced MR angiography in assessing carotid stenosis: a comparative study with DSA in 170 patients. *Radiol Med* 117(1): 54-71.

Badawi, R. D., H. Shi, P. Hu, S. Chen, T. Xu, P. M. Price, Y. Ding, B. A. Spencer, L. Nardo, W. Liu, J. Bao, T. Jones, H. Li and S. R. Cherry (2019). First Human Imaging Studies with the EXPLORER Total-Body PET Scanner. *J Nucl Med* 60(3): 299-303.

Bailey, D. (2003). Data Acquisition and Performance Characterization in PET. *Positron Emission Tomography: Basic Science and Clinical Practice.* P. Valk, D. Bailey, D. Townsend and M. Maisey. London, United Kingdom, Springer-Verlag.

Basu, S., S. Hess, P. E. Nielsen Braad, B. B. Olsen, S. Inglev and P. F. Hoilund-Carlsen (2014). The Basic Principles of FDG-PET/CT Imaging. *PET Clin* 9(4): 355-370, v.

Beheshti, M., F. M. Mottaghy, F. Paycha, F. F. F. Behrendt, T. Van den Wyngaert, I. Fogelman, K. Strobel, M. Celli, S. Fanti, F. Giammarile, B. Krause and W. Langsteger (2015). (18)F-NaF PET/CT: EANM procedure guidelines for bone imaging. *Eur J Nucl Med Mol Imaging* 42(11): 1767-1777.

Blomberg, B. A., S. R. Akers, B. Saboury, N. N. Mehta, G. Cheng, D. A. Torigian, E. Lim, C. Del Bello, T. J. Werner and A. Alavi (2013). Delayed time-point 18F-FDG PET CT imaging enhances assessment of atherosclerotic plaque inflammation. *Nucl Med Commun* 34(9): 860-867.

Blomberg, B. A., A. Thomassen, R. A. Takx, M. G. Hildebrandt, J. A. Simonsen, K. M. Buch-Olsen, A. C. Diederichsen, H. Mickley, A. Alavi and P. F. Hoilund-Carlsen (2014). Delayed 18F-fluorodeoxyglucose PET/CT imaging improves quantitation of atherosclerotic plaque inflammation: results from the CAMONA study. *J Nucl Cardiol* 21(3): 588-597.

Boellaard, R., R. Delgado-Bolton, W. J. Oyen, F. Giammarile, K. Tatsch, W. Eschner, F. J. Verzijlbergen, S. F. Barrington, L. C. Pike, W. A. Weber, S. Stroobants, D. Delbeke, K. J. Donohoe, S. Holbrook, M. M. Graham, G. Testanera, O. S. Hoekstra, J. Zijlstra, E. Visser, C. J. Hoekstra, J. Pruim, A. Willemsen, B. Arends, J. Kotzerke, A. Bockisch, T. Beyer, A. Chiti and B. J. Krause (2015). FDG PET/CT: EANM procedure guidelines for tumour imaging: version 2.0. *Eur J Nucl Med Mol Imaging* 42(2): 328-354.

Boellaard, R., M. J. O'Doherty, W. A. Weber, F. M. Mottaghy, M. N. Lonsdale, S. G. Stroobants, W. J. Oyen, J. Kotzerke, O. S. Hoekstra, J. Pruim, P. K. Marsden, K. Tatsch, C. J. Hoekstra, E. P. Visser, B. Arends, F. J. Verzijlbergen, J. M. Zijlstra, E. F. Comans, A. A. Lammertsma, A. M. Paans, A. T. Willemsen, T. Beyer, A.

Bockisch, C. Schaefer-Prokop, D. Delbeke, R. P. Baum, A. Chiti and B. J. Krause (2010). FDG PET and PET/CT: EANM procedure guidelines for tumour PET imaging: version 1.0. *Eur J Nucl Med Mol Imaging* 37(1): 181-200.

Boellaard, R., T. Sera, A. Kaalep, O. S. Hoekstra, S. F. Barrington and J. M. Zijlstra (2019). Updating PET/CT performance standards and PET/CT interpretation criteria should go hand in hand. *EJNMMI Res* 9(1): 95.

Bombardieri, E., V. Ambrosini, C. Aktolun, R. P. Baum, A. Bishof-Delaloye, S. Del Vecchio, L. Maffioli, L. Mortelmans, W. Oyen, G. Pepe, A. Chiti and E. Oncology Committee of the (2010). 111In-pentetreotide scintigraphy: procedure guidelines for tumour imaging. *Eur J Nucl Med Mol Imaging* 37(7): 1441-1448.

Brott, T. G., J. L. Halperin, S. Abbara, J. M. Bacharach, J. D. Barr, R. L. Bush, C. U. Cates, M. A. Creager, S. B. Fowler, G. Friday, V. S. Hertzberg, E. B. McIff, W. S. Moore, P. D. Panagos, T. S. Riles, R. H. Rosenwasser and A. J. Taylor (2011). 2011 ASA/ACCF/AHA/AANN/AANS/ACR/ASNR/CNS/SAIP/SCAI/SIR/SNIS/SVM/SVS guideline on the management of patients with extracranial carotid and vertebral artery disease: executive summary: a report of the American College of Cardiology Foundation/American Heart Association Task Force on Practice Guidelines, and the American Stroke Association, American Association of Neuroscience Nurses, American Association of Neurological Surgeons, American College of Radiology, American Society of Neuroradiology, Congress of Neurological Surgeons, Society of Atherosclerosis Imaging and Prevention, Society for Cardiovascular Angiography and Interventions, Society of Interventional Radiology, Society of NeuroInterventional Surgery, Society for Vascular Medicine, and Society for Vascular Surgery. *J Am Coll Cardiol* 57(8): 1002-1044.

Bucerius, J., F. Hyafil, H. J. Verberne, R. H. Slart, O. Lindner, R. Sciagra, D. Agostini, C. Ubleis, A. Gimelli, M. Hacker and M. Cardiovascular Committee of the European Association of Nuclear (2016). Position paper of the Cardiovascular Committee of the European Association of Nuclear Medicine (EANM) on PET imaging of atherosclerosis. *Eur J Nucl Med Mol Imaging* 43(4): 780-792.

Bucerius, J., V. Mani, C. Moncrieff, J. Machac, V. Fuster, M. E. Farkouh, A. Tawakol, J. H. Rudd and Z. A. Fayad (2014). Optimizing 18F-FDG PET/CT imaging of vessel wall inflammation: the impact of 18F-FDG circulation time, injected dose, uptake parameters, and fasting blood glucose levels. *Eur J Nucl Med Mol Imaging* 41(2): 369-383.

Bucerius, J., V. Mani, C. Moncrieff, J. H. Rudd, J. Machac, V. Fuster, M. E. Farkouh and Z. A. Fayad (2012). Impact of noninsulin-dependent type 2 diabetes on carotid wall 18F-fluorodeoxyglucose positron emission tomography uptake. *J Am Coll Cardiol* 59(23): 2080-2088.

Buja, L. M. (2014). Nikolai N. Anitschkow and the lipid hypothesis of atherosclerosis. *Cardiovasc Pathol* 23(3): 183-184.

Bural, G. G., D. A. Torigian, W. Chamroonrat, K. Alkhawaldeh, M. Houseni, G. El-Haddad and A. Alavi (2006). Quantitative assessment of the atherosclerotic burden of the aorta by combined FDG-PET and CT image analysis: a new concept. *Nucl Med Biol* 33(8): 1037-1043.

Burg, S., A. Dupas, S. Stute, A. Dieudonne, P. Huet, D. Le Guludec and I. Buvat (2013). Partial volume effect estimation and correction in the aortic vascular wall in PET imaging. *Phys Med Biol* 58(21): 7527-7542.

Carr, S., A. Farb, W. H. Pearce, R. Virmani and J. S. Yao (1996). Atherosclerotic plaque rupture in symptomatic carotid artery stenosis. *J Vasc Surg* 23(5): 755-765; discussion 765-756.

Chaker, S., K. Al-Dasuqi, H. Baradaran, M. Demetres, D. Delgado, S. Nehmeh, J. R. Osborne, P. J. Christos, H. Kamel and A. Gupta (2019). Carotid Plaque Positron Emission Tomography Imaging and Cerebral Ischemic Disease. *Stroke* 50(8): 2072-2079.

Chen, W. and V. Dilsizian (2015). PET assessment of vascular inflammation and atherosclerotic plaques: SUV or TBR? *J Nucl Med* 56(4): 503-504.

Chowdhury, M. M., J. M. Tarkin, N. R. Evans, E. Le, E. A. Warburton, P. D. Hayes, J. H. F. Rudd and P. A. Coughlin (2018). (18)F-FDG Uptake on PET/CT in Symptomatic versus Asymptomatic Carotid Disease: a Meta-Analysis. *Eur J Vasc Endovasc Surg* 56(2): 172-179.

Cybulsky, M. I. and M. A. Gimbrone, Jr. (1991). Endothelial expression of a mononuclear leukocyte adhesion molecule during atherogenesis. *Science* 251(4995): 788-791.

Dahlbom, M. and A. K. King (2017). Principles of SPECT and PET imaging. *Physics of PET and SPECT Imaging*. M. Dahlbom. Boca Raton, FL, CRC Press, Taylor & Francis Group.

Dalm, V. A., P. M. van Hagen, P. M. van Koetsveld, S. Achilefu, A. B. Houtsmuller, D. H. Pols, A. J. van der Lely, S. W. Lamberts and L. J. Hofland (2003). Expression of somatostatin, cortistatin, and somatostatin receptors in human monocytes, macrophages, and dendritic cells. *Am J Physiol Endocrinol Metab* 285(2): E344-353.

Davies, J. R., J. H. Rudd, T. D. Fryer, M. J. Graves, J. C. Clark, P. J. Kirkpatrick, J. H. Gillard, E. A. Warburton and P. L. Weissberg (2005). Identification of culprit lesions after transient ischemic attack by combined 18F fluorodeoxyglucose positron-emission tomography and high-resolution magnetic resonance imaging. *Stroke* 36(12): 2642-2647.

Davies, M. J. and A. C. Thomas (1985). Plaque fissuring--the cause of acute myocardial infarction, sudden ischaemic death, and crescendo angina. *Br Heart J* 53(4): 363-373.

Di Chiro, G., R. L. DeLaPaz, R. A. Brooks, L. Sokoloff, P. L. Kornblith, B. H. Smith, N. J. Patronas, C. V. Kufta, R. M. Kessler, G. S. Johnston, R. G. Manning and A. P. Wolf (1982). Glucose utilization of cerebral gliomas measured by [18F] fluorodeoxyglucose and positron emission tomography. *Neurology* 32(12): 1323-1329.

Diederichs, C. G., L. Staib, G. Glatting, H. G. Beger and S. N. Reske (1998). FDG PET: elevated plasma glucose reduces both uptake and detection rate of pancreatic malignancies. *J Nucl Med* 39(6): 1030-1033.

Dirksen, M. T., A. C. van der Wal, F. M. van den Berg, C. M. van der Loos and A. E. Becker (1998). Distribution of inflammatory cells in atherosclerotic plaques relates to the direction of flow. *Circulation* 98(19): 2000-2003.

Dweck, M. R., M. W. Chow, N. V. Joshi, M. C. Williams, C. Jones, A. M. Fletcher, H. Richardson, A. White, G. McKillop, E. J. van Beek, N. A. Boon, J. H. Rudd and D. E. Newby (2012). Coronary arterial 18F-sodium fluoride uptake: a novel marker of plaque biology. *J Am Coll Cardiol* 59(17): 1539-1548.

Elatrozy, T., A. Nicolaides, T. Tegos, A. Z. Zarka, M. Griffin and M. Sabetai (1998). The effect of B-mode ultrasonic image standardisation on the echodensity of symptomatic and asymptomatic carotid bifurcation plaques. *Int Angiol* 17(3): 179-186.

Elkhawad, M., J. H. Rudd, L. Sarov-Blat, G. Cai, R. Wells, L. C. Davies, D. J. Collier, M. S. Marber, R. P. Choudhury, Z. A. Fayad, A. Tawakol, F. V. Gleeson, J. J. Lepore, B. Davis, R. N. Willette, I. B. Wilkinson, D. L. Sprecher and J. Cheriyan (2012). Effects of p38 mitogen-activated protein kinase inhibition on vascular and systemic inflammation in patients with atherosclerosis. *JACC Cardiovasc Imaging* 5(9): 911-922.

Eskian, M., A. Alavi, M. Khorasanizadeh, B. L. Viglianti, H. Jacobsson, T. D. Barwick, A. Meysamie, S. K. Yi, S. Iwano, B. Bybel, F. Caobelli, F. Lococo, J. Gea, A. Sancho-Munoz, J. Schildt, E. Tatci, C. Lapa, G. Keramida, M. Peters, R. R. Boktor, J. John, A. G. Pitman, T. Mazurek and N. Rezaei (2019). Effect of blood glucose level on standardized uptake value (SUV) in (18)F- FDG PET-scan: a systematic review and meta-analysis of 20,807 individual SUV measurements. *Eur J Nucl Med Mol Imaging* 46(1): 224-237.

European Carotid Plaque Study Group (1995). Carotid artery plaque composition--relationship to clinical presentation and ultrasound B-mode imaging. . *Eur J Vasc Endovasc Surg* 10(1): 23-30.

European Carotid Surgery Trialists' Collaborative Group (1998). Randomised trial of endarterectomy for recently symptomatic carotid stenosis: final results of the MRC European Carotid Surgery Trial (ECST). *Lancet* 351(9113): 1379-1387.

Evans, N. R., J. M. Tarkin, M. M. Chowdhury, E. P. V. Le, P. A. Coughlin, J. H. F. Rudd and E. A. Warburton (2020). Dual-Tracer Positron-Emission Tomography for Identification of Culprit Carotid Plaques and Pathophysiology In Vivo. *Circ Cardiovasc Imaging* 13(3): e009539.

Fayad, Z. A., V. Mani, M. Woodward, D. Kallend, M. Abt, T. Burgess, V. Fuster, C. M. Ballantyne, E. A. Stein, J. C. Tardif, J. H. Rudd, M. E. Farkouh, A. Tawakol and P. I. dal (2011). Safety and efficacy of dalcetrapib on atherosclerotic disease using novel non-invasive multimodality imaging (dal-PLAQUE): a randomised clinical trial. *Lancet* 378(9802): 1547-1559.

Figueroa, A. L., A. Abdelbaky, Q. A. Truong, E. Corsini, M. H. MacNabb, Z. R. Lavender, M. A. Lawler, S. K. Grinspoon, T. J. Brady, K. Nasir, U. Hoffmann and A. Tawakol (2013). Measurement of arterial activity on routine FDG PET/CT images improves prediction of risk of future CV events. *JACC Cardiovasc Imaging* 6(12): 1250-1259.

Figueroa, A. L., S. S. Subramanian, R. C. Cury, Q. A. Truong, J. A. Gardecki, G. J. Tearney, U. Hoffmann, T. J. Brady and A. Tawakol (2012). Distribution of inflammation within carotid atherosclerotic plaques with high-risk morphological features: a comparison between positron emission tomography activity, plaque morphology, and histopathology. *Circ Cardiovasc Imaging* 5(1): 69-77.

Finessi, M., G. Bisi and D. Deandreis (2019). Hyperglycemia and 18F-FDG PET/CT, issues and problem solving: a literature review. *Acta Diabetol*.

Fjaertoft, H. and B. Indredavik (2007). [Cost-estimates for stroke]. *Tidsskr Nor Laegeforen* 127(6): 744-747.

Fukuzumi, M., H. Shinomiya, Y. Shimizu, K. Ohishi and S. Utsumi (1996). Endotoxin-induced enhancement of glucose influx into murine peritoneal macrophages via GLUT1. *Infect Immun* 64(1): 108-112.

Gaemperli, O., J. Shalhoub, D. R. Owen, F. Lamare, S. Johansson, N. Fouladi, A. H. Davies, O. E. Rimoldi and P. G. Camici (2012). Imaging intraplaque inflammation in carotid atherosclerosis with 11C-PK11195 positron emission tomography/computed tomography. *Eur Heart J* 33(15): 1902-1910.

Gallagher, B. M., J. S. Fowler, N. I. Gutterson, R. R. MacGregor, C. N. Wan and A. P. Wolf (1978). Metabolic trapping as a principle of oradiopharmaceutical design: some factors resposible for the biodistribution of [18F] 2-deoxy-2-fluoro-D-glucose. *J Nucl Med* 19(10): 1154-1161.

Gamelli, R. L., H. Liu, L. K. He and C. A. Hofmann (1996). Augmentations of glucose uptake and glucose transporter-1 in macrophages following thermal injury and sepsis in mice. *J Leukoc Biol* 59(5): 639-647.

GBD 2015 Disease and Injury Incidence and Prevalence Collaborators (2016). Global, regional, and national incidence, prevalence, and years lived with disability for 310 diseases and injuries, 1990-2015: a systematic analysis for the Global Burden of Disease Study 2015. *Lancet* 388(10053): 1545-1602.

GBD 2016 Lifetime Risk of Stroke Collaborators (2018). Global, Regional, and Country-Specific Lifetime Risks of Stroke, 1990 and 2016. *N Engl J Med* 379(25): 2429-2437.

GBD 2016 Stroke Collaborators (2019). Global, regional, and national burden of stroke, 1990-2016: a systematic analysis for the Global Burden of Disease Study 2016. *Lancet Neurol* 18(5): 439-458.

Glagov, S., E. Weisenberg, C. K. Zarins, R. Stankunavicius and G. J. Kolettis (1987). Compensatory enlargement of human atherosclerotic coronary arteries. *N Engl J Med* 316(22): 1371-1375.

Graebe, M., L. Borgwardt, L. Hojgaard, H. Sillesen and A. Kjaer (2010a). When to image carotid plaque inflammation with FDG PET/CT. *Nucl Med Commun* 31(9): 773-779.

Graebe, M., S. F. Pedersen, L. Borgwardt, L. Hojgaard, H. Sillesen and A. Kjaer (2009). Molecular pathology in vulnerable carotid plaques: correlation with [18]-fluorodeoxyglucose positron emission tomography (FDG-PET). *Eur J Vasc Endovasc Surg* 37(6): 714-721.

Graebe, M., S. F. Pedersen, L. Hojgaard, A. Kjaer and H. Sillesen (2010b). 18FDG PET and ultrasound echolucency in carotid artery plaques. *JACC Cardiovasc Imaging* 3(3): 289-295.

Grant, E. G., C. B. Benson, G. L. Moneta, A. V. Alexandrov, J. D. Baker, E. I. Bluth, B. A. Carroll, M. Eliasziw, J. Gocke, B. S. Hertzberg, S. Katanick, L. Needleman, J. Pellerito, J. F. Polak, K. S. Rholl, D. L. Wooster and R. E. Zierler (2003). Carotid artery stenosis: gray-scale and Doppler US diagnosis--Society of Radiologists in Ultrasound Consensus Conference. *Radiology* 229(2): 340-346.

Gronholdt, M. L., B. G. Nordestgaard, J. Bentzon, B. M. Wiebe, J. Zhou, E. Falk and H. Sillesen (2002). Macrophages are associated with lipid-rich carotid artery plaques, echolucency on B-mode imaging, and elevated plasma lipid levels. *J Vasc Surg* 35(1): 137-145.

Gronholdt, M. L., B. G. Nordestgaard, T. V. Schroeder, S. Vorstrup and H. Sillesen (2001). Ultrasonic echolucent carotid plaques predict future strokes. *Circulation* 104(1): 68-73.

Gupta, A., K. Kesavabhotla, H. Baradaran, H. Kamel, A. Pandya, A. E. Giambrone, D. Wright, K. J. Pain, E. E. Mtui, J. S. Suri, P. C. Sanelli and A. I. Mushlin (2015). Plaque echolucency and stroke risk in asymptomatic carotid stenosis: a systematic review and meta-analysis. *Stroke* 46(1): 91-97.

Hadar, N., G. Raman, D. Moorthy, T. F. O'Donnell, D. E. Thaler, E. Feldmann, J. Lau, G. D. Kitsios and I. J. Dahabreh (2014). Asymptomatic carotid artery stenosis treated with medical therapy alone: temporal trends and implications for risk assessment and the design of future studies. *Cerebrovasc Dis* 38(3): 163-173.

Hardie, A. D., C. M. Kramer, P. Raghavan, E. Baskurt and K. R. Nandalur (2007). The impact of expansive arterial remodeling on clinical presentation in carotid artery disease: a multidetector CT angiography study. *AJNR Am J Neuroradiol* 28(6): 1067-1070.

Hart, R. G., H. C. Diener, S. B. Coutts, J. D. Easton, C. B. Granger, M. J. O'Donnell, R. L. Sacco, S. J. Connolly and E. I. W. G. Cryptogenic Stroke (2014). Embolic strokes of undetermined source: the case for a new clinical construct. *Lancet Neurol* 13(4): 429-438.

Hawkins, R. A., A. L. Miller, J. E. Cremer and R. L. Veech (1974). Measurement of the rate of glucose utilization by rat brain in vivo. *J Neurochem* 23(5): 917-923.

Hop, H., S. A. de Boer, M. Reijrink, P. W. Kamphuisen, M. H. de Borst, R. A. Pol, C. J. Zeebregts, J. L. Hillebrands, R. Slart, H. H. Boersma, J. Doorduin and D. J. Mulder (2019). (18)F-sodium fluoride positron emission tomography assessed microcalcifications in culprit and non-culprit human carotid plaques. *J Nucl Cardiol* 26(4): 1064-1075.

Howard, D. P., G. W. van Lammeren, J. N. Redgrave, F. L. Moll, J. P. de Vries, D. P. de Kleijn, G. J. de Borst, G. Pasterkamp and P. M. Rothwell (2013). Histological features of carotid plaque in patients with ocular ischemia versus cerebral events. *Stroke* 44(3): 734-739.

Huet, P., S. Burg, D. Le Guludec, F. Hyafil and I. Buvat (2015). Variability and uncertainty of 18F-FDG PET imaging protocols for assessing inflammation in atherosclerosis: suggestions for improvement. *J Nucl Med* 56(4): 552-559.

Hyafil, F., W. Ferrag, C. Kefti and D. Le Guludec (2019a). Fluoride imaging of atherosclerotic plaques: Moving from macro to microcalcifications? *J Nucl Cardiol* 26(4): 1076-1078.

Hyafil, F., A. Schindler, D. Sepp, T. Obenhuber, A. Bayer-Karpinska, T. Boeckh-Behrens, S. Hohn, M. Hacker, S. G. Nekolla, A. Rominger, M. Dichgans, M. Schwaiger, T. Saam and H. Poppert (2016). High-risk plaque features can be detected in non-stenotic carotid plaques of patients with ischaemic stroke classified as cryptogenic using combined (18)F-FDG PET/MR imaging. *Eur J Nucl Med Mol Imaging* 43(2): 270-279.

Hyafil, F. and J. Vigne (2019b). Nuclear Imaging: Focus on Vascular Probes. *Arterioscler Thromb Vasc Biol* 39(7): 1369-1378.

Irkle, A., A. T. Vesey, D. Y. Lewis, J. N. Skepper, J. L. Bird, M. R. Dweck, F. R. Joshi, F. A. Gallagher, E. A. Warburton, M. R. Bennett, K. M. Brindle, D. E. Newby, J. H. Rudd and A. P. Davenport (2015). Identifying active vascular microcalcification by (18)F-sodium fluoride positron emission tomography. *Nat Commun* 6: 7495.

Jamar, F., J. Buscombe, A. Chiti, P. E. Christian, D. Delbeke, K. J. Donohoe, O. Israel, J. Martin-Comin and A. Signore (2013). EANM/SNMMI guideline for 18F-FDG use in inflammation and infection. *J Nucl Med* 54(4): 647-658.

Jander, S., M. Sitzer, R. Schumann, M. Schroeter, M. Siebler, H. Steinmetz and G. Stoll (1998). Inflammation in high-grade carotid stenosis: a possible role for macrophages and T cells in plaque destabilization. *Stroke* 29(8): 1625-1630.

Johal, A. S., I. M. Loftus, J. R. Boyle, A. R. Naylor, S. Waton, K. Heikkila and D. A. Cromwell (2019). Changing Patterns of Carotid Endarterectomy Between 2011 and 2017 in England. *Stroke* 50(9): 2461-2468.

Johnsrud, K., K. Skagen, T. Seierstad, M. Skjelland, D. Russell and M. E. Revheim (2019). (18)F-FDG PET/CT for the quantification of inflammation in large carotid artery plaques. *J Nucl Cardiol* 26(3): 883-893.

Joseph, P. and A. Tawakol (2016). Imaging atherosclerosis with positron emission tomography. *Eur Heart J* 37(39): 2974-2980.

Joshi, N. V., A. T. Vesey, M. C. Williams, A. S. Shah, P. A. Calvert, F. H. Craighead, S. E. Yeoh, W. Wallace, D. Salter, A. M. Fletcher, E. J. van Beek, A. D. Flapan, N. G. Uren, M. W. Behan, N. L. Cruden, N. L. Mills, K. A. Fox, J. H. Rudd, M. R. Dweck and D. E. Newby (2014). 18F-fluoride positron emission tomography for identification of ruptured and high-risk coronary atherosclerotic plaques: a prospective clinical trial. *Lancet* 383(9918): 705-713.

Kaalep, A., T. Sera, S. Rijnsdorp, M. Yaqub, A. Talsma, M. A. Lodge and R. Boellaard (2018). Feasibility of state of the art PET/CT systems performance harmonisation. *Eur J Nucl Med Mol Imaging* 45(8): 1344-1361.

Karp, J. S., S. Surti, M. E. Daube-Witherspoon and G. Muehllehner (2008). Benefit of time-of-flight in PET: experimental and clinical results. *J Nucl Med* 49(3): 462-470.

Kelly, P. J., P. Camps-Renom, N. Giannotti, J. Marti-Fabregas, J. P. McNulty, J. C. Baron, M. Barry, S. B. Coutts, S. Cronin, R. Delgado-Mederos, E. Dolan, A. Fernandez-Leon, S. Foley, J. Harbison, G. Horgan, E. Kavanagh, M. Marnane, J. McCabe, C. McDonnell, V. K. Sharma, D. J. Williams, M. O'Connell and S. Murphy (2020). A Risk Score Including Carotid Plaque Inflammation and Stenosis Severity Improves Identification of Recurrent Stroke. *Stroke* 51(3): 838-845.

Kelly, P. J., P. Camps-Renom, N. Giannotti, J. Marti-Fabregas, S. Murphy, J. McNulty, M. Barry, P. Barry, D. Calvet, S. B. Coutts, S. Cronin, R. Delgado-Mederos, E. Dolan, A. Fernandez-Leon, S. Foley, J. Harbison, G. Horgan, E. Kavanagh, M. Marnane, C. McDonnell, M. O'Donohoe, V. Sharma, C. Walsh, D. Williams and M. O'Connell (2019). Carotid Plaque Inflammation Imaged by (18)F-Fluorodeoxyglucose Positron Emission Tomography and Risk of Early Recurrent Stroke. *Stroke* 50(7): 1766-1773.

Keyes, J. W., Jr. (1995). SUV: standard uptake or silly useless value? *J Nucl Med* 36(10): 1836-1839.

Khan, A. A., C. Koudelka, C. Goldstein, L. Zhao, J. Yokemick, M. Dux, S. Sikdar and B. K. Lal (2017). Semiautomatic quantification of carotid plaque volume with three-dimensional ultrasound imaging. *J Vasc Surg* 65(5): 1407-1417.

King, A. and H. S. Markus (2009). Doppler embolic signals in cerebrovascular disease and prediction of stroke risk: a systematic review and meta-analysis. *Stroke* 40(12): 3711-3717.

Kolodgie, F. D., G. Nakazawa, G. Sangiorgi, E. Ladich, A. P. Burke and R. Virmani (2007). Pathology of atherosclerosis and stenting. *Neuroimaging Clin N Am* 17(3): 285-301, vii.

Kolodgie, F. D., K. Yahagi, H. Mori, M. E. Romero, H. H. R. Trout, A. V. Finn and R. Virmani (2017). High-risk carotid plaque: lessons learned from histopathology. *Semin Vasc Surg* 30(1): 31-43.

Komatsu, T., Y. Iguchi, A. Arai, K. Sakuta, K. Sakai, Y. Terasawa, H. Mitsumura and M. Matsushima (2018). Large but Nonstenotic Carotid Artery Plaque in Patients With a History of Embolic Stroke of Undetermined Source. *Stroke* 49(12): 3054-3056.

Koopman, D., J. A. van Dalen, M. C. Lagerweij, H. Arkies, J. de Boer, A. H. Oostdijk, C. H. Slump and P. L. Jager (2015). Improving the detection of small lesions using a state-of-the-art time-of-flight PET/CT system and small-voxel reconstructions. *J Nucl Med Technol* 43(1): 21-27.

Kubota, R., S. Yamada, K. Kubota, K. Ishiwata, N. Tamahashi and T. Ido (1992). Intratumoral distribution of fluorine-18-fluorodeoxyglucose in vivo: high accumulation in macrophages and granulation tissues studied by microautoradiography. *J Nucl Med* 33(11): 1972-1980.

Kvåle, R., G. Forland, I. J. Bakken, T. Nguyen Trung, R. Akerkar, J. Dyngeland, G. Egeland, G. S. Tell, M. Altreuther, J. Bjørnstad, K. H. Bønaa, H. Fjærtoft, O. Geiran, R. E. Govatsmark, M. Grundtvig, S. Hovland, B. Indredavik, J. Kramer-Johansen, S. Rotevatn, T. Saltnes, E. Slind Kjøl, T. Steen, I. Tjelmeland and M. Ebbing (2018). Hjerte- og karregisteret: Rapport for 2012–2016. *Oslo: Folkehelseinstituttet*.

Kwee, R. M., M. T. Truijman, W. H. Mess, G. J. Teule, J. W. ter Berg, C. L. Franke, A. G. Korten, B. J. Meems, M. H. Prins, J. M. van Engelshoven, J. E. Wildberger, R. J. van Oostenbrugge and M. E. Kooi (2011). Potential of integrated [18F] fluorodeoxyglucose positron-emission tomography/CT in identifying vulnerable carotid plaques. *AJNR Am J Neuroradiol* 32(5): 950-954.

Kwekkeboom, D. J. and E. P. Krenning (1997). Radiolabeled somatostatin analog scintigraphy in oncology and immune diseases: an overview. *Eur Radiol* 7(7): 1103-1109.

Lamanna, A., J. Maingard, C. D. Barras, H. K. Kok, G. Handelman, R. V. Chandra, V. Thijs, D. M. Brooks and H. Asadi (2019). Carotid artery stenting: Current state of evidence and future directions. *Acta Neurol Scand* 139(4): 318-333.

Largeau, B., A. C. Dupont, D. Guilloteau, M. J. Santiago-Ribeiro and N. Arlicot (2017). TSPO PET Imaging: From Microglial Activation to Peripheral Sterile Inflammatory Diseases? *Contrast Media Mol Imaging* 2017: 6592139.

Libby, P. (2002). Inflammation in atherosclerosis. *Nature* 420(6917): 868-874.

Libby, P., J. E. Buring, L. Badimon, G. K. Hansson, J. Deanfield, M. S. Bittencourt, L. Tokgozoglu and E. F. Lewis (2019a). Atherosclerosis. *Nat Rev Dis Primers* 5(1): 56.

Libby, P. and B. M. Everett (2019b). Novel Antiatherosclerotic Therapies. *Arterioscler Thromb Vasc Biol* 39(4): 538-545.

Libby, P. and G. K. Hansson (2019c). From Focal Lipid Storage to Systemic Inflammation: JACC Review Topic of the Week. *J Am Coll Cardiol* 74(12): 1594-1607.

Lindholm, H., F. Brolin, C. Jonsson and H. Jacobsson (2013). The relation between the blood glucose level and the FDG uptake of tissues at normal PET examinations. *EJNMMI Res* 3(1): 50.

Lodge, M. A., M. A. Chaudhry and R. L. Wahl (2012). Noise considerations for PET quantification using maximum and peak standardized uptake value. *J Nucl Med* 53(7): 1041-1047.

Lonneux, M., I. Borbath, A. Bol, A. Coppens, M. Sibomana, R. Bausart, M. Defrise, S. Pauwels and C. Michel (1999). Attenuation correction in whole-body FDG oncological studies: the role of statistical reconstruction. *Eur J Nucl Med* 26(6): 591-598.

Ly, J., D. Minarik, L. Edenbrandt, P. Wollmer and E. Tragardh (2019). The use of a proposed updated EARL harmonization of (18)F-FDG PET-CT in patients with lymphoma yields significant differences in Deauville score compared with current EARL recommendations. *EJNMMI Res* 9(1): 65.

Maki-Petaja, K. M., M. Elkhawad, J. Cheriyan, F. R. Joshi, A. J. Ostor, F. C. Hall, J. H. Rudd and I. B. Wilkinson (2012). Anti-tumor necrosis factor-alpha therapy reduces aortic inflammation and stiffness in patients with rheumatoid arthritis. *Circulation* 126(21): 2473-2480.

Malek, A. M., S. L. Alper and S. Izumo (1999). Hemodynamic shear stress and its role in atherosclerosis. *JAMA* 282(21): 2035-2042.

Markus, H. S., A. King, M. Shipley, R. Topakian, M. Cullinane, S. Reihill, N. M. Bornstein and A. Schaafsma (2010). Asymptomatic embolisation for prediction of stroke in the Asymptomatic Carotid Emboli Study (ACES): a prospective observational study. *Lancet Neurol* 9(7): 663-671.

Marnane, M., A. Merwick, O. C. Sheehan, N. Hannon, P. Foran, T. Grant, E. Dolan, J. Moroney, S. Murphy, K. O'Rourke, K. O'Malley, M. O'Donohoe, C. McDonnell, I. Noone, M. Barry, M. Crowe, E. Kavanagh, M. O'Connell and P. J. Kelly (2012). Carotid plaque inflammation on 18F-fluorodeoxyglucose positron emission tomography predicts early stroke recurrence. *Ann Neurol* 71(5): 709-718.

Marnane, M., S. Prendeville, C. McDonnell, I. Noone, M. Barry, M. Crowe, N. Mulligan and P. J. Kelly (2014). Plaque inflammation and unstable morphology are associated with early stroke recurrence in symptomatic carotid stenosis. *Stroke* 45(3): 801-806.

Mathiesen, E. B., K. H. Bonaa and O. Joakimsen (2001). Echolucent plaques are associated with high risk of ischemic cerebrovascular events in carotid stenosis: the tromso study. *Circulation* 103(17): 2171-2175.

McKenney-Drake, M. L., M. C. Moghbel, K. Paydary, M. Alloosh, S. Houshmand, S. Moe, A. Salavati, J. M. Sturek, P. R. Territo, C. Weaver, T. J. Werner, P. F. Hoilund-Carlsen, M. Sturek and A. Alavi (2018). (18)F-NaF and (18)F-FDG as molecular probes in the evaluation of atherosclerosis. *Eur J Nucl Med Mol Imaging* 45(12): 2190-2200.

Menezes, L. J., C. W. Kotze, B. F. Hutton, R. Endozo, J. C. Dickson, I. Cullum, S. W. Yusuf, P. J. Ell and A. M. Groves (2009). Vascular inflammation imaging with 18F-FDG PET/CT: when to image? *J Nucl Med* 50(6): 854-857.

Mochizuki, T., E. Tsukamoto, Y. Kuge, K. Kanegae, S. Zhao, K. Hikosaka, M. Hosokawa, M. Kohanawa and N. Tamaki (2001). FDG uptake and glucose transporter subtype expressions in experimental tumor and inflammation models. *J Nucl Med* 42(10): 1551-1555.

Moses, W. W. (2011). Fundamental Limits of Spatial Resolution in PET. *Nucl Instrum Methods Phys Res A* 648 Supplement 1: S236-S240.

Moustafa, R. R., D. Izquierdo-Garcia, T. D. Fryer, M. J. Graves, J. H. Rudd, J. H. Gillard, P. L. Weissberg, J. C. Baron and E. A. Warburton (2010). Carotid plaque inflammation is associated with cerebral microembolism in patients with recent transient ischemic attack or stroke: a pilot study. *Circ Cardiovasc Imaging* 3(5): 536-541.

Mueckler, M. (1994). Facilitative glucose transporters. *Eur J Biochem* 219(3): 713-725.

Muller, H. F., A. Viaccoz, L. Fisch, C. Bonvin, K. O. Lovblad, O. Ratib, P. Lalive, S. Pagano, N. Vuilleumier, J. P. Willi and R. Sztajzel (2014). 18FDG-PET-CT: an imaging biomarker of high-risk carotid plaques. Correlation to symptoms and microembolic signals. *Stroke* 45(12): 3561-3566.

Munk, O. L., L. P. Tolbod, S. B. Hansen and T. V. Bogsrud (2017). Point-spread function reconstructed PET images of sub-centimeter lesions are not quantitative. *EJNMMI Phys* 4(1): 5.

Myers, W. G. (1979). Georg Charles de Hevesy: the father of nuclear medicine. *J Nucl Med* 20(6): 590-594.

Nakashima, Y., H. Fujii, S. Sumiyoshi, T. N. Wight and K. Sueishi (2007). Early human atherosclerosis: accumulation of lipid and proteoglycans in intimal thickenings followed by macrophage infiltration. *Arterioscler Thromb Vasc Biol* 27(5): 1159-1165.

Naylor, A. R. (2015). Why is the management of asymptomatic carotid disease so controversial? *Surgeon* 13(1): 34-43.

Naylor, A. R., P. A. Gaines and P. M. Rothwell (2009). Who benefits most from intervention for asymptomatic carotid stenosis: patients or professionals? *Eur J Vasc Endovasc Surg* 37(6): 625-632.

Naylor, A. R., J. B. Ricco, G. J. de Borst, S. Debus, J. de Haro, A. Halliday, G. Hamilton, J. Kakisis, S. Kakkos, S. Lepidi, H. S. Markus, D. J. McCabe, J. Roy, H. Sillesen, J. C. van den Berg, F. Vermassen, C. Esvs Guidelines, P. Kolh, N. Chakfe, R. J. Hinchliffe, I. Koncar, J. S. Lindholt, M. Vega de Ceniga, F. Verzini, R. Esvs Guideline, J. Archie, S. Bellmunt, A. Chaudhuri, M. Koelemay, A. K. Lindahl, F. Padberg and M. Venermo (2018). Editor's Choice - Management of Atherosclerotic Carotid and Vertebral Artery Disease: 2017 Clinical Practice Guidelines of the European Society for Vascular Surgery (ESVS). *Eur J Vasc Endovasc Surg* 55(1): 3-81.

Nicholls, M. (2019). Adolf Otto Reinhold Windaus. *Eur Heart J* 40(32): 2659-2660.

North American Symptomatic Carotid Endarterectomy Trial Collaborators (1998). Benefit of carotid endarterectomy in patients with symptomatic moderate or severe stenosis. *N Engl J Med* 339(20): 1415-1425.

Ntaios, G. and R. G. Hart (2017). Embolic Stroke. *Circulation* 136(25): 2403-2405.

Oh, M., J. Y. Kim, K. H. Shin, S. H. Park, J. S. Ryu, J. S. Kim, H. J. Kim, D. W. Kang and D. H. Moon (2010). Imaging Atherosclerosis in the Carotid Arteries with F-18-Fluoro-2-deoxy-D-glucose Positron Emission Tomography: Effect of Imaging Time after Injection on Quantitative Measurement. *Nucl Med Mol Imaging* 44(4): 261-266.

Pedersen, S. F., B. V. Sandholt, S. H. Keller, A. E. Hansen, A. E. Clemmensen, H. Sillesen, L. Hojgaard, R. S. Ripa and A. Kjaer (2015). 64Cu-DOTATATE PET/MRI for Detection of Activated Macrophages in Carotid Atherosclerotic Plaques: Studies in Patients Undergoing Endarterectomy. *Arterioscler Thromb Vasc Biol* 35(7): 1696-1703.

Quirce, R., I. Martinez-Rodriguez, I. Banzo, J. Jimenez-Bonilla, N. Martinez-Amador, S. Ibanez-Bravo, J. Lopez-Defillo, M. Jimenez-Alonso, M. A. Revilla and J. M. Carril (2016). New insight of functional molecular imaging into the atheroma biology: 18F-NaF and 18F-FDG in symptomatic and asymptomatic carotid plaques after recent CVA. Preliminary results. *Clin Physiol Funct Imaging* 36(6): 499-503.

Rabkin, Z., O. Israel and Z. Keidar (2010). Do hyperglycemia and diabetes affect the incidence of false-negative 18F-FDG PET/CT studies in patients evaluated for infection or inflammation and cancer? A Comparative analysis. *J Nucl Med* 51(7): 1015-1020.

Razifar, P., M. Sandstrom, H. Schnieder, B. Langstrom, E. Maripuu, E. Bengtsson and M. Bergstrom (2005). Noise correlation in PET, CT, SPECT and PET/CT data evaluated using autocorrelation function: a phantom study on data, reconstructed using FBP and OSEM. *BMC Med Imaging* 5: 5.

Redgrave, J. N., J. K. Lovett, P. J. Gallagher and P. M. Rothwell (2006). Histological assessment of 526 symptomatic carotid plaques in relation to the nature and timing of ischemic symptoms: the Oxford plaque study. *Circulation* 113(19): 2320-2328.

Reeps, C., R. A. Bundschuh, J. Pellisek, M. Herz, S. van Marwick, M. Schwaiger, H. H. Eckstein, S. G. Nekolla and M. Essler (2013). Quantitative assessment of glucose metabolism in the vessel wall of abdominal aortic aneurysms: correlation with histology and role of partial volume correction. *Int J Cardiovasc Imaging* 29(2): 505-512.

Reivich, M., D. Kuhl, A. Wolf, J. Greenberg, M. Phelps, T. Ido, V. Casella, J. Fowler, E. Hoffman, A. Alavi, P. Som and L. Sokoloff (1979). The [18F]fluorodeoxyglucose method for the measurement of local cerebral glucose utilization in man. *Circ Res* 44(1): 127-137.

Ridker, P. M., B. M. Everett, T. Thuren, J. G. MacFadyen, W. H. Chang, C. Ballantyne, F. Fonseca, J. Nicolau, W. Koenig, S. D. Anker, J. J. P. Kastelein, J. H. Cornel, P. Pais, D. Pella, J. Genest, R. Cifkova, A. Lorenzatti, T. Forster, Z. Kobalava, L. Vida-Simiti, M. Flather, H. Shimokawa, H. Ogawa, M. Dellborg, P. R. F. Rossi, R. P. T. Troquay, P. Libby, R. J. Glynn and C. T. Group (2017). Antiinflammatory Therapy with Canakinumab for Atherosclerotic Disease. *N Engl J Med* 377(12): 1119-1131.

Ridker, P. M., C. H. Hennekens, J. E. Buring and N. Rifai (2000). C-reactive protein and other markers of inflammation in the prediction of cardiovascular disease in women. *N Engl J Med* 342(12): 836-843.

Rogers, I. S., K. Nasir, A. L. Figueroa, R. C. Cury, U. Hoffmann, D. A. Vermylen, T. J. Brady and A. Tawakol (2010). Feasibility of FDG imaging of the coronary arteries: comparison between acute coronary syndrome and stable angina. *JACC Cardiovasc Imaging* 3(4): 388-397.

Rothwell, P. M., M. Eliasziw, S. A. Gutnikov, A. J. Fox, D. W. Taylor, M. R. Mayberg, C. P. Warlow, H. J. Barnett and C. Carotid Endarterectomy Trialists (2003). Analysis of pooled data from the randomised controlled trials of endarterectomy for symptomatic carotid stenosis. *Lancet* 361(9352): 107-116.

Rothwell, P. M., M. Eliasziw, S. A. Gutnikov, C. P. Warlow, H. J. Barnett and C. Carotid Endarterectomy Trialists (2004). Endarterectomy for symptomatic carotid stenosis in relation to clinical subgroups and timing of surgery. *Lancet* 363(9413): 915-924.

Rudd, J. H., K. S. Myers, S. Bansilal, J. Machac, C. A. Pinto, C. Tong, A. Rafique, R. Hargeaves, M. Farkouh, V. Fuster and Z. A. Fayad (2008). Atherosclerosis inflammation imaging with 18F-FDG PET: carotid, iliac, and femoral uptake reproducibility, quantification methods, and recommendations. *J Nucl Med* 49(6): 871-878.

Rudd, J. H., K. S. Myers, S. Bansilal, J. Machac, A. Rafique, M. Farkouh, V. Fuster and Z. A. Fayad (2007). (18)Fluorodeoxyglucose positron emission tomography imaging of atherosclerotic plaque inflammation is highly reproducible: implications for atherosclerosis therapy trials. *J Am Coll Cardiol* 50(9): 892-896.

Rudd, J. H., E. A. Warburton, T. D. Fryer, H. A. Jones, J. C. Clark, N. Antoun, P. Johnstrom, A. P. Davenport, P. J. Kirkpatrick, B. N. Arch, J. D. Pickard and P. L. Weissberg (2002). Imaging atherosclerotic plaque inflammation with [18F]-fluorodeoxyglucose positron emission tomography. *Circulation* 105(23): 2708-2711.

Russell, D., K. P. Madden, W. M. Clark, P. M. Sandset and J. A. Zivin (1991). Detection of arterial emboli using Doppler ultrasound in rabbits. *Stroke* 22(2): 253-258.

Saba, L., T. Saam, H. R. Jager, C. Yuan, T. S. Hatsukami, D. Saloner, B. A. Wasserman, L. H. Bonati and M. Wintermark (2019). Imaging biomarkers of vulnerable carotid plaques for stroke risk prediction and their potential clinical implications. *Lancet Neurol* 18(6): 559-572.

Saba, L., C. Yuan, T. S. Hatsukami, N. Balu, Y. Qiao, J. K. DeMarco, T. Saam, A. R. Moody, D. Li, C. C. Matouk, M. H. Johnson, H. R. Jager, M. Mossa-Basha, M. E. Kooi, Z. Fan, D. Saloner, M. Wintermark, D. J. Mikulis, B. A. Wasserman and N. Vessel Wall Imaging Study Group of the American Society of (2018). Carotid Artery Wall Imaging: Perspective and Guidelines from the ASNR Vessel Wall Imaging Study Group and Expert Consensus Recommendations of the American Society of Neuroradiology. *AJNR Am J Neuroradiol* 39(2): E9-E31.

Sacco, R. L., S. E. Kasner, J. P. Broderick, L. R. Caplan, J. J. Connors, A. Culebras, M. S. Elkind, M. G. George, A. D. Hamdan, R. T. Higashida, B. L. Hoh, L. S. Janis, C. S. Kase, D. O. Kleindorfer, J. M. Lee, M. E. Moseley, E. D. Peterson, T. N. Turan, A. L. Valderrama, H. V. Vinters, C. o. C. S. American Heart Association Stroke Council, Anesthesia, R. Council on Cardiovascular, Intervention, C. Council on, N. Stroke, E. Council on, Prevention, D. Council on Peripheral Vascular, P. A. Council on Nutrition and Metabolism (2013). An updated definition of stroke for the 21st century: a statement for healthcare professionals from the American Heart Association/American Stroke Association. *Stroke* 44(7): 2064-2089.

Schillinger, M., M. Exner, W. Mlekusch, S. Sabeti, J. Amighi, R. Nikowitsch, E. Timmel, B. Kickinger, C. Minar, M. Pones, W. Lalouschek, H. Rumpold, G. Maurer, O. Wagner and E. Minar (2005). Inflammation and Carotid Artery--Risk for Atherosclerosis Study (ICARAS). *Circulation* 111(17): 2203-2209.

Shreve, P. D., Y. Anzai and R. L. Wahl (1999). Pitfalls in oncologic diagnosis with FDG PET imaging: physiologic and benign variants. *Radiographics* 19(1): 61-77; quiz 150-151.

Siegler, J. E., J. M. Thon, J. H. Woo, D. Do, S. R. Messe and B. Cucchiara (2019). Prevalence of Nonstenotic Carotid Plaque in Stroke Due to Atrial Fibrillation Compared to Embolic Stroke of Undetermined Source. *J Stroke Cerebrovasc Dis* 28(10): 104289.

Silverman, S. (2019). Management of Asymptomatic Carotid Artery Stenosis. *Curr Treat Options Cardiovasc Med* 21(12): 80.

Skretting, A. (2009). 'Intensity diffusion' is a better description than 'partial volume effect'. *Eur J Nucl Med Mol Imaging* 36(3): 536-537.

Skretting, A. (2010a). A method for on-site measurements of the effective spatial resolution in PET image volumes reconstructed with OSEM and Gaussian post-filters. *Radiat Prot Dosimetry* 139(1-3): 195-198.

Skretting, A., O. Glomset and T. V. Bogsrud (2010b). A phantom for investigation of tumour signal and noise in PET reconstruction with various smoothing filters: experiments and comparisons with simulated intensity diffusion. *Radiat Prot Dosimetry* 139(1-3): 191-194.

Slart, R., g. Writing, g. Reviewer, E. C. Members of, E. I. Members of, Inflammation, S. C. Members of Committees, P. E. T. I. G. Members of Council, A. Members of and E. C. Coordinator (2018). FDG-PET/CT(A) imaging in large vessel vasculitis and polymyalgia rheumatica: joint procedural recommendation of the EANM, SNMMI, and the PET Interest Group (PIG), and endorsed by the ASNC. *Eur J Nucl Med Mol Imaging* 45(7): 1250-1269.

Slomka, P. J., T. Pan and G. Germano (2016). Recent Advances and Future Progress in PET Instrumentation. *Semin Nucl Med* 46(1): 5-19.

Sokoloff, L., M. Reivich, C. Kennedy, M. H. Des Rosiers, C. S. Patlak, K. D. Pettigrew, O. Sakurada and M. Shinohara (1977). The [14C]deoxyglucose method for the measurement of local cerebral glucose utilization: theory, procedure, and normal values in the conscious and anesthetized albino rat. *J Neurochem* 28(5): 897-916.

Sols, A. and R. K. Crane (1954). Substrate specificity of brain hexokinase. *J Biol Chem* 210(2): 581-595.

Soret, M., S. L. Bacharach and I. Buvat (2007). Partial-volume effect in PET tumor imaging. *J Nucl Med* 48(6): 932-945.

Sprinz, C., S. Altmayer, M. Zanon, G. Watte, K. Irion, E. Marchiori and B. Hochhegger (2018). Effects of blood glucose level on 18F-FDG uptake for PET/CT in normal organs: A systematic review. *PLoS One* 13(2): e0193140.

Stary, H. C., D. H. Blankenhorn, A. B. Chandler, S. Glagov, W. Insull, Jr., M. Richardson, M. E. Rosenfeld, S. A. Schaffer, C. J. Schwartz, W. D. Wagner and et al. (1992). A definition of the intima of human arteries and of its atherosclerosis-prone regions. A report from the Committee on Vascular Lesions of the Council on Arteriosclerosis, American Heart Association. *Circulation* 85(1): 391-405.

Stary, H. C., A. B. Chandler, R. E. Dinsmore, V. Fuster, S. Glagov, W. Insull, Jr., M. E. Rosenfeld, C. J. Schwartz, W. D. Wagner and R. W. Wissler (1995). A definition of advanced types of atherosclerotic lesions and a histological classification of atherosclerosis. A report from the Committee on Vascular Lesions of the Council on Arteriosclerosis, American Heart Association. *Arterioscler Thromb Vasc Biol* 15(9): 1512-1531.

Stary, H. C., A. B. Chandler, S. Glagov, J. R. Guyton, W. Insull, Jr., M. E. Rosenfeld, S. A. Schaffer, C. J. Schwartz, W. D. Wagner and R. W. Wissler (1994). A definition of initial, fatty streak, and intermediate lesions of atherosclerosis. A report from the Committee on Vascular Lesions of the Council on Arteriosclerosis, American Heart Association. *Arterioscler Thromb* 14(5): 840-856.

Surti, S., A. Kuhn, M. E. Werner, A. E. Perkins, J. Kolthammer and J. S. Karp (2007). Performance of Philips Gemini TF PET/CT scanner with special consideration for its time-of-flight imaging capabilities. *J Nucl Med* 48(3): 471-480.

Surti, S. and J. Scheuermann (2017). Data corrections and quantitative PET *Physics of PET and SPECT Imaging*. M. Dahlbom. Boca Raton, FL, CRC Press, Taylor & Francis Group.

Tahari, A. K., D. Chien, J. R. Azadi and R. L. Wahl (2014). Optimum lean body formulation for correction of standardized uptake value in PET imaging. *J Nucl Med* 55(9): 1481-1484.

Tarkin, J. M., F. R. Joshi, N. R. Evans, M. M. Chowdhury, N. L. Figg, A. V. Shah, L. T. Starks, A. Martin-Garrido, R. Manavaki, E. Yu, R. E. Kuc, L. Grassi, R. Kreuzhuber, M. A. Kostadima, M. Frontini, P. J. Kirkpatrick, P. A. Coughlin, D. Gopalan, T. D. Fryer, J. R. Buscombe, A. M. Groves, W. H. Ouwehand, M. R. Bennett, E. A. Warburton, A. P. Davenport and J. H. Rudd (2017). Detection of Atherosclerotic Inflammation by (68)Ga-DOTATATE PET Compared to [(18)F]FDG PET Imaging. *J Am Coll Cardiol* 69(14): 1774-1791.

Tarkin, J. M., F. R. Joshi and J. H. Rudd (2014). PET imaging of inflammation in atherosclerosis. *Nat Rev Cardiol* 11(8): 443-457.

Tawakol, A., Z. A. Fayad, R. Mogg, A. Alon, M. T. Klimas, H. Dansky, S. S. Subramanian, A. Abdelbaky, J. H. Rudd, M. E. Farkouh, I. O. Nunes, C. R. Beals and S. S. Shankar (2013). Intensification of statin therapy results in a rapid reduction in atherosclerotic inflammation: results of a multicenter fluorodeoxyglucose-positron emission tomography/computed tomography feasibility study. *J Am Coll Cardiol* 62(10): 909-917.

Tawakol, A., R. Q. Migrino, G. G. Bashian, S. Bedri, D. Vermylen, R. C. Cury, D. Yates, G. M. LaMuraglia, K. Furie, S. Houser, H. Gewirtz, J. E. Muller, T. J. Brady and A. J. Fischman (2006). In vivo 18F-fluorodeoxyglucose positron emission tomography imaging provides a noninvasive measure of carotid plaque inflammation in patients. *J Am Coll Cardiol* 48(9): 1818-1824.

Tawakol, A., P. Singh, J. H. Rudd, J. Soffer, G. Cai, E. Vucic, S. P. Brannan, E. A. Tarka, B. C. Shaddinger, L. Sarov-Blat, P. Matthews, S. Subramanian, M. Farkouh and Z. A. Fayad (2014). Effect of treatment for 12 weeks with

rilapladib, a lipoprotein-associated phospholipase A2 inhibitor, on arterial inflammation as assessed with 18F-fluorodeoxyglucose-positron emission tomography imaging. *J Am Coll Cardiol* 63(1): 86-88.

van der Valk, F. M., S. L. Verweij, K. A. Zwinderman, A. C. Strang, Y. Kaiser, H. A. Marquering, A. J. Nederveen, E. S. Stroes, H. J. Verberne and J. H. Rudd (2016). Thresholds for Arterial Wall Inflammation Quantified by 18F-FDG PET Imaging: Implications for Vascular Interventional Studies. *JACC Cardiovasc Imaging* 9(10): 1198-1207.

van der Vos, C. S., D. Koopman, S. Rijnsdorp, A. J. Arends, R. Boellaard, J. A. van Dalen, M. Lubberink, A. T. M. Willemsen and E. P. Visser (2017). Quantification, improvement, and harmonization of small lesion detection with state-of-the-art PET. *Eur J Nucl Med Mol Imaging* 44(Suppl 1): 4-16.

Varrone, A., S. Asenbaum, T. Vander Borght, J. Booij, F. Nobili, K. Nagren, J. Darcourt, O. L. Kapucu, K. Tatsch, P. Bartenstein, K. Van Laere and C. European Association of Nuclear Medicine Neuroimaging (2009). EANM procedure guidelines for PET brain imaging using [18F]FDG, version 2. *Eur J Nucl Med Mol Imaging* 36(12): 2103-2110.

Venermo, M., G. Wang, A. Sedrakyan, J. Mao, N. Eldrup, R. DeMartino, K. Mani, M. Altreuther, B. Beiles, G. Menyhei, G. Danielsson, I. Thomson, G. Heller, C. Setacci, M. Bjorck and J. Cronenwett (2017). Editor's Choice - Carotid Stenosis Treatment: Variation in International Practice Patterns. *Eur J Vasc Endovasc Surg* 53(4): 511-519.

Verel, I., G. W. Visser and G. A. van Dongen (2005). The promise of immuno-PET in radioimmunotherapy. *J Nucl Med* 46 Suppl 1: 164S-171S.

Vesey, A. T., W. S. Jenkins, A. Irkle, A. Moss, G. Sng, R. O. Forsythe, T. Clark, G. Roberts, A. Fletcher, C. Lucatelli, J. H. Rudd, A. P. Davenport, N. L. Mills, R. Al-Shahi Salman, M. Dennis, W. N. Whiteley, E. J. van Beek, M. R. Dweck and D. E. Newby (2017). (18)F-Fluoride and (18)F-Fluorodeoxyglucose Positron Emission Tomography After Transient Ischemic Attack or Minor Ischemic Stroke: Case-Control Study. *Circ Cardiovasc Imaging* 10(3).

Virgolini, I., V. Ambrosini, J. B. Bomanji, R. P. Baum, S. Fanti, M. Gabriel, N. D. Papathanasiou, G. Pepe, W. Oyen, C. De Cristoforo and A. Chiti (2010). Procedure guidelines for PET/CT tumour imaging with 68Ga-DOTA-conjugated peptides: 68Ga-DOTA-TOC, 68Ga-DOTA-NOC, 68Ga-DOTA-TATE. *Eur J Nucl Med Mol Imaging* 37(10): 2004-2010.

Wahl, R. L., C. A. Henry and S. P. Ethier (1992). Serum glucose: effects on tumor and normal tissue accumulation of 2-[F-18]-fluoro-2-deoxy-D-glucose in rodents with mammary carcinoma. *Radiology* 183(3): 643-647.

Walrand, S., M. Hesse and F. Jamar (2018). Update on novel trends in PET/CT technology and its clinical applications. *Br J Radiol* 91(1081): 20160534.

Warburg, O. (1956). On the origin of cancer cells. *Science* 123(3191): 309-314.

Wardlaw, J. M., F. M. Chappell, M. Stevenson, E. De Nigris, S. Thomas, J. Gillard, E. Berry, G. Young, P. Rothwell, G. Roditi, M. Gough, A. Brennan, J. Bamford and J. Best (2006). Accurate, practical and cost-effective assessment of carotid stenosis in the UK. *Health Technol Assess* 10(30): iii-iv, ix-x, 1-182.

World Health Organization. (2017, 2017.17.05). "Cardiovascular diseases." from https://www.who.int/news-room/fact-sheets/detail/cardiovascular-diseases-(cvds).

Wu, Y. W., H. L. Kao, M. F. Chen, B. C. Lee, W. Y. Tseng, J. S. Jeng, K. Y. Tzen, R. F. Yen, P. J. Huang and W. S. Yang (2007). Characterization of plaques using 18F-FDG PET/CT in patients with carotid atherosclerosis and correlation with matrix metalloproteinase-1. *J Nucl Med* 48(2): 227-233.

Yamada, S., K. Kubota, R. Kubota, T. Ido and N. Tamahashi (1995). High accumulation of fluorine-18-fluorodeoxyglucose in turpentine-induced inflammatory tissue. *J Nucl Med* 36(7): 1301-1306.

Yamamoto, T., Y. Seino, H. Fukumoto, G. Koh, H. Yano, N. Inagaki, Y. Yamada, K. Inoue, T. Manabe and H. Imura (1990). Over-expression of facilitative glucose transporter genes in human cancer. *Biochem Biophys Res Commun* 170(1): 223-230.

Zaidi, H. and N. Karakatsanis (2018). Towards enhanced PET quantification in clinical oncology. *Br J Radiol* 91(1081): 20170508.

Zamani, M., K. Skagen, H. Scott, B. Lindberg, D. Russell and M. Skjelland (2019). Carotid Plaque Neovascularization Detected With Superb Microvascular Imaging Ultrasound Without Using Contrast Media. *Stroke* 50(11): 3121-3127.

Zasadny, K. R. and R. L. Wahl (1993). Standardized uptake values of normal tissues at PET with 2-[fluorine-18]-fluoro-2-deoxy-D-glucose: variations with body weight and a method for correction. *Radiology* 189(3): 847-850.

Zhao, S., Y. Kuge, E. Tsukamoto, T. Mochizuki, T. Kato, K. Hikosaka, M. Hosokawa, M. Kohanawa and N. Tamaki (2001). Effects of insulin and glucose loading on FDG uptake in experimental malignant tumours and inflammatory lesions. *Eur J Nucl Med* 28(6): 730-735.

Zhao, S., Y. Kuge, E. Tsukamoto, T. Mochizuki, T. Kato, K. Hikosaka, K. Nakada, M. Hosokawa, M. Kohanawa and N. Tamaki (2002). Fluorodeoxyglucose uptake and glucose transporter expression in experimental inflammatory lesions and malignant tumours: effects of insulin and glucose loading. *Nucl Med Commun* 23(6): 545-550.

Zhuang, H. M., A. Cortes-Blanco, M. Pourdehnad, L. E. Adam, A. J. Yamamoto, R. Martinez-Lazaro, J. H. Lee, J. C. Loman, M. D. Rossman and A. Alavi (2001). Do high glucose levels have differential effect on FDG uptake in inflammatory and malignant disorders? *Nucl Med Commun* 22(10): 1123-1128.

11. PAPERS

I

Carotid plaque inflammation assessed with ^{18}F-FDG PET/CT is higher in symptomatic compared with asymptomatic patients

Karolina Skagen[1]*, Kjersti Johnsrud[2], Kristin Evensen[1], Helge Scott[3], Kirsten Krohg-Sørensen[4], Frode Reier-Nilsen[5], Mona-Elisabeth Revheim[6], Jan Gunnar Fjeld[7], Mona Skjelland[1], and David Russell[1]

Background **Carotid artery plaque inflammation is thought to be an important marker of plaque vulnerability and increased stroke risk.**

Aim **The main aim of this study was to assess the level of agreement between 2-deoxy-2-[^{18}F] fluoro-D-glucose (18F-FDG) uptake on PET (positron emission tomography) scan in carotid plaques, with cerebrovascular symptoms, carotid plaque ultrasound echogenicity and histological assessments of plaque inflammation.**

Methods **Thirty-six patients with ≥70% carotid stenosis scheduled for carotid endarterectomy underwent a Colour Duplex ultrasound, ^{18}F-FDG PET/CT and blood tests less than 24 h prior to surgery. Plaques were defined as symptomatic when associated with ipsilateral cerebral ischemic symptoms within 30 days prior to inclusion. Plaques were assessed histologically following endarterectomy. The level of agreement between ^{18}F-FDG uptake (mean SUV_{max} and SUV_{max}), and target-to-background ratio, symptoms, plaque echolucency, and histological evidence of inflammation was assessed.**

Results **The amount of ^{18}F-FDG uptake in plaques and the amount of inflammation on histological assessment were significantly correlated (r = 0·521, *P* = 0·003). ^{18}F-FDG uptake was significantly higher in symptomatic plaques with median SUV_{max} 1·75 (1·26–2·04) in symptomatic, and 1·43 (1·15–2·28) in asymptomatic patients (*P* = 0·03). ^{18}F-FDG uptake was also positively correlated with echolucency on Doppler ultrasound (*P* = 0·03).**

Conclusion **^{18}F-FDG uptake on PET/CT correlated with histological assessments of inflammation and was higher in patients with symptomatic compared with asymptomatic carotid artery plaques. These results support the use of ^{18}F-FDG PET/CT in the detection inflammation in carotid atherosclerosis, which may be of help in the detection of vulnerable plaques.**

Key words: carotid plaque echogenicity, carotid plaque, carotid stenosis, carotid ultrasound, ischemic stroke, positron emission tomography

Introduction

A significant proportion of strokes are thromboembolic, arising from a vulnerable atherosclerotic plaque at the carotid bifurcation. Such strokes have been shown to be effectively preventable by carotid endarterectomy (CEA) (1,2). In current clinical practice patient selection for revascularization primarily involves identification of the severity of luminal stenosis. It has, however, become increasingly clear that the degree of luminal stenosis alone is not the best predictor of stroke risk and the composition of an atherosclerotic plaque is considered more important. Owing to the process of arterial remodeling, the lumen of an artery may not be compromised despite the presence of a significant atherosclerotic burden with vulnerable plaques prone to rupture (3). Strokes may occur as a result of nonstenotic carotid disease, and conversely, a non-negligible proportion of patients with significant carotid stenosis may remain completely asymptomatic throughout their lifetime (3,4). Identifying markers of plaque destabilization is therefore central for improving treatment decisions and reducing the risk of embolic stroke for patients with carotid artery atherosclerosis. Inflammation is thought to be central in plaque destabilization and has been proposed as a major criterion for defining a high-risk vulnerable plaque (5–7). Due to the infiltration and retention of oxidized lipids in the arterial wall, vulnerable plaques contain a greater density of macrophages compared with asymptomatic plaques (8). Activated macrophages have a significantly increased metabolic rate and therefore increased 2-deoxy-2-[^{18}F] fluoro-D-glucose (^{18}F-FDG) uptake. Rudd *et al.* found increased ^{18}F-FDG in macrophage-rich regions of carotid plaques, removed at endarterectomy, in eight symptomatic patients compared with contralateral asymptomatic plaques in the same patients (9). Tawakol *et al.* demonstrated that *in vivo* ^{18}F-FDG uptake correlated with the degree of plaque inflammation in 17 patients when macrophage staining was assessed histologically (10).

^{18}F-FDG uptake has also been shown to correlate with factors that are associated with plaque vulnerability. Carotid plaques with decreased ultrasound echogenicity and patients with increased serum lipids have been found to have higher degrees of ^{18}F-FDG uptake on PET (11,12). Evidence from longitudinal studies also suggests that arterial ^{18}F-FDG uptake may be related to patient outcome. Figueroa *et al.* followed 513 patients without

Correspondence: Karolina Skagen*, Department of Neurology, Oslo University Hospital and University of Oslo, Oslo, Norway.
E-mail: kskagen@ous-hf.no
[1]Department of Neurology, Oslo University Hospital and University of Oslo, Oslo, Norway
[2]Department of Radiology and Nuclear Medicine, Oslo University Hospital and University of Oslo, Oslo, Norway
[3]Department of Pathology, Oslo University Hospital and University of Oslo, Oslo, Norway
[4]Department of Thoracic Surgery, Oslo University Hospital and University of Oslo, Oslo, Norway
[5]Department of Vascular and Thoracic surgery, Akershus University Hospital, Oslo, Norway
[6]Department of Radiology and Nuclear Medicine, Oslo University Hospital, Oslo, Norway
[7]Department of Radiology and Nuclear Medicine, Oslo University Hospital and Akershus University College of Applied Sciences, Oslo, Norway

Received: 26 August 2014; Accepted: 5 November 2014

Conflict of interest: None declared.

Funding: This research was funded by the National Association of Public Health.

DOI: 10.1111/ijs.12430

symptomatic cardiovascular disease for a mean of 4·2 years. They found that ^{18}F-FDG uptake within the wall of the ascending aorta was an independent predictor of future cardiovascular events (13). Results from The Dublin Carotid Atherosclerosis Stroke Study showed, in 44 patients, that carotid plaque inflammation, measured by ^{18}F-FDG PET, was associated with a high risk of early stroke recurrence, independent of the degree of stenosis (14).

Previous studies have, however, been limited by relatively small sample sizes and time delays of weeks or months from symptoms to ^{18}F-FDG PET imaging and histology following endarterectomy. There is therefore a possibility that plaque inflammation may have been modified by medications and lifestyle changes during time-delays from symptoms to imaging and histological assessments (15,16). Increased ^{18}F-FDG uptake must be closely correlated with ipsilateral ischemic cerebral events and higher in symptomatic compared with asymptomatic patients if this method is to be of value in the clinical management of these patients.

Aim

The main aim of this study was therefore to assess level of agreement between carotid plaque ^{18}F-FDG uptake on PET/CT and histological assessments of the degree of inflammation in plaques from symptomatic and asymptomatic patients.

Methods

Subjects

Consecutive patients with internal carotid artery stenosis ≥70% scheduled for CEA were included in the study from April 2009 to November 2013. Plaques were defined as symptomatic when associated with ipsilateral cerebral ischemia (minor strokes, transitory ischemic attack or amaurosis fugax) within 30 days prior to inclusion. Exclusion criteria were prior CEA, stenting, carotid occlusion, vasculitis, malignancy, prior radiation therapy to the neck, treatment with immunomodulating drugs or oncological disease.

All patients underwent a clinical neurological examination and registration of the following cardiovascular risk factors: hypercholesterolemia, hypertension, coronary artery disease and diabetes. The Regional Committee for Medical and Health Research Ethics (REC) approved the study, and informed written consent was obtained from all patients.

Carotid ultrasound

Colour duplex ultrasound was performed with a General Electric Vivid 7 (General Electric, Horten, Norway) using a M12L probe (14 MHz) on both carotid arteries. The degree of stenosis was based on velocities according to consensus criteria of the Society of Radiologists in Ultrasound (17). Plaque echogenicity was assessed with the vessel lumen as the reference structure for defining echolucency, and the bright echo zone produced by the media-adventitia interface as the reference for defining echogenicity (18–20). Echogenicity was graded from 1 to 4 as: echolucent, predominantly echolucent, predominantly echogenic, or echogenic by an experienced examiner blinded for the PET results (18).

^{18}F-FDG PET/CT

Patients were examined with a hybrid PET/CT scanner (Siemens Biograph 64, Siemens Medical Systems, Erlangen, Germany). After an overnight fast (minimum six-hours), an ^{18}F-FDG PET/CT was performed from the base of the skull to the aortic arch, approximately 90 mins after the injection of 5Mbq/kg ^{18}F-FDG Blood glucose levels were measured. The PET data were reconstructed to 2 mm thick slices with a matrix size of 256 x 256 pixels (pixel size 2·67 mm) using the OSEM 2D algorithm with four iterations (i), eight subsets (s) (4i/8s), and Gaussian post-reconstruction filter with full-width at half maximum (FWHM) of 3·5 mm (21). A CT without contrast for attenuation correction was performed immediately before the PET scan with the patient in the same position. A contrast-enhanced CT of the carotid arteries was also performed on those patients that did not have a recent CT angiography available. The contrast-enhanced CT was used for localizing the carotid artery plaque. A specialist in nuclear medicine blinded for patient data placed the regions of interest (ROI). The contrast-enhanced CT angiography was used as a guide for drawing the ROI on the PET slice (fused with noncontrast CT). ROIs covering the whole plaque including vessel wall thickening and the lumen contrast-filling defect (22) were drawn on each axial slice from the most cranial to the most caudal slice of the plaque. The ROI was minimized to only cover parts of the plaque uptake when nearby ^{18}F-FDG activity, e.g. lymph nodes, paravertebral muscles or salivary glands could have influenced the measured ^{18}F-FDG activity in the ROIs. Four ROIs were placed in the lumen of the jugular vein close to the plaque for calculation of the target-to-background ratio (TBR). Maximum standardized uptake values (SUV_{max}); the highest activity concentration per injected dose per lean body mass (lbm – a factor derived from each patients height, weight and gender) after correction for decay in each ROI were measured. SUV normalized to lbm is an established parameter for the quantification of ^{18}F-FDG uptake (23). The following uptake parameters were used for the statistical analysis for each plaque: (1) SUV_{max} = the single highest SUV_{max} value, (2) Mean SUV_{max} = mean of all plaque SUV_{max} values, (3) TBR = mean SUV_{max} divided by mean SUV_{mean} in the four venous regions.

Tissue processing and histological analysis

The plaques were removed en bloc (intact) at CEA, fixed in 4% formaldehyde, decalcified in ethylenediaminetetraacetic acid, and cut into 2–3 mm slices. After dehydration the slices were embedded in paraffin, and histological sections were cut at 5 µm and stained with hematoxylin and eosin. Plaques were assessed by a pathologist and a research physician blinded for clinical and ^{18}F-FDG PET findings. A section from each slice was evaluated with 120 times magnification and the percentage of inflammatory cells (macrophages and leukocytes) was estimated as the area with inflammatory cells as a percentage of the total area. The amount of inflammation per plaque was calculated as the sum of all areas with inflammatory activity divided by the total area of the sections to give a percentage of inflammatory cells per plaque. This method for evaluating and grading inflammation has been shown to have good to excellent intra- and inter-rater variability (24).

Histological assessments were made on 11 slices from three plaques on two occasions more than two-months apart to assess the reproducibility of the findings. For this analysis the percentage inflammatory cells per slice was classified into the following categories: 0–5%, 5–10%, 10–15% and 15–20% and the results assessed using Kappa statistics.

Statistical analysis

SPSS for Windows statistical software (version 18·0; SPSS Inc., Chicago, IL) was used for data analysis. Student's *t* test or Mann–Whitney *U*-test was used depending on the distribution of data. The chi-square test was used for analyzing contingency data. Coefficients of correlation were calculated by the Spearman correlation. All statistical results were considered significant when $P < 0{\cdot}05$.

Results

Clinical characteristics

Thirty-six patients took part in the study. There were 26 men (66·8 ± 9 years) and 10 women (67·9 ± 7 years). Eighteen patients were symptomatic, and 18 patients asymptomatic. Plaques were not delivered for histology after endarterectomy due to practical reasons in six patients; four of these were in the symptomatic and two were in the asymptomatic group. All other data from these patients were retained in the analyses. Clinical characteristics of the patients are shown in Table 1. There were no statistically significant differences between the symptomatic and asymptomatic patients with respect to age or gender. Mean age was 67·5 years in the symptomatic group and 66·7 in the asymptomatic group. Thirteen patients (72·2%) were male in both groups. For symptomatic patients ($n = 18$), mean time from last symptom to CEA was 12 days ranging from 3 to 30 days. Although not reaching statistical significance, patients in the symptomatic group had higher average plasma leukocyte levels at 9·2 10 × 9/L compared with 7·6 10 × 9/L in the asymptomatic group ($P = 0{\cdot}05$). Plasma levels of CRP, total cholesterol, low-density lipoprotein (LDL), high-density lipoprotein (HDL) and glucose were similar in the two groups.

Plaque inflammation on histological analysis and correlation to ^{18}F-FDG uptake and echogenicity on ultrasound

There was a significant correlation (Fig. 1) between the amount of inflammation on histology and all ^{18}F-FDG uptake parameters (mean SUV_{max} $P = 0{\cdot}003$, SUV_{max} $P = 0{\cdot}009$ and TBR $P = 0{\cdot}002$).

Higher amounts of inflammation on histology were also significantly correlated with low echogenicity on carotid Doppler ultrasound ($P = 0{\cdot}014$).

When the histopathological assessments were repeated on two occasions more than two-months apart we found that the amount of inflammatory cells was in the same 5% category at both assessment for 8 of 11 slices (73%, Kappa = 0·73).

^{18}F-FDG uptake and correlation to clinical symptoms

Figure 2 shows that the amount of ^{18}F-FDG uptake measured by mean SUV_{max} was significantly higher in symptomatic compared with asymptomatic plaques (Fig. 4). Median mean SUV_{max} in the symptomatic group was 1·75 (range: 1·26–2·04) compared with 1·43 (range: 1·15–2·28) in the asymptomatic group. This difference was statistically significant with $P = 0{\cdot}03$. TBR was not significantly higher in the symptomatic compared with asymptomatic patients. The highest mean SUV_{max} 2·28 was measured in an asymptomatic patient.

^{18}F-FDG uptake and correlation to echogenicity on ultrasound

There was a positive correlation for mean SUV_{max} and low echolucency on carotid Doppler ultrasound ($r = 0{\cdot}378$, $P < 0{\cdot}03$) (Fig. 3). Mean SUV_{max} was significantly increased ($P = 0{\cdot}028$) for echolucent plaques 1·67 (1·2–2·28) compared with echogenic plaques 1·5 (1·2–2·04). Mean SUV_{max} remained significantly higher in echolucent plaques compared with predominantly echolucent plaques ($P = 0{\cdot}01$). Lower ultrasound echogenicity was associated with a higher TBR values ($P = 0{\cdot}005$).

Table 1 Clinical characteristics of symptomatic and asymptomatic patients

	Symptomatic ($n = 18$)	Asymptomatic ($n = 18$)	*P*
Age, yrs; (mean ± SD)	67·5 ± 9·5	66·7 ± 7·2	0·77
Gender, male; *n* (%)	13 (72·2)	13 (72·2)	1·00
Hypercholesterolemia, no of patients	13 (72·2)	14 (77·8)	0·60
Antihypertensive medication, yes	10 (55·6)	12 (66·7)	0·56
Coronary artery disease, no of patients	4 (22·2)	10 (55·6)	0·04
Diabetes, yes	2 (14·3)	3 (16·7)	0·68
Plasma levels: (mean ± SD)			
Leukocytes, 10 × 9/l	9·2 ± 2·4	7·6 ± 1·9	0·05
CRP, mg/l	11·2 ± 27	4·9 ± 4·5	0·44
Cholesterol mmol/l	4·9 ± 1·5	4·0 ± 0·8	0·17
LDL, mmol/l	3·1 ± 1·4	2·0 ± 0·6	0·06
HDL, mmol/l	1·22 ± 0·6	1·1 ± 0·7	0·84
Glucose, mmol/l	5·9 ± 0·8	6·5 ± 2·2	0·33

CRP, high sensitivity C- reactive protein; LDL, low density lipoprotein; HDL, high density lipoprotein.

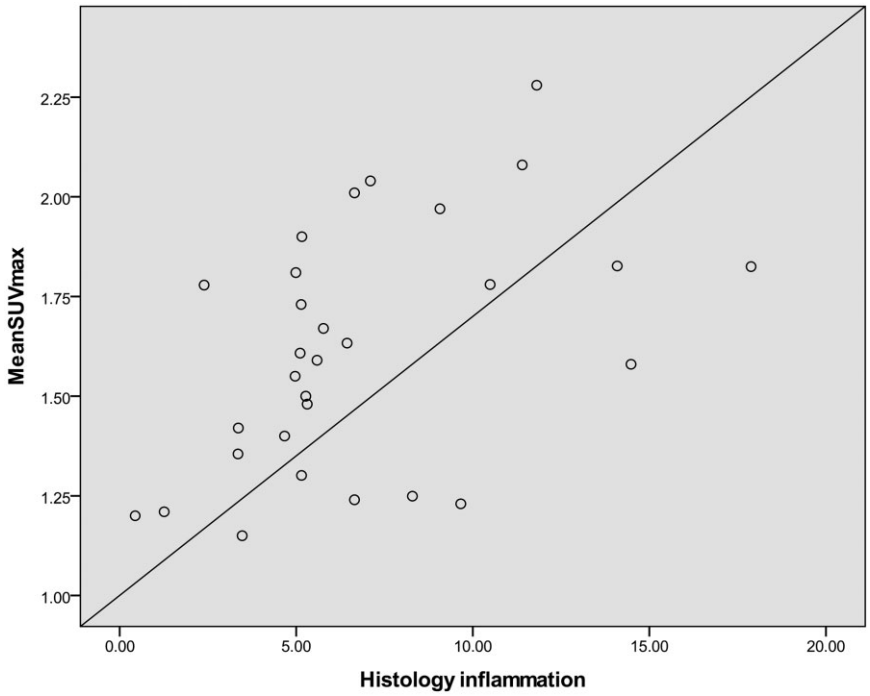

Fig. 1 Correlations between mean SUV_{max} values and percentage plaque inflammation on histology. $P = 0{\cdot}003$. SD, standard deviation.

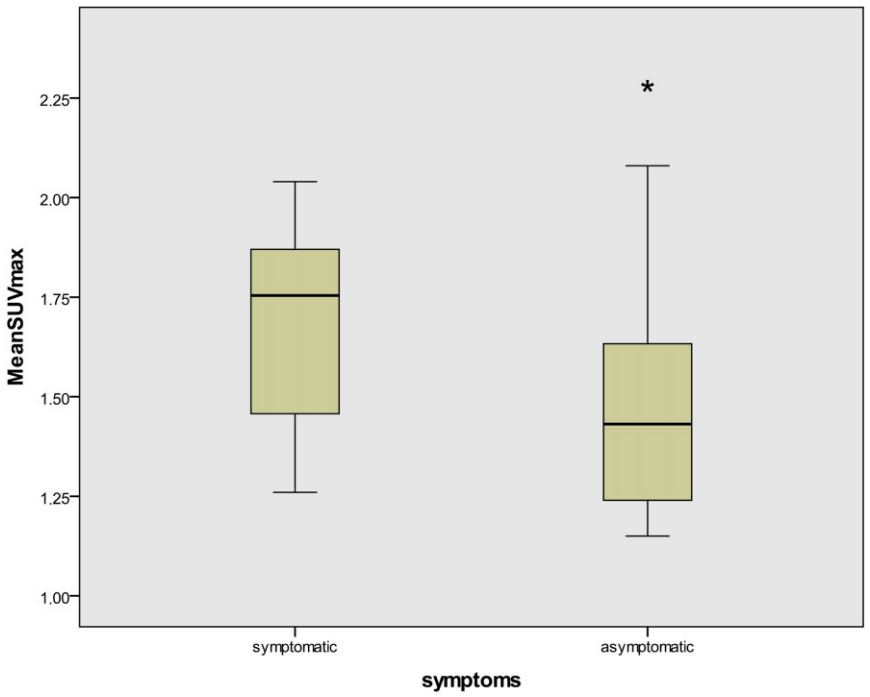

Fig. 2 Box plot showing distribution of FDG uptake values (median mean SUV_{max}) in symptomatic and asymptomatic patients. The bottom and top of the box represent the first and third quartile. Horizontal lines in boxes represent the median value (second quartile) and the whiskers the range limits. Median mean SUV_{max} was 1·68 (range 1·26–2·04) in symptomatic compared with 1·52 (1·15–2·28) in asymptomatic patients ($P = 0{\cdot}03$). The *P*-value is from a Mann–Whitney *U*-test. *Represents the outlier in the asymptomatic patient group.

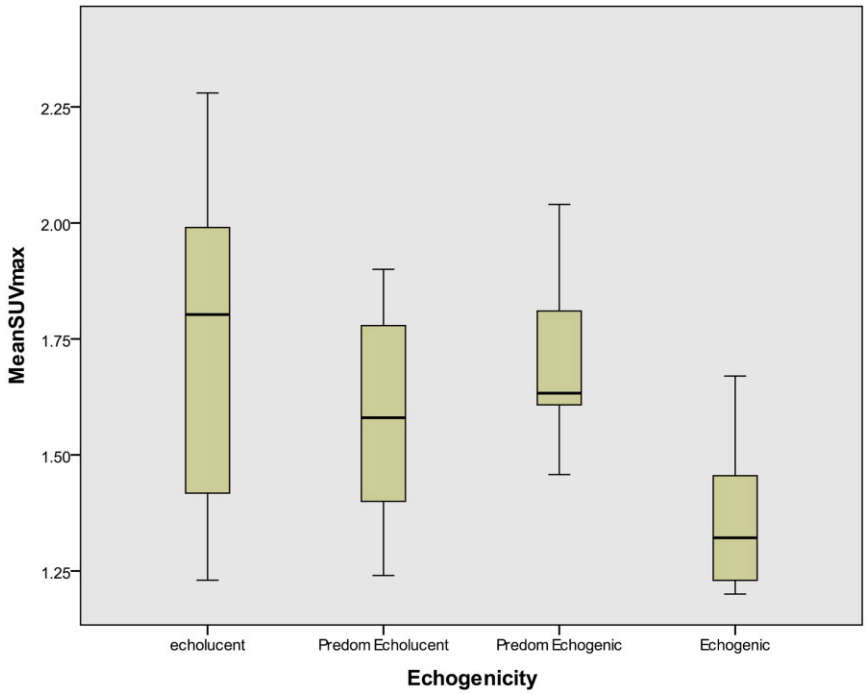

Fig. 3 Correlation of mean SUV_{max} and plaque ultrasound echogenicity. Box plot showing distribution of FDG uptake values (median mean SUVmax) and ultrasound echogenicity Horizontal lines in boxes represent the median value and the whiskers the range limits. Mean SUV_{max} was significantly increased ($P = 0{\cdot}028$) for echolucent plaques; 1·67 (1·2–2·28) compared with echogenic plaques; 1·5 (1·2–2·04). Echolucent vs. Echogenic plaques ($P = 0{\cdot}028$). SUV, standardized uptake value; Predom, predominantly.

Discussion

In this study we found a significantly higher ^{18}F-FDG uptake in carotid artery plaques from symptomatic compared with those from asymptomatic patients. There was also a significant correlation between the amount of inflammation on plaque histology and ^{18}F-FDG uptake.

The findings of increased ^{18}F-FDG uptake in symptomatic carotid artery plaques in this study confirm the results of previous reports (9–11). Rudd *et al.* found higher ^{18}F-FDG uptake-values in carotid plaques obtained from patients with clinical evidence of plaque instability (9). In this small study histological assessments of the degree of plaque inflammation were not carried out and the relationship between inflammation and ^{18}F-FDG uptake was therefore not established. This association was first demonstrated by Tawakol *et al.* who found that histological evidence of plaque inflammation correlated with the degree of ^{18}F-FDG uptake (10). However, the time from the ^{18}F-FDG examinations and the histological assessments in this study was up to one-month and a change in the inflammatory status of the plaques during this time interval can therefore not be excluded.

To our knowledge, this is the first study, which has, in addition to demonstrating higher ^{18}F-FDG uptake values in plaques from symptomatic compared with asymptomatic patients also found a correlation between ^{18}F-FDG uptake and the degree of plaque inflammation on histological assessment. Higher ^{18}F-FDG uptake was demonstrated in plaques from symptomatic patients for both mean SUV_{max} and SUV_{max} values. These results show the potential of ^{18}F-FDG PET for evaluating carotid atherosclerosis with higher ^{18}F-FDG uptake in vulnerable plaques, which have a higher risk of causing embolic stroke. There are at present no established 18F-FDG uptake limits that can be used to detect vulnerable carotid artery plaques. In this study, the range of SUV_{max} values, although significantly higher in symptomatic patients, overlapped in the two groups with the highest mean SUVmax uptake being recorded in a patient without symptoms. This patient was imaged 100 mins after 18-FDG injection and the increased 18-FDG uptake can therefore not be explained by longer circulation time of ^{18}F-FDG. Despite not reporting cerebrovascular symptoms, this patient had findings on magnetic resonance imaging (MRI) consistent with a small cerebral infarction in the ipsilateral cerebral hemisphere. This plaque had also low ultrasound echogenicity and a high inflammatory content on histology, which increases the probability that this was a vulnerable plaque. White matter lesions on cerebral MRI are known to indicate higher risk of stroke (25). Labeling carotid plaques as vulnerable in asymptomatic patients when the patient has ipsilateral silent brain infarcts on cerebral MRI imaging should therefore be considered in future studies where the aim is to identify unstable plaques.

In current studies different measurements of uptake are being used to quantify arterial^{18}F-FDG uptake (9,10,12,26). In this study, blood background corrected TBR assessments of ^{18}F-FDG uptake did not show an association between FDG uptake and symptoms. This may be due to the early timing of PET/CT imaging in this study relative to the time of ^{18}F-FDG injection. Previous studies have found that TBR was a reliable and reproducible parameter when quantifying arterial ^{18}F-FDG uptake in late (>90 mins) acquisitions, but not for early imaging within

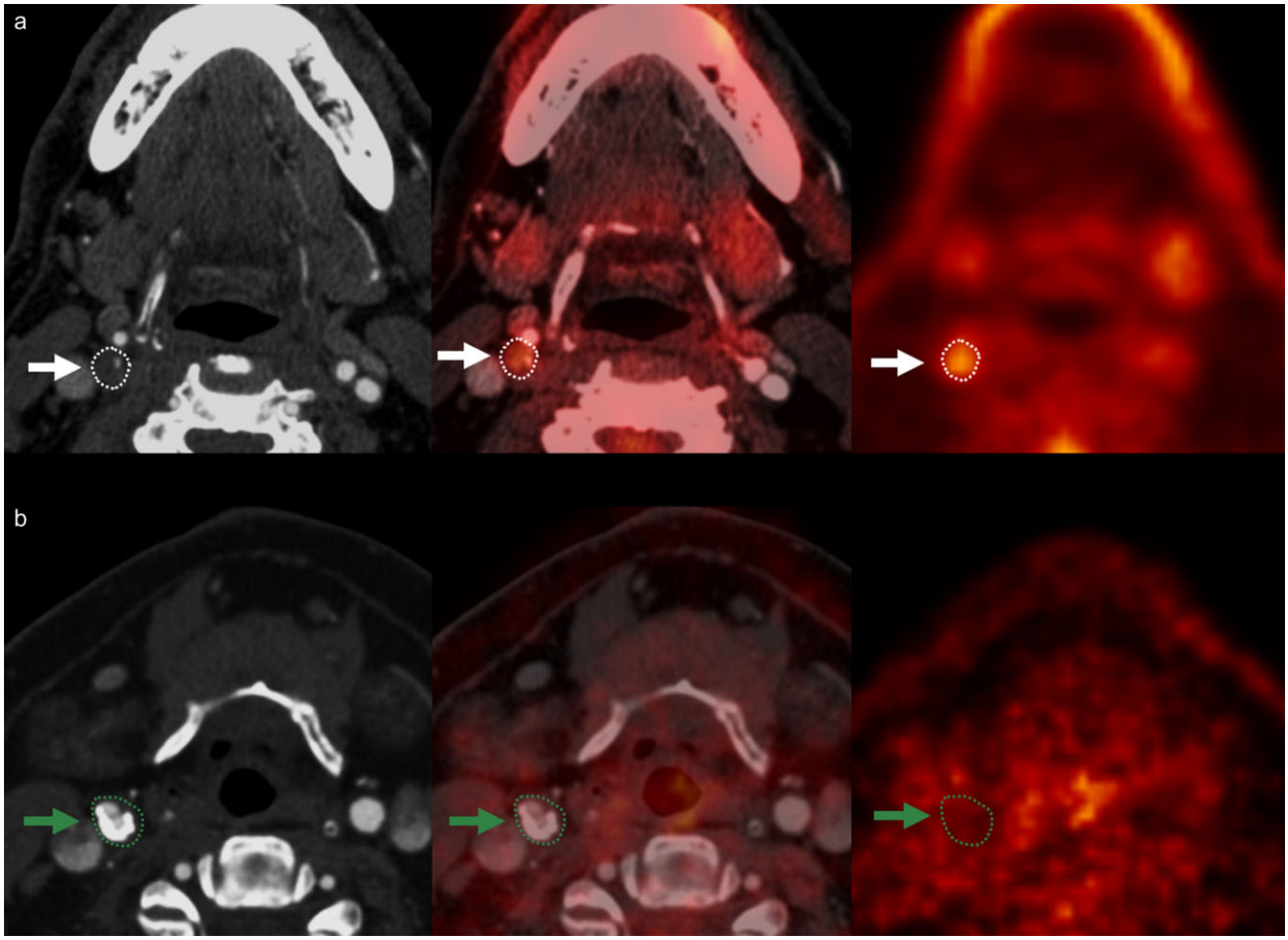

Fig. 4 ^{18}F-FDG PET/CT images of carotid artery plaques from symptomatic (a) and asymptomatic (b) patients. From left to right the images shown are contrast-enhanced CT, co-registered PET/CT and PET. Patient a has a noncalcified plaque with a high degree stenosis in the right internal carotid artery (white circle). The small white spot inside the circle on the CT image is contrast media in the stenotic ICA. The plaque had a high focal ^{18}F-FDG uptake (orange spot on PET images). The plaque was also echolucent on ultrasound and showed a large amount of inflammation on histology. Patient b has a calcified plaque in the right bifurcation (green circle) with no focal ^{18}F-FDG uptake. The plaque was echogenic on ultrasound and showed a small amount of inflammation on histology.

90 mins of ^{18}F-FDG injection (22). Graebe *et al.* compared ^{18}F-FDG uptake at one-hour and three-hours after ^{18}F-FDG injection in 19 patients and concluded that TBR measurements, using venous blood pool activity as background were not accurate for early scans (imaging <90 mins of ^{18}F-FDG injection) because of a mismatch observed in the relative ^{18}F-FDG plaque uptake between the two time-points; TBR values generally increases over time as blood pool activity decreased (22).

The method used in our histological evaluations allows the assessment of the total amount of inflammatory cells in the plaque, including both macrophages and leucocytes. Several methods have previously been described for estimating plaque inflammation histologically. These have included counting labeled macrophages (9–11). Leukocytes are also hypermetabolic cells that increase ^{18}F-FDG uptake. We therefore assessed both macrophage and leukocyte activity, as we believe that this is more accurate when comparing histological evidence of inflammation with ^{18}F-FDG uptake. All methods that are used to correlate histological findings with ^{18}F-FDG uptake on PET/CT imaging have, however, potential weaknesses. Despite careful removal of the plaque at surgery, fragmentation of the CEA specimen is sometimes unavoidable resulting in a reduction of the observed amount of inflammation on histology.

We found that ^{18}F-FDG uptake was higher in plaques with low ultrasound echogenicity compared with those with high ultrasound echogenicity. This is in agreement with previous reports that have found that echolucent plaques are associated with both an increased risk of ipsilateral cerebrovascular events and increased presence of plaque macrophages on histology, independent of the degree of artery stenosis (18,27). Graebe *et al.* also found that echolucency on ultrasound correlated with ^{18}F-FDG uptake on PET (26). We did not find more patients who had plaques with low echogenicity in the symptomatic compared with the asymptomatic group. This may be explained by the sample size, which was underpowered to show such a difference.

Patients in the symptomatic group had higher LDL levels compared with patients in the asymptomatic group (mean 3·1 vs. 2·0 mml/l), approaching statistical significance ($P = 0{\cdot}06$). The number of patients on statin therapy was, however, comparable for the two groups with 13 patients in the symptomatic group

taking statins, compared to 14 in the asymptomatic group. Chronin *et al.* found that increased ^{18}F-FDG uptake was associated with increased LDL, cholesterol and triglycerides and decreased high-density lipoprotein values. They suggested that increased LDL and cholesterol contribute to plaque inflammation (12). LDL and cholesterol are key mediators of inflammation, and studies have found that increased ^{18}F-FDG uptake correlated with an atherosclerotic lipid core, macrophage infiltration and matrix metalloproteinase immunoreactivity (10,28). Modifying atherosclerosis with statins and other anti-atherogenic therapy may also reduce plaque ^{18}F-FDG uptake (15).

In conclusion this study provides further evidence supporting the use of ^{18}F-FDG PET/CT for the detection of inflammation in vulnerable atherosclerotic plaques. Confirmation of this method in larger prospective clinical studies is, however, needed to clarify if ^{18}F-FDG PET/CT may be used to predict outcome in atherosclerotic carotid artery disease, especially in asymptomatic subjects and patients with less severe stenosis.

Acknowledgement

The authors would like to acknowledge the contribution from Are Pripp, PhD, University of Oslo, Department of Biostatistics.

References

1 Barnett HJ, Taylor DW, Eliasziw M *et al.* Benefit of carotid endarterectomy in patients with symptomatic moderate or severe stenosis. North American Symptomatic Carotid Endarterectomy Trial Collaborators. *N Engl J Med* 1998; **339:**1415–25.
2 European Carotid Surgery Trialists' Collaborative Group. Randomised trial of endarterectomy for recently symptomatic carotid stenosis: final results of the MRC European Carotid Surgery Trial (ECST). *Lancet* 1998; **351:**1379–87.
3 Trivedi RA, U-King-Im JM, Graves MJ, Gillard J, Kirkpatrick PJ. Non-stenotic ruptured atherosclerotic plaque causing thrombo-embolic stroke. *Cerebrovasc Dis* 2005; **20:**53–5.
4 Halliday A, Mansfield A, Marro J *et al.* Prevention of disabling and fatal strokes by successful carotid endarterectomy in patients without recent neurological symptoms: randomised controlled trial. *Lancet* 2004; **363:**1491–502.
5 Libby P. Inflammation in atherosclerosis. *Nature* 2002; **420:**868–74.
6 Virmani R, Ladich ER, Burke AP, Kolodgie FD. Histopathology of carotid atherosclerotic disease. *Neurosurgery* 2006; **59**(5 Suppl. 3)**:**S219–27, discussion S3–13.
7 Naghavi M, Libby P, Falk E *et al.* From vulnerable plaque to vulnerable patient: a call for new definitions and risk assessment strategies: part II. *Circulation* 2003; **108:**1772–8.
8 Virmani R, Burke AP, Farb A, Kolodgie FD. Pathology of the vulnerable plaque. *J Am Coll Cardiol* 2006; **47**(8 Suppl.)**:**C13–8.
9 Rudd JH, Warburton EA, Fryer TD *et al.* Imaging atherosclerotic plaque inflammation with [18F]-fluorodeoxyglucose positron emission tomography. *Circulation* 2002; **105:**2708–11.
10 Tawakol A, Migrino RQ, Bashian GG *et al.* In vivo 18F-fluorodeoxyglucose positron emission tomography imaging provides a noninvasive measure of carotid plaque inflammation in patients. *J Am Coll Cardiol* 2006; **48:**1818–24.
11 Graebe M, Pedersen SF, Borgwardt L, Hojgaard L, Sillesen H, Kjaer A. Molecular pathology in vulnerable carotid plaques: correlation with [18]-fluorodeoxyglucose positron emission tomography (FDG-PET). *Eur J Vasc Endovasc Surg* 2009; **37:**714–21.
12 Chroinin DN, Marnane M, Akijian L *et al.* Serum lipids associated with inflammation-related PET-FDG uptake in symptomatic carotid plaque. *Neurology* 2014; **82:**1693–9.
13 Figueroa AL, Abdelbaky A, Truong QA *et al.* Measurement of arterial activity on routine FDG PET/CT images improves prediction of risk of future CV events. *JACC Cardiovasc Imaging* 2013; **6:**1250–9.
14 Marnane M, Merwick A, Sheehan OC *et al.* Carotid plaque inflammation on 18F-fluorodeoxyglucose positron emission tomography predicts early stroke recurrence. *Ann Neurol* 2012; **71:**709–18.
15 Tahara N, Kai H, Ishibashi M *et al.* Simvastatin attenuates plaque inflammation: evaluation by fluorodeoxyglucose positron emission tomography. *J Am Coll Cardiol* 2006; **48:**1825–31.
16 Lee SJ, On YK, Lee EJ, Choi JY, Kim BT, Lee KH. Reversal of vascular 18F-FDG uptake with plasma high-density lipoprotein elevation by atherogenic risk reduction. *J Nucl Med* 2008; **49:**1277–82.
17 Grant EG, Benson CB, Moneta GL *et al.* Carotid artery stenosis: gray-scale and Doppler US diagnosis–Society of Radiologists in Ultrasound Consensus Conference. *Radiology* 2003; **229:**340–6.
18 Mathiesen EB, Bonaa KH, Joakimsen O. Echolucent plaques are associated with high risk of ischemic cerebrovascular events in carotid stenosis: the tromso study. *Circulation* 2001; **103:**2171–5.
19 Nordestgaard BG, Gronholdt ML, Sillesen H. Echolucent rupture-prone plaques. *Curr Opin Lipidol* 2003; **14:**505–12.
20 European Carotid Plaque Study Group. Carotid artery plaque composition – relationship to clinical presentation and ultrasound B-mode imaging. European Carotid Plaque Study Group. *Eur J Vasc Endovasc Surg* 1995; **10:**23–30.
21 Boellaard R, O'Doherty MJ, Weber WA *et al.* FDG PET and PET/CT: EANM procedure guidelines for tumour PET imaging: version 1·0. *Eur J Nucl Med Mol Imaging* 2010; **37:**181–200.
22 Graebe M, Borgwardt L, Hojgaard L, Sillesen H, Kjaer A. When to image carotid plaque inflammation with FDG PET/CT. *Nucl Med Commun* 2010; **31:**773–9.
23 Shankar LK, Hoffman JM, Bacharach S *et al.* Consensus recommendations for the use of 18F-FDG PET as an indicator of therapeutic response in patients in National Cancer Institute Trials. *J Nucl Med* 2006; **47:**1059–66.
24 Mannon RB, Matas AJ, Grande J *et al.* Inflammation in areas of tubular atrophy in kidney allograft biopsies: a potent predictor of allograft failure. *Am J Transplant* 2010; **10:**2066–73.
25 Vermeer SE, Hollander M, van Dijk EJ *et al.* Silent brain infarcts and white matter lesions increase stroke risk in the general population: the Rotterdam Scan Study. *Stroke* 2003; **34:**1126–9.
26 Graebe M, Pedersen SF, Hojgaard L, Kjaer A, Sillesen H. 18FDG PET and ultrasound echolucency in carotid artery plaques. *JACC Cardiovasc Imaging* 2010; **3:**289–95.
27 Gronholdt ML, Nordestgaard BG, Bentzon J *et al.* Macrophages are associated with lipid-rich carotid artery plaques, echolucency on B-mode imaging, and elevated plasma lipid levels. *J Vasc Surg* 2002; **35:**137–45.
28 Shaw JA, Bobik A, Murphy A *et al.* Infusion of reconstituted high-density lipoprotein leads to acute changes in human atherosclerotic plaque. *Circ Res* 2008; **103:**1084–91.

II

^{18}F-FDG PET/CT for the quantification of inflammation in large carotid artery plaques

Kjersti Johnsrud, MD,[a,b] Karolina Skagen, MD, PhD,[c] Therese Seierstad, PhD, MHA,[a] Mona Skjelland, MD, PhD,[c] David Russell, MD, PhD,[b,c] and Mona-Elisabeth Revheim, MD, PhD[a,b]

[a] Division of Radiology and Nuclear Medicine, Oslo University Hospital, Oslo, Norway
[b] Institute of Clinical Medicine, University of Oslo, Oslo, Norway
[c] Department of Neurology, Oslo University Hospital, Oslo, Norway

Received Mar 6, 2017; accepted Oct 19, 2017
doi:10.1007/s12350-017-1121-7

Background. **There is currently no consensus on the methodology for quantification of ^{18}F-FDG uptake in inflammation in atherosclerosis. In this study, we explore different methods for quantification of ^{18}F-FDG uptake in carotid atherosclerotic plaques and correlate the uptake values to histological assessments of inflammation.**

Methods and Results. **Forty-four patients with atherosclerotic stenosis ≥70% of the internal carotid artery underwent ^{18}F-FDG PET/CT. Maximum standardized uptake values (SUV_{max}) from all plaque-containing slices were collected. SUV_{max} for the single highest and the mean of multiple slices with and without blood background correction (by subtraction (cSUV) or by division (target-to-background ratio (TBR)) were calculated. Following endarterectomy 30 plaques were assessed histologically. The length of the plaques at CT was 6-32 mm. The ^{18}F-FDG uptake in the plaques was 1.15-2.66 for uncorrected SUVs, 1.16-3.19 for TBRs, and 0.20-1.79 for cSUVs. There were significant correlations between the different uptake values (r = 0.57-0.99, P < 0.001). Methods with and without blood background correction showed similar, moderate correlations to the amount of inflammation assessed at histology (r = 0.44-0.59, P < 0.02).**

Conclusions. **In large stenotic carotid plaques, ^{18}F-FDG uptake reflects the inflammatory status as assessed at histology. Increasing number of PET slices or background correction did not change the correlation. (J Nucl Cardiol 2019;26:883–93.)**

Key Words: ^{18}F-FDG PET/CT • carotid plaque • atherosclerosis • inflammation • quantification method

Abbreviations

PET	Positron emission tomography	ROI	Region of interest
^{18}F-FDG	2-deoxy-2-(^{18}F)-fluoro-D-glucose	MDS	Most diseased segment
SUV_{max}	Maximum standardized uptake value	TBR	Target-to-background ratio
		cSUV	Corrected SUV

Electronic supplementary material The online version of this article (https://doi.org/10.1007/s12350-017-1121-7) contains supplementary material, which is available to authorized users.

The authors of this article have provided a PowerPoint file, available for download at SpringerLink, which summarises the contents of the paper and is free for re-use at meetings and presentations. Search for the article DOI on SpringerLink.com

David Russell and Mona-Elisabeth Revheim have contributed equally to this work.

Funding This project received funding from the South-Eastern Norway Regional Health Authority and the National Association of Public Health.

Reprint requests: Kjersti Johnsrud, MD, Division of Radiology and Nuclear Medicine, Oslo University Hospital, Postbox 4950, Nydalen, 0424 Oslo, Norway; *kjersti@slogum.no*

1071-3581/$34.00

See related editorial, pp. 894–898

INTRODUCTION

Inflammation is a key factor in the pathophysiology of atherosclerosis with regard to progression and destabilization of plaques.[1] Patients with unstable carotid plaques have increased risk of plaque rupture and ischemic stroke,[2,3] and there is increasing interest in imaging carotid plaque inflammation in order to detect these unstable plaques.

Positron emission tomography (PET) imaging with 2-deoxy-2-(^{18}F)-fluoro-D-glucose (^{18}F-FDG) of inflammation in atherosclerotic plaques has rapidly evolved since Rudd et al first reported ^{18}F-FDG accumulation in macrophage-rich areas of carotid artery plaques over a decade ago.[4] In contrast to oncology,[5] there is no consensus on methodological guidelines for ^{18}F-FDG PET/CT in atherosclerosis imaging. A recent position paper from the Cardiovascular Committee of the European Association of Nuclear Medicine[6] proposed optimized and standardized protocols for the imaging and interpretation of ^{18}F-FDG PET scans in atherosclerosis. However, they admitted that many of the recommendations suffer from the absence of conclusive evidence. Compared to a solid tumor, the cells responsible for ^{18}F-FDG uptake in carotid artery plaques are generally fewer, more dispersed, and spread around parts of the circumference of a tubular vascular structure.[3,7] Consequently, limited spatial resolution of the PET scanner and blood background activity are of great concern. Two parallel phenomena are known to influence measured activity in a lesion:[8] signal from the lesion lost to the surroundings (spill-out), and signal added to the lesion from the vessel lumen and adjacent anatomic structures (spill-in).[8,9]

Different acquisition protocols and quantification methods have been suggested.[10-17] They all address the same concerns but have diverging solutions. A literature search identified 53 different acquisition protocols, 51 different reconstruction protocols, and 46 different quantification methods used in 49 studies.[9] The most common measure is the mean of all the maximum standardized uptake values (SUVs) (mean SUV_{max}) of the regions of interest (ROIs). The ROIs include the whole plaque (in localized stenosis), or one or more vessel segments (in subclinical/generalized disease). Bural et al calculated the atherosclerotic burden of the aorta by multiplying the mean uptake values for each aorta segment with the vessel wall volume.[18] Subanalysis looking for the most metabolically active areas of a vessel segment have been used in therapy response studies.[16] The uptake values are either normalized to the blood background activity,[15,17,19,20] corrected for the background activity with subtraction[11] or not corrected for background activity.[13,21,22] The rationale for background correction has been strongly criticized.[9,23]

The aim of this study was to explore different methods for the quantification of ^{18}F-FDG uptake in large carotid artery plaques, and to correlate the uptake values to the amount of inflammation on histology.

METHODS

Study Population

Forty-four patients referred to the Department of Neurology at our institution for the evaluation of carotid artery disease were included (Table 1). Inclusion criteria were ultrasound-confirmed atherosclerosis with internal carotid artery stenosis $\geq$ 70% according to consensus criteria of the Society of Radiologists in Ultrasound.[24] Exclusion criteria were prior carotid endarterectomy/angioplasty with stenting, carotid occlusion, vasculitis, malignancy, prior radiation therapy to the neck, or immunotherapy. The Regional Committee for Medical and Health Research Ethics approved the study and all patients provided informed written consent.

Of the 44 included patients, 38 underwent carotid endarterectomy due to ipsilateral ischemic events or as prophylactic treatment before heart surgery. Eight of these plaques were lost to histological assessment due to logistical reasons.

^{18}F-FDG PET/CT Examination

Following overnight fasting blood glucose level was measured before the patient received *i.v.* injection of 5 MBq/

Table 1. Patient characteristics (n = 44)

Age, years; mean ± SD	66.3±8.4
Sex, male; *n* (%)	30 (68.2)
Statin therapy; *n* (%)	34 (77.3)
Blood glucose, mmol L^{-1}; mean ± SD (range)	6.8 ± 2.2 (4.9-14.9)
Bodyweight, kg; mean ± SD (range)	83.5 ± 16 (55-110)
Body mass index, kg/m^2; mean ± SD (range)	27.4 ± 4.5 (19.9-34.8)

A subgroup of the patient material is included in a previously published study.[25]

kg (0.14 mCi/kg). After a mean circulation time of 100 minutes (range 68-156), a ^{18}F-FDG PET/CT scan from the base of the skull to the aortic arch was performed with 15 minutes per bed position using a hybrid PET/CT scanner (Siemens Biograph 64, Siemens Medical Systems, Erlangen, Germany). The PET data were reconstructed to 2-mm slices with a pixel size of 2.67 mm using the ordered subset expectation-maximization 2D algorithm with four iterations (i), eight subsets (s)(4i/8s), and Gaussian post-reconstruction filter with full-width at half maximum of 3.5 mm. For attenuation correction, low-dose CT without the use of *i.v.* contrast was performed immediately before ^{18}F-FDG PET. For patients without a recent CT angiography of the carotid arteries, this was performed after ^{18}F-FDG PET.

^{18}F-FDG Uptake Quantification

The Hybrid Viewer 2.0 software (Hermes Medical Solutions AB, Stockholm, Sweden) was used for image fusion and ^{18}F-FDG uptake quantification. The CT angiography was used to guide drawing of the ROIs on the fused PET/CT slices. A plaque was defined as vessel wall thickening and a lumen contrast-filling defect on CT angiography (Figure 1).[13] An experienced nuclear medicine physician (K.J.) drew ROIs around the entire vessel wall and lumen on all plaque-containing axial PET slices (Figure 2). ROIs were carefully placed to minimize the influence from ^{18}F-FDG uptake in structures close to the plaque (e.g., lymph nodes, paravertebral muscles, or salivary glands). Blood pool activity was obtained from four ROIs placed in the lumen of the jugular vein away from structures with ^{18}F-FDG uptake. Plaque localization in relation to the carotid bifurcation was recorded. The most cranial slice of the common carotid artery before the division was defined as the bifurcation. The pixel values in the PET images were converted into SUV normalized to lean body mass.[5]

For all plaque ROIs, SUV_{max} was obtained and the ^{18}F-FDG uptake was quantified using the following approaches (Figure 2):

(1) Max SUV_{max} = the single highest SUV,
(2) Mean SUV_{max} = the mean of all plaque SUV_{max},
(3) Most Diseased Segment (MDS)3 = the mean SUV_{max} of the three contiguous slices centered on the slice with the highest SUV_{max},
(4) MDS5 = the mean SUV_{max} of the five contiguous slices centered on the slice with the highest SUV_{max},
(5) Mean $SUV_{max}4$ = the mean SUV_{max} of the four slices with highest SUV_{max}.

For all blood pool ROIs, SUV_{mean} was obtained. Blood background-corrected values for all the SUV measurements were calculated (target-to-background ratio (TBR); SUV divided by the blood pool activity (mean SUV_{mean} in four venous regions) and corrected SUV (cSUV); blood pool-corrected SUV (subtraction of the blood pool activity (mean SUV_{mean}) from SUV).

A second independent experienced nuclear medicine physician (MER) drew ROIs on the 20 initial patients to assess inter-observer variability of the different quantification methods.

Endarterectomy and Histological Analysis

The mean time between PET/CT and endarterectomy was 6 days (range; 0-116, median; 0). The histological analysis has been described previously.[25] In brief, plaques were removed *en bloc* at carotid endarterectomy, fixed in 4% formaldehyde, decalcified in ethylenediaminetetraacetic acid, and cut into 2- to 3-mm slices. After dehydration, the slices were embedded in paraffin and a 5-μm histological section from each slice was cut and stained with hematoxylin and eosin (H&E). The number of histology sections obtained from each plaque

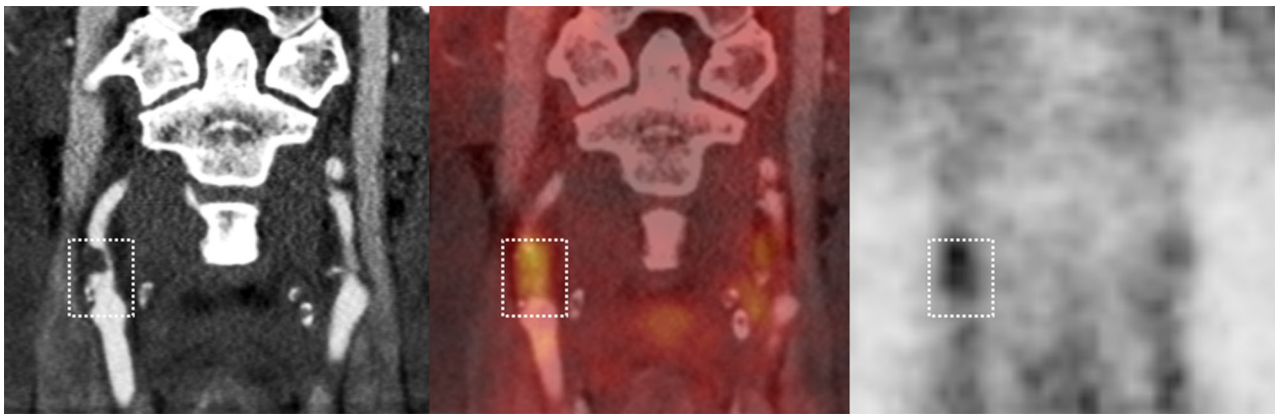

Figure 1. ^{18}F-FDG PET/CT of stenotic plaque in the right internal carotid artery. From left to right: CT angiography, co-registered PET/CT, and ^{18}F-FDG PET. The white box shows the plaque extension craniocaudally with lumen contrast-filling defect and vessel wall thickening on CT angiography (left image).

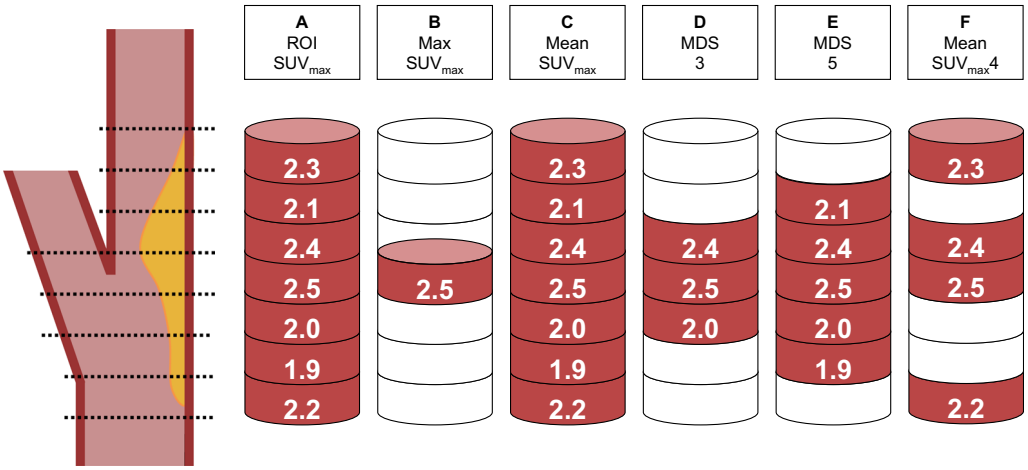

Figure 2. [18]F-FDG uptake quantification was based on the SUV_{max} of all the plaque-containing axial PET slices (**A**): Max SUV_{max} = the single highest SUV_{max} (**B**), mean SUV_{max} = the mean of all plaque SUV_{max} (**C**), MDS3 = the mean SUV_{max} of the three contiguous slices centered on the slice with the highest SUV_{max} (**D**), MDS5 = the mean SUV_{max} of the five contiguous slices centered on the slice with the highest SUV_{max} (**E**), and mean $SUV_{max}4$ = the mean SUV_{max} of the four slices with highest SUV_{max} within the plaque(F) (based on a figure by Tawakol et al [32]).

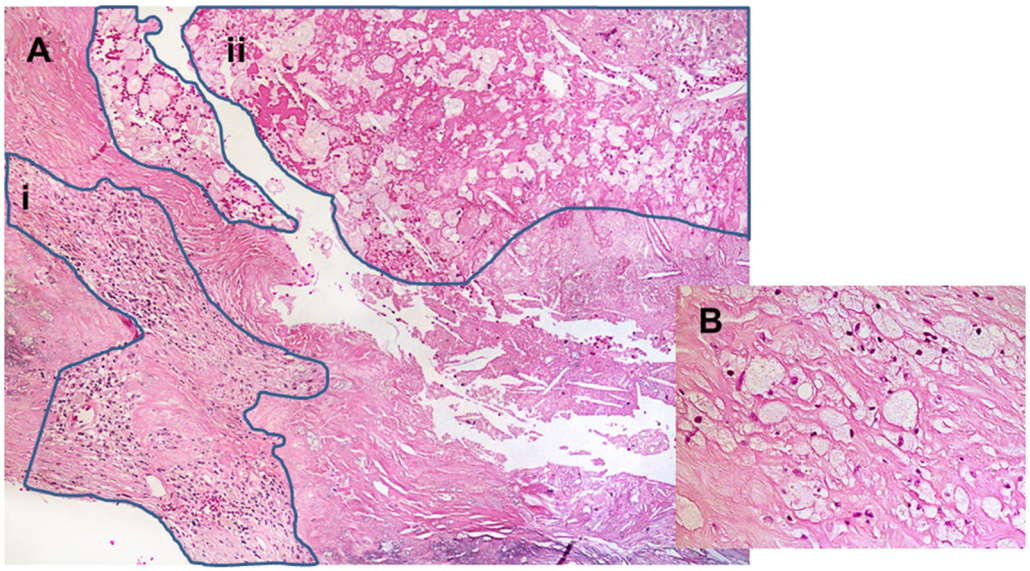

Figure 3. The histological quantification of inflammation was performed on H&E stained samples. The ocular micrometer was used to measure the total plaque area and area occupied by inflammatory cells in all the fields of view from all sections. The amount of inflammation per plaque was defined as the sum of all areas with inflammatory cells divided by the total area of all sections. **A**: ×200 magnification with inflammatory areas (marked by blue lines) containing mainly lymphocytes (*i*) and lipid macrophages (*ii*). **B**: ×400 magnification of areas with lipid macrophages.

ranged from 2 to 9 (mean 4.9, SD 2.0). The plaques were assessed by a pathologist and a research physician blinded for the clinical and the [18]F-FDG PET findings. Inflammation was quantified using a modified version of the method used by Jander et al.[3] The sections were evaluated with 120× magnification and the percentage area of inflammatory cells (macrophages and leucocytes) per plaque was obtained (Figure 3): For each section, the total area and the area occupied by inflammatory cells were measured manually. The amount of inflammation per plaque was defined as the sum of all areas with inflammatory cells divided by the total area of all the sections. We performed repeated histopathological

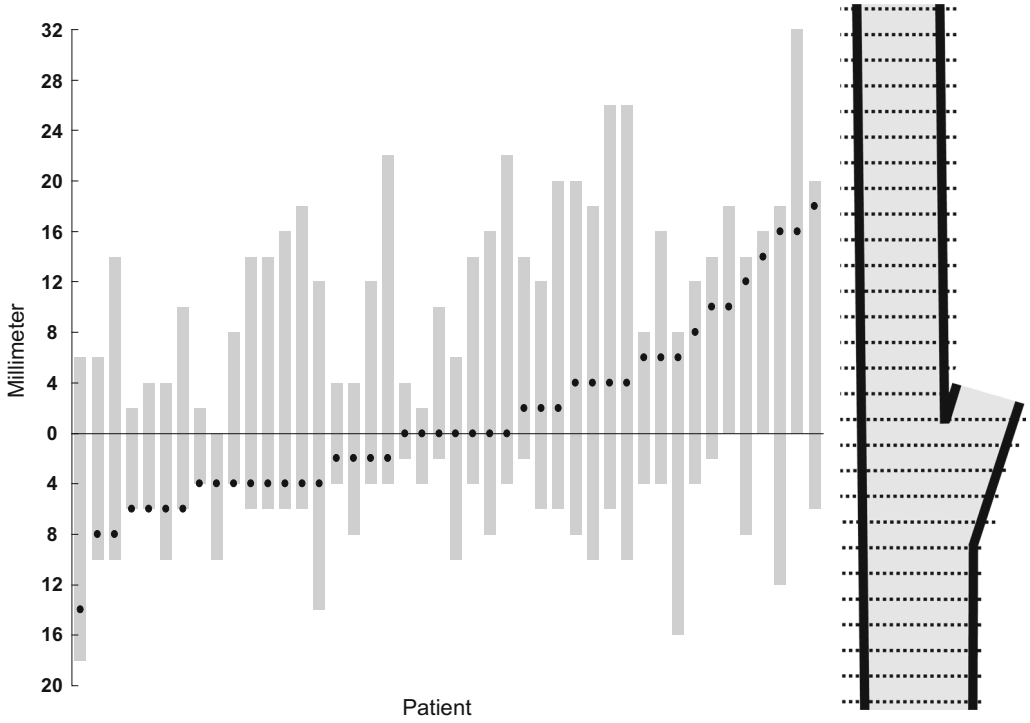

Figure 4. Plaque extension (gray bars) and max SUV_{max} location (black dots) per patient along the *x*-axis. The *y*-axis shows the distance in millimeter from the bifurcation (0) cranially in the internal carotid artery and caudally in the common carotid artery.

assessment on selected sections from this study cohort and found that the amount of inflammatory cells was in the same 5% category at both assessments for 73% of the sections (Kappa = 0.73).[25] The amount of inflammation per plaque was 6.8% (SD 4.0; range 0.4-17.9).

Statistical Analysis

The SPSS Statistics software for Windows (IBM, version 21.0; SPSS Inc., Chicago, Ill) was used. Groups of data were compared using two-sided *t*-test and Pearson correlation for normally distributed variables. For non-normal distributions Mann-Whitney test and Spearman correlation were used. Statistical significance was set to 0.05.

RESULTS

Localization of Plaque and Highest ^{18}F-FDG Uptake

The length of the plaques in the cranio-caudal direction was 6-32 mm (mean 19, SD 7.6) and all included the carotid artery bifurcation (Figure 4). Max SUV_{max} was located between 14 mm below to 18 mm above the bifurcation (mean 1.2 mm below the bifurcation) (Figure 4).

Inter-observer Variability

The correlation coefficients between ^{18}F-FDG uptakes calculated from plaques delineated by two nuclear medicine physicians independently were 0.96-0.98 for uncorrected SUVs, 0.63-0.68 for TBRs, and 0.90-0.93 for cSUVs. The correlation coefficient for background blood pool activity was 0.75.

Quantification of ^{18}F-FDG Uptake

Mean values, SDs, and ranges for the different quantification methods are summarized in Table 2. The ^{18}F-FDG uptake was significantly different for the different quantification approaches (paired samples *t*-test, $P < 0.004$ for all pairs). TBR gave the highest mean values and the widest ranges, whereas the background-subtracted values (cSUV) showed the lowest mean values and the narrowest ranges.

^{18}F-FDG uptake for the different quantification methods and corresponding background values for all patients are shown in Figure 5. Mean difference between max SUV_{max} and mean SUV_{max} was 0.08 and ranged from 0.02 to 0.66. The effect of background correction is shown in Figure 6. Correlations between ^{18}F-FDG uptake within the groups were 0.93-0.99 for the uncorrected SUV, 0.94-1.0 for TBR, and 0.92-0.99 for cSUV (Table 3).

Histology and ^{18}F-FDG Uptake

There were significant moderate (0.44-0.59) correlations between the amount of inflammation and all the different ^{18}F-FDG quantification methods (Table 4). The highest correlations were found for mean SUV_{max}, and the lowest for max SUV_{max} independent of background correction. Figure 7 shows scatter plots of inflammation versus max and mean SUV_{max} with and without background correction.

Table 2. Plaque SUV for different quantification methods ($n = 44$)

	Uncorrected	TBR	cSUV
Max SUV_{max}	1.76 ± 0.35 (1.18-2.66)	2.07 ± 0.44 (1.34-3.19)	0.90 ± 0.33 (0.42-1.79)
Mean SUV_{max}	1.56 ± 0.28 (1.11-2.28)	1.83 ± 0.38 (1.16-2.91)	0.69 ± 0.28 (0.20-1.29)
MDS3	1.70 ± 0.34 (1.17-2.51)	2.00 ± 0.43 (1.26-3.16)	0.83 ± 0.32 (0.33-1.64)
MDS5	1.66 ± 0.32 (1.15-2.32)	1.95 ± 0.41 (1.22-3.14)	0.79 ± 0.31 (0.28-1.45)
Mean SUV_{max}4	1.68 ± 0.33 (1.15-2.45)	1.98 ± 0.42 (1.26-3.16)	0.82 ± 0.31 (0.32-1.58)

Data are given as mean ± SD (range)
TBR, target-to-background ratio; *SUV*, standardized uptake value; *cSUV*, corrected SUV (background-subtracted SUV); *MDS*, most diseased segment

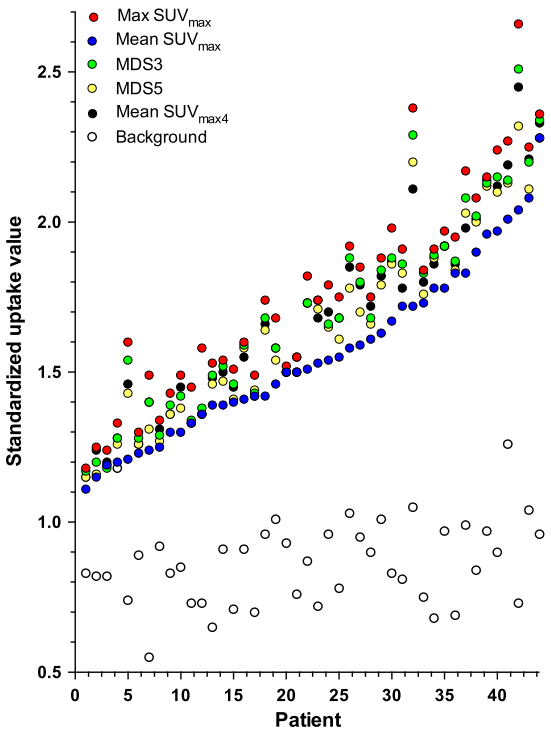

Figure 5. Uncorrected ^{18}F-FDG uptake values for individual patients sorted according to increasing mean SUV_{max}. Each color represents separate quantification methods. The black dots are the background values (mean SUV_{mean}).

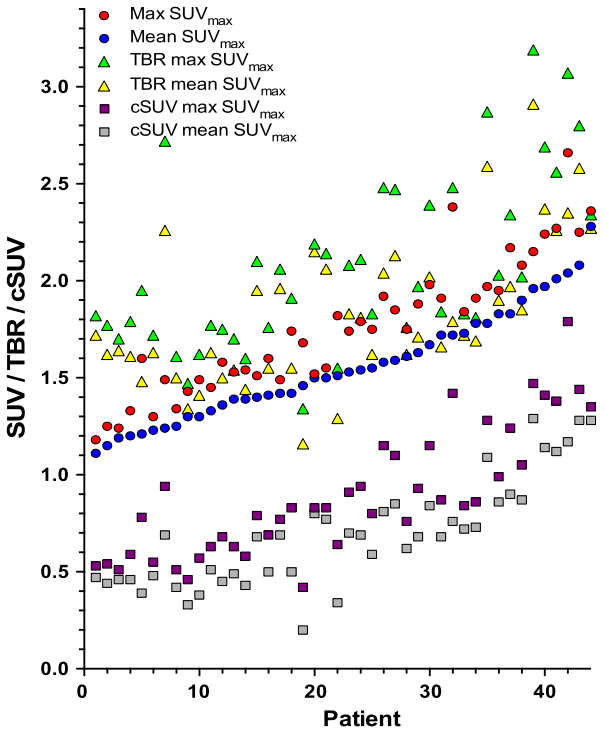

Figure 6. Uncorrected and background-corrected (TBR and cSUV) max and mean SUV_{max} per patient sorted according to increasing mean SUV_{max}.

Table 3. Correlation coefficients between different methods for ^{18}F-FDG uptake quantification ($n = 44$)

	Uncorrected				TBR					cSUV				
	Mean SUV_{max}	**MDS3**	**MDS5**	**Mean $SUV_{max}4$**	**Max SUV_{max}**	**Mean SUV_{max}**	**MDS3**	**MDS5**	**Mean $SUV_{max}4$**	**Max SUV_{max}**	**Mean SUV_{max}**	**MDS3**	**MDS5**	**Mean $SUV_{max}4$**
Uncorrected														
Max SUV_{max}	.93*	.99*	.99*	.99*	.68*	.57*	.68*	.67*	.65*	.91*	.79*	.89*	.89*	.88*
Mean SUV_{max}	1	.96*	.96*	.96*	.64*	.65*	.65*	.66*	.65*	.85*	.87*	.86*	.87*	.86*
MDS3		1	.99*	.99*	.69*	.59*	.69*	.68*	.67*	.91*	.81*	.91*	.90*	.89*
MDS5			1	.99*	.67*	.59*	.67*	.68*	.65*	.89*	.81*	.89*	.90*	.88*
Mean $SUV_{max}4$				1	.69*	.62*	.69*	.69*	.68*	.91*	.83*	.90*	.90*	.90*
TBR														
Max SUV_{max}					1	.94*	.99*	.99*	.99*	.91*	.89*	.92*	.91*	.92*
Mean SUV_{max}						1	.96*	.97*	.97*	.82*	.93*	.85*	.86*	.87*
MDS3							1	1.0*	1.0*	.91*	.90*	.92*	.92*	.93*
MDS5								1	.99*	.90*	.91*	.91*	.92*	.92*
Mean $SUV_{max}4$									1	.89*	.90*	.90*	.90*	.92*
cSUV														
Max SUV_{max}										1	.92*	.99*	.99*	.99*
Mean SUV_{max}											1	.94*	.95*	.96*
MDS3												1	.99*	.99*
MDS5													1	.99*
Mean $SUV_{max}4$														1

SUV, standardized uptake value; *MDS*, most diseased segment, background-corrected data; *TBR*, target-to-background ratio; *cSUV*, background-subtracted SUV
*Correlation is significant at the 0.01 level

Table 4. Correlation between ^{18}F-FDG PET uptake values and histology ($n = 30$)

^{18}F-FDG quantification method	Spearman correlation coefficient
Max SUV_{max}	0.48 (0.008)
Mean SUV_{max}	0.54 (0.002)
MDS3	0.48 (0.007)
MDS5	0.49 (0.006)
Mean SUV_{max}4	0.52 (0.003)
TBR max SUV_{max}	0.44 (0.016)
TBR mean SUV_{max}	0.58 (0.001)
TBR MDS3	0.47 (0.009)
TBR MDS5	0.48 (0.008)
TBR mean SUV_{max}4	0.48 (0.007)
cSUV max SUV_{max}	0.47 (0.009)
cSUV mean SUV_{max}	0.59 (0.001)
cSUV MDS3	0.52 (0.004)
cSUV MDS5	0.52 (0.003)
cSUV mean SUV_{max}4	0.54 (0.002)

Data given as correlation coefficient (*P* value)

DISCUSSION

In this clinical study, we explored different methods for the quantification of ^{18}F-FDG uptake in carotid plaques causing artery stenosis equal to or above 70%. ^{18}F-FDG uptake was homogenously disseminated throughout the entire plaques. Although there were differences in magnitude, quantification of ^{18}F-FDG uptake with and without background correction showed similar, moderate correlations to inflammation on histology.

Mean max SUV_{max} (mean of the max SUV_{max} for the study population) was only 13% higher than mean mean SUV_{max} (Figure 8), whereas the three other quantification methods gave values in between, increasing with decreasing number of included slices. Homogenous ^{18}F-FDG uptake throughout the plaque contrasts findings from microPET of endarterectomized plaques showing patchy ^{18}F-FDG uptake.[26] The presence of macrophages reduces the thickness of the fibrous capsule and therefore an increasing number is likely to correlate to increasing vulnerability. As such, the highest ^{18}F-FDG uptake within a plaque could be the most appropriate parameter for risk assessment. Currently, the most used measure for assessment of plaque inflammation has been the mean SUV_{max}.[17,21,22] No clinical studies have assessed the use of whole plaque max SUV_{max}. Max SUV_{max} is easily obtained, highly reproducible, and less influenced by partial-volume effects.[8,27] Although max SUV_{max} is prone to image noise,[8] our findings suggest that for atherosclerotic plaque assessment in clinical PET, max SUV_{max} should be explored further.

The strong correlation between the different quantification methods suggests that for this group of patients uncorrected ^{18}F-FDG uptake values may provide similar information as background-corrected values. As such, our findings do not support the superiority of TBR as quantification method as suggested by others.[4,10,14-17] For circulation times above one hour, the blood background is low, but highly variable, whereas carotid plaques have consistent uptake over time.[11,13] A slight variation in blood background will therefore give significant variability in TBR. From a physics perspective, Huet et al [9] have explained that there is no legitimate rationale for using TBR instead of SUV because blood contamination is an additive and not a multiplicative process. A purely additive process would require subtraction of the mean luminal blood pool activity from the SUVs (cSUVs).

The inter-observer variability analysis of ^{18}F-FDG quantification revealed superior reproducibility of uncorrected SUV_{max} compared to blood background-corrected SUVs (TBR and cSUV). SUV measurements are highly dependent on the size, shape, and location of the drawn ROI because the ROI can either miss the voxel with the highest intensity or the ROI can inadvertently include contribution from adjacent ^{18}F-FDG-avid organs. The use of contrast-enhanced CT to localize the plaques is likely to have contributed to the low inter-observer variability in the SUV_{max} in our study. Our correlation coefficient for blood background of 0.75

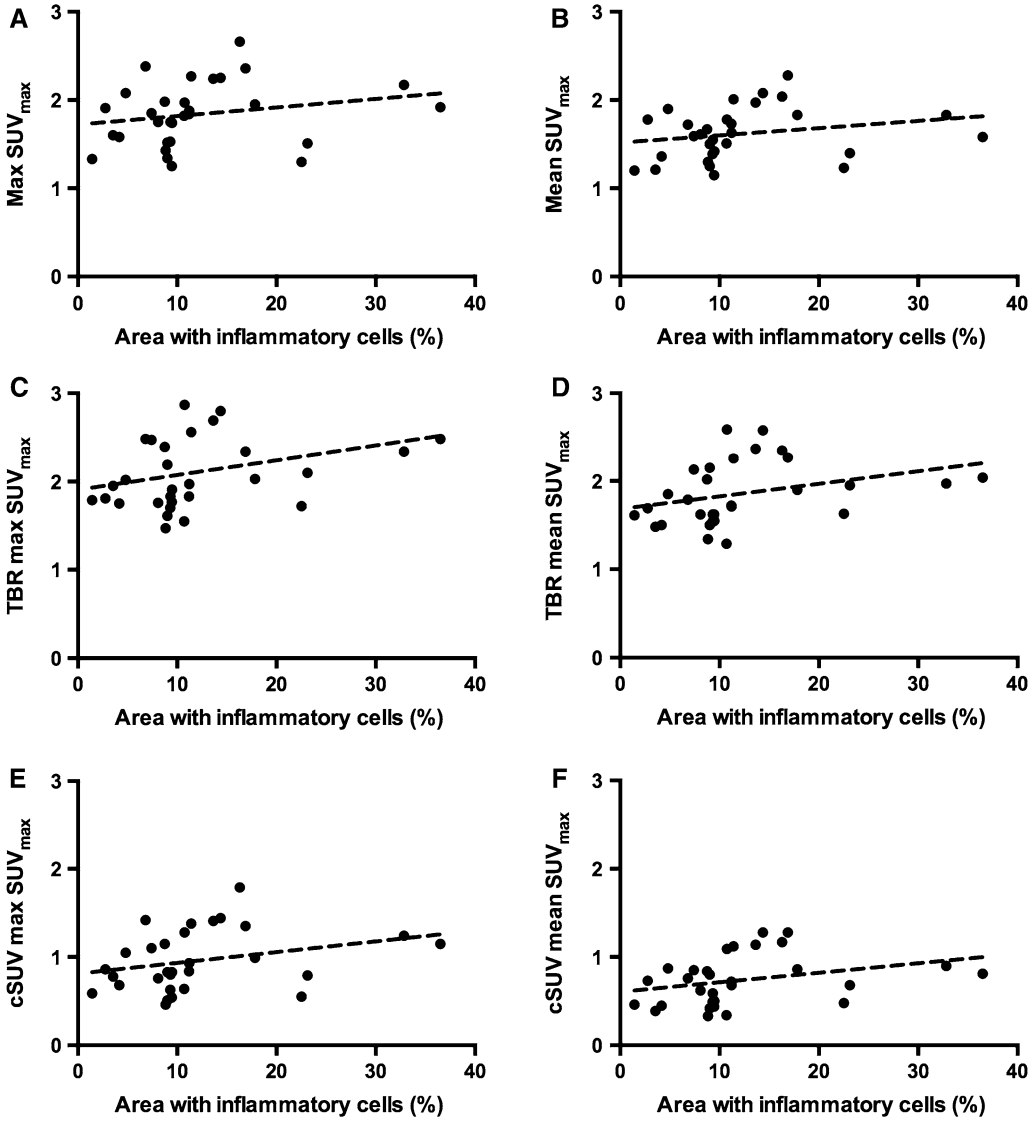

Figure 7. Scatter plots with correlation lines of total area with inflammatory cells versus uncorrected (**A**, **B**) and background-corrected (TBR: **C**, **D** and cSUV: **E**, **F**) max and mean SUV_{max}.

inevitably increases the inter-observer variability of all background-corrected values. Other ^{18}F-FDG uptake reproducibility studies in localized carotid artery plaques have reported moderate (background corrected)[28] to excellent (with and without background correction)[22,29] inter-observer agreement. The slightly inferior inter-observer agreement for background-corrected values found in our study could be related to differences in the placement of the ROI in the jugular vein as the diameter of the jugular vein often was small, making the measurement susceptible to image noise. However, this is an inherent limitation of all quantification methods with background correction.

The optimal method should predict plaque vulnerability and clinical outcome. In the present study, all quantification methods for ^{18}F-FDG uptake showed moderate correlation to inflammation on histopathology (Table 4). The correlations were systematically slightly higher when mean SUV_{max} was used instead of max SUV_{max}. This was not unexpected as total plaque inflammation score and mean SUV_{max} are both multislice methodologies. Total plaque inflammation score is a well-established method to correlate histology to ischemic symptoms,[2,3] or to ^{18}F-FDG uptake.[17] When comparing max SUV_{max} with the slice with the highest percentage inflammatory area, the correlation did not

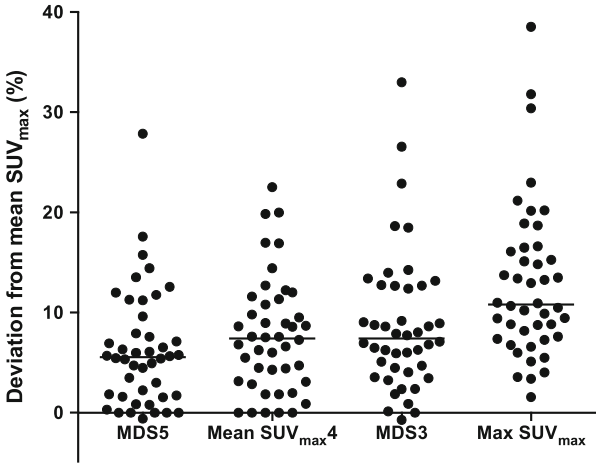

Figure 8. Deviation from the mean SUV_{max} for different quantification methods for individual patients. The black bar represents the mean values.

increase (data not shown). This is in accordance with Tawakol et al[17] who found slightly higher correlations between overall plaque inflammation and histology than a slice-by-slice comparison of uptake value and histology. How to use histology as a gold standard to imaging is challenging. We know that excised plaques both shrink[17] and may be partly damaged.[17,25]

The strength of our study was the close timing between the PET examinations and the endarterectomies. Our study patients had plaques not only presumed highly inflammatory giving recent symptoms, but also plaques removed prophylactically from asymptomatic patients.

A limitation of our study is the inclusion of patients with elevated blood glucose. Four had blood glucose values > 11 mmol/L (198 mg/dL) and three 7-11 mmol/L (126-198 mg/dL) at the time of the ^{18}F-FDG injection. Elevated blood glucose is known to reduce the uptake of ^{18}F-FDG into metabolic active cells in malignant diseases.[30] Guidelines for the clinical use of ^{18}F-FDG in inflammation and infection[31] also recommend the reduction of blood glucose to the lowest possible level. In studies on atherosclerosis, there is no consensus on a cut-off value.[12] Some studies do not report on blood glucose level, whereas in other studies the cut-off values have ranged from 8 mmol/L (144 mg/dL)[21] to 11.1 mmol/L (200 mg/dL).[16] Our correlations between histology and the different ^{18}F-FDG quantification methods were slightly increased when excluding the four patients with blood glucose level > 11 mmol/L. We have not excluded patients with high blood glucose in the correlation analysis of the different uptake parameters and thereby we do not know if this has contaminated our results. In the 44 included patients, there was no correlation between blood glucose and background SUV_{mean}. Another limitation is the wide range of circulation times (68-156 minutes) that could have influenced the plaque ^{18}F-FDG uptake by underestimating background-corrected values for patients with shorter circulation times and by overestimating background-corrected values for patients with longer circulation times. However, for 38 of the 44 patients the PET acquisition started between 85 and 115 minutes after ^{18}F-FDG injection, and thus, it is unlikely that difference in circulation time would change the findings in our study.

NEW KNOWLEDGE GAINED

Our study showed that SUVs without background correction from large plaques in the carotid artery can be used as inflammatory parameter in atherosclerosis.

CONCLUSION

In conclusion, in carotid artery stenosis equal to or above 70%, ^{18}F-FDG uptake reflects the inflammatory status as assessed on histology. Increasing number of PET slices or background correction did not improve the correlation.

Acknowledgement

The authors thank Trine Hjørnevik, PhD for helping with quantification software and figures.

Disclosure

KJ, KS, TS, MS, DR, and MER report no conflicts of interest.

References

1. Libby P. Inflammation in atherosclerosis. Nature. 2002;420:868–74.
2. Redgrave JN, Lovett JK, Gallagher PJ, Rothwell PM. Histological assessment of 526 symptomatic carotid plaques in relation to the nature and timing of ischemic symptoms: the Oxford plaque study. Circulation. 2006;113:2320–8.

3. Jander S, Sitzer M, Schumann R, Schroeter M, Siebler M, Steinmetz H, et al. Inflammation in high-grade carotid stenosis: a possible role for macrophages and T cells in plaque destabilization. Stroke. 1998;29:1625–30.
4. Rudd JH, Warburton EA, Fryer TD, Jones HA, Clark JC, Antoun N, et al. Imaging atherosclerotic plaque inflammation with [^{18}F]-fluorodeoxyglucose positron emission tomography. Circulation. 2002;105:2708–11.
5. Boellaard R, Delgado-Bolton R, Oyen WJ, Giammarile F, Tatsch K, Eschner W, et al. FDG PET/CT: EANM procedure guidelines for tumour imaging: version 2.0. Eur J Nucl Med Mol Imaging. 2015;42:328–54.
6. Bucerius J, Hyafil F, Verberne HJ, Slart RH, Lindner O, Sciagra R, et al. Position paper of the Cardiovascular Committee of the European Association of Nuclear Medicine (EANM) on PET imaging of atherosclerosis. Eur J Nucl Med Mol Imaging. 2016;43:780–92.
7. Kolodgie FD, Nakazawa G, Sangiorgi G, Ladich E, Burke AP, Virmani R. Pathology of atherosclerosis and stenting. Neuroimaging Clin N Am. 2007;17:285–301.
8. Soret M, Bacharach SL, Buvat I. Partial-volume effect in PET tumor imaging. J Nucl Med. 2007;48:932–45.
9. Huet P, Burg S, Le Guludec D, Hyafil F, Buvat I. Variability and uncertainty of 18F-FDG PET imaging protocols for assessing inflammation in atherosclerosis: suggestions for improvement. J Nucl Med. 2015;56:552–9.
10. Blomberg BA, Akers SR, Saboury B, Mehta NN, Cheng G, Torigian DA, et al. Delayed time-point 18F-FDG PET CT imaging enhances assessment of atherosclerotic plaque inflammation. Nucl Med Commun. 2013;34:860–7.
11. Blomberg BA, Thomassen A, Takx RA, Hildebrandt MG, Simonsen JA, Buch-Olsen KM, et al. Delayed ^{18}F-fluorodeoxyglucose PET/CT imaging improves quantitation of atherosclerotic plaque inflammation: results from the CAMONA study. J Nucl Cardiol. 2014;21:588–97.
12. Bucerius J, Mani V, Moncrieff C, Machac J, Fuster V, Farkouh ME, et al. Optimizing ^{18}F-FDG PET/CT imaging of vessel wall inflammation: the impact of 18F-FDG circulation time, injected dose, uptake parameters, and fasting blood glucose levels. Eur J Nucl Med Mol Imaging. 2014;41:369–83.
13. Graebe M, Borgwardt L, Hojgaard L, Sillesen H, Kjaer A. When to image carotid plaque inflammation with FDG PET/CT. Nucl Med Commun. 2010;31:773–9.
14. Niccoli Asabella A, Ciccone MM, Cortese F, Scicchitano P, Gesualdo M, Zito A, et al. Higher reliability of 18F-FDG target background ratio compared to standardized uptake value in vulnerable carotid plaque detection: a pilot study. Ann Nucl Med. 2014;28:571–9.
15. Rudd JH, Myers KS, Bansilal S, Machac J, Pinto CA, Tong C, et al. Atherosclerosis inflammation imaging with 18F-FDG PET: carotid, iliac, and femoral uptake reproducibility, quantification methods, and recommendations. J Nucl Med. 2008;49:871–8.
16. Tawakol A, Fayad ZA, Mogg R, Alon A, Klimas MT, Dansky H, et al. Intensification of statin therapy results in a rapid reduction in atherosclerotic inflammation: results of a multicenter fluorodeoxyglucose-positron emission tomography/computed tomography feasibility study. J Am Coll Cardiol. 2013;62:909–17.
17. Tawakol A, Migrino RQ, Bashian GG, Bedri S, Vermylen D, Cury RC, et al. In vivo 18F-fluorodeoxyglucose positron emission tomography imaging provides a noninvasive measure of carotid plaque inflammation in patients. J Am Coll Cardiol. 2006;48:1818–24.
18. Bural GG, Torigian DA, Chamroonrat W, Alkhawaldeh K, Houseni M, El-Haddad G, et al. Quantitative assessment of the atherosclerotic burden of the aorta by combined FDG-PET and CT image analysis: a new concept. Nucl Med Biol. 2006;33:1037–43.
19. Rudd JH, Myers KS, Bansilal S, Machac J, Rafique A, Farkouh M, et al. (18)Fluorodeoxyglucose positron emission tomography imaging of atherosclerotic plaque inflammation is highly reproducible: implications for atherosclerosis therapy trials. J Am Coll Cardiol. 2007;50:892–6.
20. Fayad ZA, Mani V, Woodward M, Kallend D, Abt M, Burgess T, et al. Safety and efficacy of dalcetrapib on atherosclerotic disease using novel non-invasive multimodality imaging (dal-PLAQUE): a randomised clinical trial. Lancet. 2011;378:1547–59.
21. Graebe M, Pedersen SF, Hojgaard L, Kjaer A, Sillesen H. 18FDG PET and ultrasound echolucency in carotid artery plaques. JACC Cardiovasc Imaging. 2010;3:289–95.
22. Marnane M, Merwick A, Sheehan OC, Hannon N, Foran P, Grant T, et al. Carotid plaque inflammation on ^{18}F-fluorodeoxyglucose positron emission tomography predicts early stroke recurrence. Ann Neurol. 2012;71:709–18.
23. Chen W, Dilsizian V. PET assessment of vascular inflammation and atherosclerotic plaques: SUV or TBR? J Nucl Med. 2015;56:503–4.
24. Grant EG, Benson CB, Moneta GL, Alexandrov AV, Baker JD, Bluth EI, et al. Carotid artery stenosis: gray-scale and Doppler US diagnosis—Society of Radiologists in Ultrasound Consensus Conference. Radiology. 2003;229:340–6.
25. Skagen K, Johnsrud K, Evensen K, Scott H, Krohg-Sorensen K, Reier-Nilsen F, et al. Carotid plaque inflammation assessed with (18)F-FDG PET/CT is higher in symptomatic compared with asymptomatic patients. Int J Stroke. 2015;10:730–6.
26. Masteling MG, Zeebregts CJ, Tio RA, Breek JC, Tietge UJ, de Boer JF, et al. High-resolution imaging of human atherosclerotic carotid plaques with micro 18F-FDG PET scanning exploring plaque vulnerability. J Nucl Cardiol. 2011;18:1066–75.
27. Lodge MA, Chaudhry MA, Wahl RL. Noise considerations for PET quantification using maximum and peak standardized uptake value. J Nucl Med. 2012;53:1041–7.
28. Kwee RM, Truijman MT, Mess WH, Teule GJ, ter Berg JW, Franke CL, et al. Potential of integrated [^{18}F] fluorodeoxyglucose positron-emission tomography/CT in identifying vulnerable carotid plaques. AJNR Am J Neuroradiol. 2011;32:950–4.
29. Li X, Heber D, Rausch I, Beitzke D, Mayerhoefer ME, Rasul S, et al. Quantitative assessment of atherosclerotic plaques on (18)F-FDG PET/MRI: comparison with a PET/CT hybrid system. Eur J Nucl Med Mol Imaging. 2016;43:1503–12.
30. Wahl RL, Henry CA, Ethier SP. Serum glucose: effects on tumor and normal tissue accumulation of 2-[F-18]-fluoro-2-deoxy-D-glucose in rodents with mammary carcinoma. Radiology. 1992;183:643–7.
31. Jamar F, Buscombe J, Chiti A, Christian PE, Delbeke D, Donohoe KJ, et al. EANM/SNMMI guideline for 18F-FDG use in inflammation and infection. J Nucl Med. 2013;54:647–58.
32. Tawakol A, Singh P, Rudd JH, Soffer J, Cai G, Vucic E, et al. Effect of treatment for 12 weeks with rilapladib, a lipoprotein-associated phospholipase A2 inhibitor, on arterial inflammation as assessed with 18F-fluorodeoxyglucose-positron emission tomography imaging. J Am Coll Cardiol. 2014;63:86–8.

III

Inter-reader agreement of ^{18}F-FDG PET/CT for the quantification of carotid artery plaque inflammation

Kjersti Johnsrud, MD[1,2], Therese Seierstad, PhD, MHA[3], David Russell, MD, PhD[2,4], Mona-Elisabeth Revheim, MD, PhD[1,2]

[1] Department of Nuclear Medicine, Division of Radiology and Nuclear Medicine, Oslo University Hospital, Oslo, Norway

[2] Institute of Clinical Medicine, University of Oslo, Oslo, Norway

[3] Department for Research and Development, Division of Radiology and Nuclear Medicine, Oslo University Hospital, Oslo, Norway

[4] Department of Neurology, Oslo University Hospital, Oslo, Norway

Funding: South-Eastern Norway Regional Health Authority, grant number: 2009006.

Corresponding author:

Kjersti Johnsrud, Division of Radiology and Nuclear Medicine, Oslo University Hospital, Postbox 4950 Nydalen, 0424 Oslo, Norway. Tel: +4799246753. Fax: +4723073837.

E-mail: kjersti@slogum.no

Abstract

A significant proportion of ischemic strokes are caused by emboli from unstable atherosclerotic carotid artery plaques. Inflammation is a key feature of plaque instability. Positron emission tomography/computed tomography (PET/CT) with 2-deoxy-2-(^{18}F)-fluoro-D-glucose (**(**^{18}F-FDG) is a promising technique to quantify plaque inflammation, but a consensus on the methodology has not been established. High inter-reader agreement is essential if ^{18}F-FDG PET/CT is to be used as a clinical tool for the assessment of unstable plaques and stroke risk. We assessed the inter-reader variability of different methods for quantification of ^{18}F-FDG uptake in 43 patients with carotid artery stenosis ≥70%. Two independent readers delineated the plaque and collected maximum standardized uptake value (SUV_{max}) from all axial PET slices containing the atherosclerotic plaque. Uptake values with and without background correction were calculated. Intraclass correlation coefficients were highest for uncorrected uptake values (0.97-0.98) followed by those background corrected by subtraction (0.89-0.94) and lowest for those background corrected by division (0.74-0.79).

Quantification methods without background correction have the highest inter-reader agreement for ^{18}F-FDG PET of carotid artery plaque inflammation. The use of the single highest uptake value (max SUV_{max}) from the plaque will facilitate the method's clinical utility in stroke prevention.

Introduction

Ischemic strokes caused by thromboembolism from an unstable atherosclerotic plaque in the carotid artery can be prevented by carotid endarterectomy (CEA).[1-3] Patients are selected for CEA based on the degree of carotid artery stenosis and presence or absence of cerebral ischemic symptoms. In recent years it has become increasingly clear that the degree of stenosis alone is not the best predictor of stroke risk. This has led to the concept of the 'unstable plaque' describing carotid plaques that carry high risk of stroke irrespective of the degree of artery stenosis and increased focus on factors that destabilize the plaque. Inflammation plays a key role in the development of an unstable plaque.[4-6]

Positron emission tomography (PET) imaging of atherosclerosis has been rapidly evolving since the first reports of 2-deoxy-2-(^{18}F)-fluoro-D-glucose (^{18}F-FDG) uptake localized to the inflammatory macrophage rich areas in carotid artery plaques.[7] The goal of the imaging technique is to detect carotid plaques that are at high risk of rupture and therefore carry high risk of stroke.[18] F-FDG PET for the detection of unstable plaques is not in clinical use,[8] partly due to lack of feasible PET protocols and consensus regarding imaging procedure, method for ^{18}F-FDG uptake quantification and assessment of stroke risk, although several recommendations exist.[9, 10] PET is an imaging modality with limited anatomical information, and it might therefore be challenging to define the vessel-segment-of-interest. Computed tomography angiography (CTA) is often used together with ^{18}F-FDG PET when assessing patients with carotid artery stenosis, but selection of the plaque area for uptake measurements varies.[11-13] A requirement for introducing a diagnostic method into clinical routine is high inter-reader agreement. Inter-reader agreement has been studied for a few selected uptake parameters with generalized vascular inflammation[14, 15] and in patients with symptomatic carotid stenosis,[12, 13] but to our knowledge no study has compared inter-reader agreement for different quantification methods.

The aim of this study was to assess inter-reader variability of different methods used for quantification of ^{18}F-FDG uptake at PET/CT of carotid artery plaques.

Materials and methods

Study population

The study cohort consisted of forty-three patients with ultrasound-confirmed atherosclerosis with internal carotid artery stenosis ≥70% according to consensus criteria of the Society of Radiologists in Ultrasound.[16] Patient characteristics are summarized in Table 1. There were 30 men (66 ± 9 years) and 13 women (67 ± 8 years) with a mean age of 66.2 years. The study protocol conformed with the ethical guidelines of the 1975 Declaration of Helsinki and was approved by the Norwegian Regional Committee for Medical and Health Research Ethics South-East A (approval number S-09233a). Written informed consent was obtained from all patients prior to study inclusion.

Table 1. Patient characteristics (n = 43) *

Age, years; mean ± SD	66.2 ± 8.4
Sex, male; n (%)	30 (69.8)
Blood glucose, mmol·L^{-1}; mean ± SD (range)	6.8 ± 2.2 (4.9 - 14.9)
Bodyweight, kg; mean ± SD (range)	82.4 ± 15 (55 - 110)
Body mass index, kg/m^2; mean ± SD (range)	27.5 ± 4.5 (19.9 - 34.8)

*The patient material is included in previously published studies.[17, 18]

^{18}F-FDG PET/CT examination

After a minimum of six hours fasting the patients were injected with 5 MBq/kg ^{18}F-FDG and blood glucose, weight, and height were recorded. After approximately 90 minutes a two-bed position PET/CT from the base of the skull to the aortic arch was performed with 15 minutes per bed position using a hybrid PET/CT scanner (Siemens Biograph 64, Siemens Medical Systems, Erlangen, Germany). The PET images were acquired with a 256 x 256 matrix and the images were reconstructed to two millimetre thick slices, with four iterations/eight subsets ordered subset expectation–maximization (OSEM) algorithm and Gaussian post-reconstruction filter with 3.5 mm full width half maximum (FWHM). In addition to a non-contrast CT for attenuation correction a CTA with contrast filling of the arteries (minimum 40 mL Iomeron (iodine 350 mg/mL; Bracco Imaging S.P.A, Milan, Italy) or Visipaque (iodine 320 mg/mL); GE Healthcare, Chicago, USA) was acquired immediately after the PET when still lying in the scanner for 16 of the 43 patients. For 24 patients CTA was performed at other radiologic departments. For three patients no CTA was available when the PET images were analysed.

Image analyses and ^{18}F-FDG quantification

The images were assessed with Hybrid Viewer 2.0 software (Hermes Medical Solutions AB, Stockholm, Sweden). Two experienced nuclear medicine senior consultants independently evaluated the ^{18}F-FDG PET/CT examinations. The two readers (R1 and R2) did not undergo any joint training before assessing the images, but they agreed on how to perform the analyses. The instructions were to use the CTA as guide for drawing the region of interests (ROIs) on the fused slices (PET and non-contrast CT). The plaque was defined as vessel wall thickening and a lumen contrast-filling defect on CTA.[11] The ROIs were drawn around the

entire vessel wall and lumen on all plaque-containing axial PET slices (Figure 1). For patients without CTA available, the plaque was defined as vessel wall with calcification and fat deposits in the level of the carotid bifurcation. Uptake in structures close to the plaque (e.g. lymph nodes, paravertebral muscles or salivary glands) that could falsify the plaque uptake values were excluded from the ROI. The number of plaque-containing slices for each patient was recorded. The pixel values in the PET images were converted into SUV and normalized to lean body mass.[19] SUV_{max} in all plaque containing ROIs were recorded. Background blood pool activity was obtained from four ROIs placed in the lumen of the jugular vein away from structures with ^{18}F-FDG uptake but preferably in the same craniocaudal level as the plaque. The background was calculated as the mean of the SUV_{mean} in these four ROIs. Different measures of ^{18}F-FDG uptake were calculated (Table 2) as previously described in detail.[17] Blood background corrected values were calculated as the ^{18}F-FDG uptake values divided by the mean blood pool activity (TBR) and subtraction of the blood pool activity from the ^{18}F-FDG uptake values (corrected SUV (cSUV)).

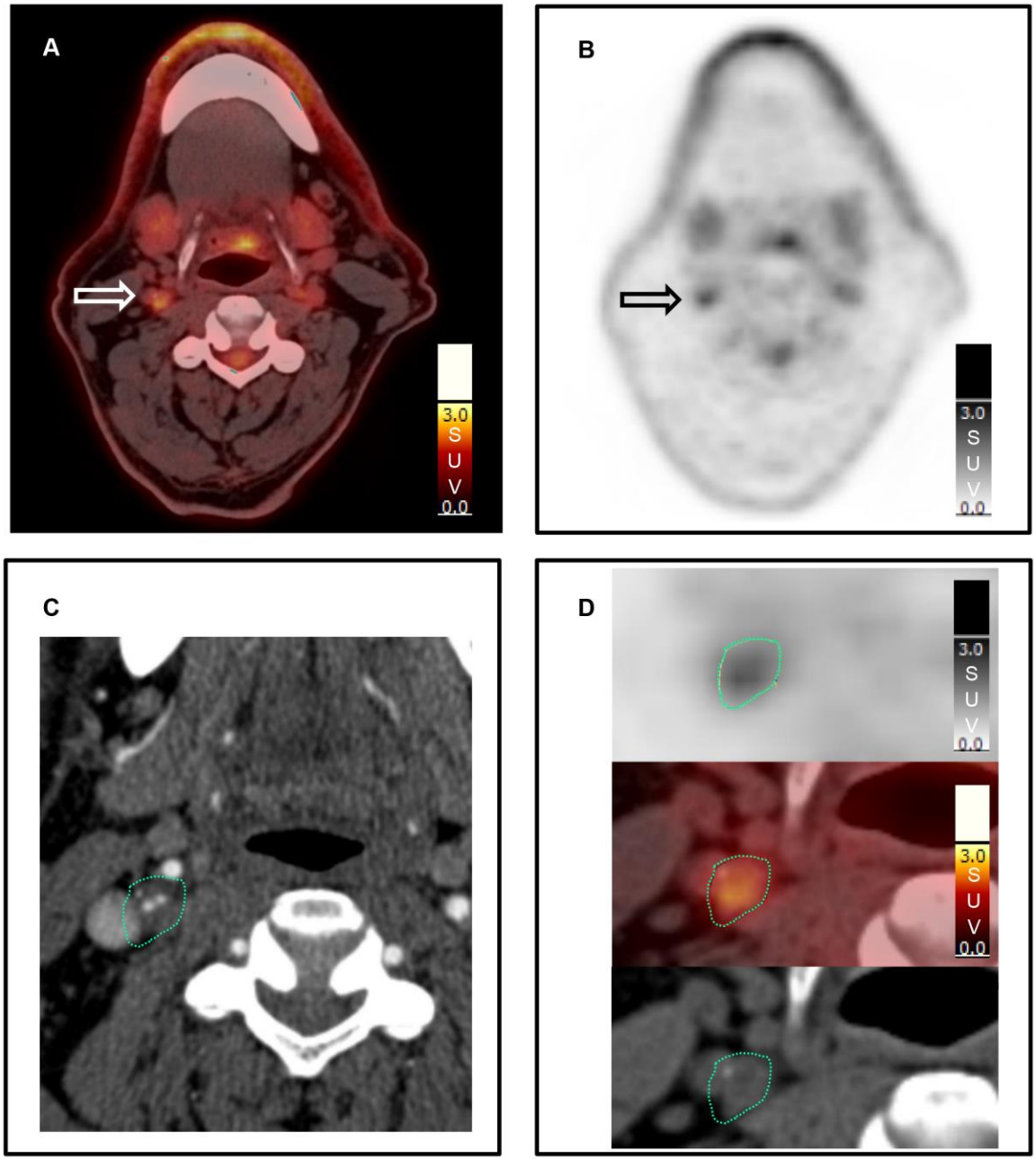

Fig 1. Region of interest. On each plaque-containing axial slice a region of interest (ROI) was drawn manually around the entire vessel wall including the plaque and the lumen. A (fused PET/non-contrast CT) and B (PET) show increased uptake (arrow) in the plaque in the right internal carotid artery. C shows how the plaque location on contrast enhanced CT (low attenuation plaque with thin contrast filled lumen in the centre) guides the actual drawing of the ROI (green dotted line) on the fused PET/non-contrast CT (D).

Table 2. Plaque ^{18}F-FDG uptake measures.

Uptake measure	Description
max SUV_{max}	the single highest SUV_{max}
mean SUV_{max}	mean of all plaque SUV_{max}
MDS3*	mean SUV_{max} of the three contiguous slices centered on the slice with the highest SUV_{max}
MDS5*	mean SUV_{max} of the five contiguous slices centered on the slice with the highest SUV_{max}
mean $SUV_{max}4$	mean SUV_{max} of the four slices with highest SUV_{max}

*MDS, most diseased segment

Statistical analysis

The IBM SPSS Statistics software for Windows (version 25.0; IBM Corp., Armonk, USA) was used for data analyses. Groups of paired data were compared using the Wilcoxon signed rank test for non-normally distributed variables. Inter-reader agreement was calculated using intraclass correlation coefficients (ICC's; model two-way random, type absolute agreement). All statistical results were considered significant when $p < 0.05$.

Results

The different ^{18}F-FDG uptake values for the two readers are summarized in Table 3. Reader 2 identified significantly more slices as plaque containing (median; 10, range; 4-23) than reader 1 (median; 9, range; 3-18) (p = 0.001).

Table 3. ^{18}F-FDG uptake values and intraclass correlation coefficients between the two readers (n = 43 patients).

Quantification method	^{18}F-FDG uptake values			ICC
	Reader 1	Reader 2	*p*	
Max SUV_{max}	1.74 (1.18 - 2.66)	1.74 (1.20 - 2.66)	0.304	.979
Mean SUV_{max}	1.51 (1.11 - 2.28)	1.51 (1.06 - 2.15)	0.687	.973
MDS3	1.68 (1.17 - 2.51)	1.68 (1.19 - 2.51)	0.400	.978
MDS5	1.64 (1.15 - 2.32)	1.63 (1.17 - 2.45)	0.438	.972
Mean SUV_{max}4	1.68 (1.15 - 2.45)	1.68 (1.13 - 2.45)	0.060	.972
Background	0.87 (0.55 - 1.26)	0.89 (0.55 - 1.30)	0.245	.767
TBR max SUV_{max}	1.95 (1.34 - 3.07)	2.02 (1.34 - 2.68)	0.314	.792
TBR mean SUV_{max}	1.72 (1.16 - 2.59)	1.76 (1.25 - 2.37)	0.232	.741
TBR MDS3	1.87 (1.26 - 2,89)	1.97 (1.30 - 2.55)	0.296	.775
TBR MDS5	1.80 (1.22 - 2.79)	1.94 (1.24 - 2.53)	0.241	.769
TBR mean SUV_{max} 4	1.81 (1.26 - 2.82)	1.93 (1.31 - 2.61)	0.358	.758
cSUV max SUV_{max}	0.83 (0.42 - 1.79)	0.87 (0.38 - 1.67)	0.837	.944
cSUV mean SUV_{max}	0.68 (0.20 - 1.28)	0.68 (0.28 - 1.19)	0.435	.893
cSUV MDS3	0.80 (0.33 - 1.64)	0.79 (0.34 - 1.51)	0.769	.931
cSUV MDS5	0.75 (0.28 - 1.45)	0.76 (0.27 - 1.45)	0.595	.916
cSUV mean SUV_{max}4	0.74 (0.32 - 1.58)	0.77 (0.35 - 1.45)	0.975	.919

Data are given as median (range). *P*-value from Wilcoxon signed ranks test. SUV, standardized uptake value; MDS, most diseased segment; TBR, target-to-background ratio; cSUV, background subtracted SUV; ICC, intraclass correlation coefficient.

There were no differences in ^{18}F-FDG uptake between the two readers (Table 3). The ICC for the different ^{18}F-FDG quantification methods was highest for uncorrected SUVs (0.97-0.98) followed by cSUVs (0.89-0.94) and TBRs (0.74-0.79), and 0.77 for the

background blood pool (Table 3). The differences in the median for the uptake values between the readers ranged from 0.00 and 0.01 for the uncorrected SUVs to 0.04-0.14 for TBRs (0.14 for TBR MDS5). The difference for the background value was 0.02 (Table 3).

Figure 2 shows the differences in max SUV_{max} and mean SUV_{max} for individual patients for the two readers without background correction (A and B), and the corresponding values when the ^{18}F-FDG uptake is corrected for background blood pool by division (TBR; 2C and 2D) and by subtraction (cSUV; 2E and 2F). The difference in venous background is shown in Figure 2G. The difference between the readers is highest for the uptake values corrected for background blood pool by division (2C and 2D), and lowest for the uptake values without background correction (2A and 2B).

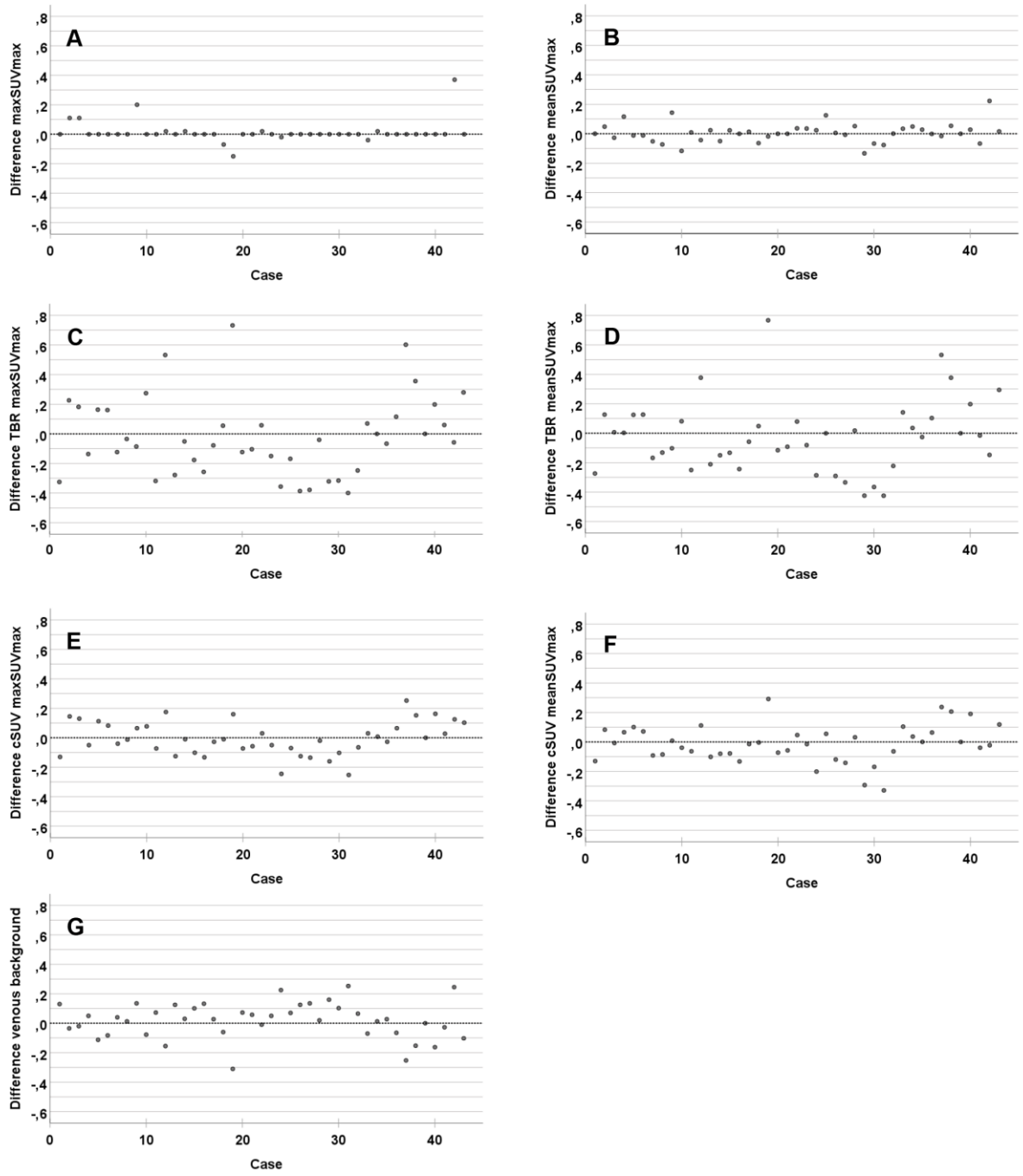

Fig 2. Inter-reader difference for the ^{18}F-FDG quantification methods. Difference between the readers (R2 minus R1, y-axis)) for the included patients (x-axis). Max SUV_{max} (A), mean SUV_{max} (B), TBR max SUV_{max} (C), TBR mean SUV_{max} (D), cSUV max SUV_{max} (E), cSUV mean SUV_{max} (F), and venous background (G).

Discussion

In this study we found high inter-reader agreement between different methods for ^{18}F-FDG uptake quantification of inflammation in high grade carotid artery stenosis. The inter-reader agreement was highest for the methods without background correction. Two studies in patients with carotid stenosis supports our finding that methods without correction for background blood activity have higher inter-reader agreement than background corrected values: Kwee et al.[12] reported an ICC of 0.61 for TBR mean SUV_{max} and 0.65 for TBR max $SUV_{max,}$ and Marnane et al.[13] found an ICC of 0.99 for mean SUV_{max}.

In our study the highest ICC was found for max SUV_{max} (0.98). For the methods without background blood pool correction only 12% of the max SUV_{max} and 14% of the mean SUV_{max} measurements differed with more than ± 0.10 (Figure 2A, B). Patient number 42 is an outlier with an inter-reader difference of 0.38. This is probably due to different delineations of the plaque ROIs as this patient had high uptake in neighbouring muscle (Figure 3). Reader 1 can have excluded more of the plaque ROIs to be sure to avoid spill-in activity than reader 2. The problem with spill-in from neighbouring structures is due to the relatively low spatial resolution of PET combined with unspecific uptake of ^{18}F-FDG.

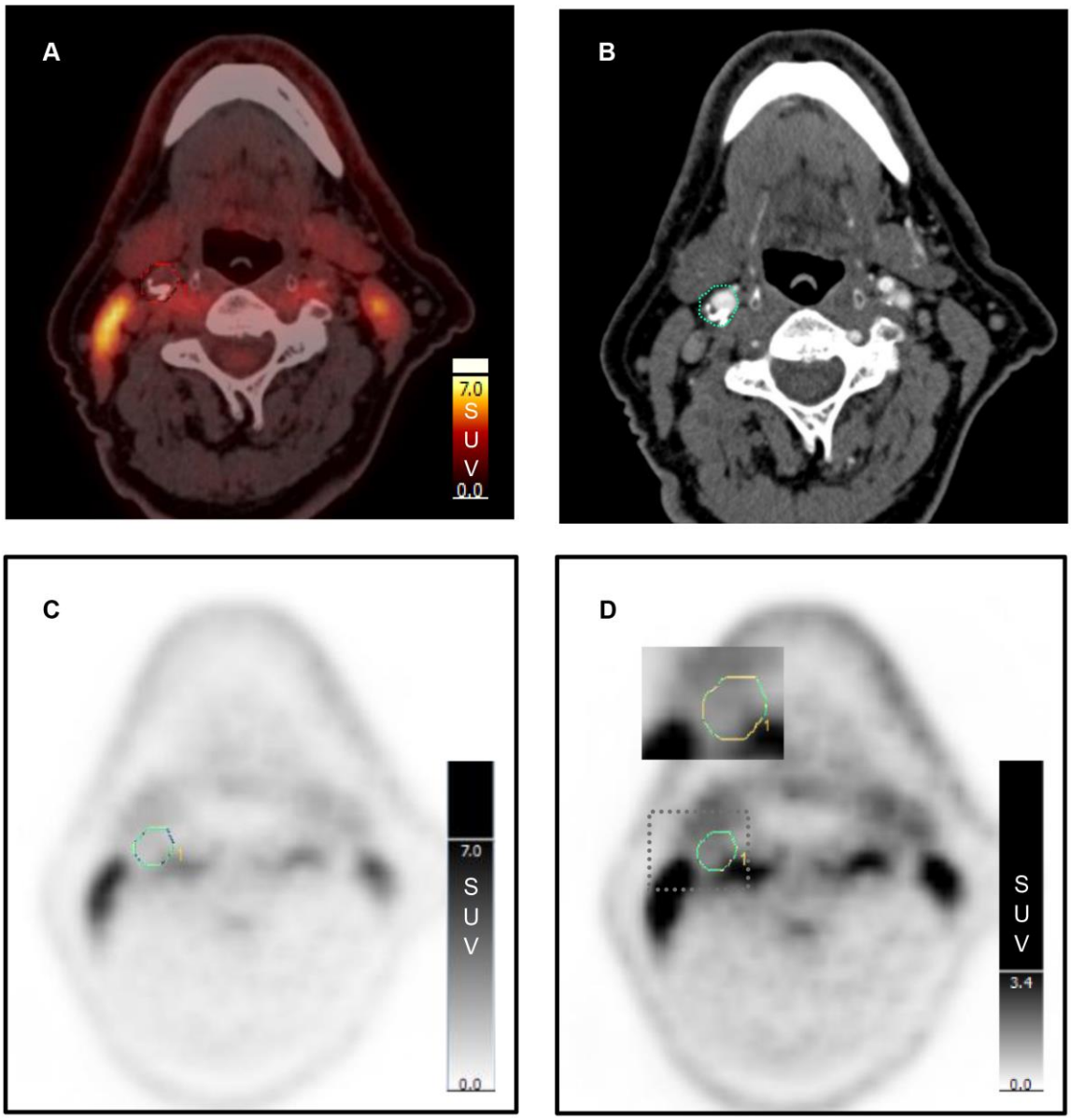

Fig 3. Spill-in activity. Fused image of non-contrast CT and PET (A) and contrast enhanced CT (B) show a plaque in the level of the right carotid bifurcation with low uptake but with high uptake in nearby muscles. PET with normal intensity on the SUV scale (C) and PET with high intensity on the SUV scale (D) show that ^{18}F-FDG uptake from nearby muscle activity influences the ROI around the plaque (inserted picture at 4 to 5 o'clock position).

For the background corrected values, the difference was larger with 40% of TBR max SUV_{max} and 30% of TBR mean SUV_{max} having a difference of ± 0.25 or more (Figure 2C, D). In our previous study exploring ^{18}F-FDG-uptake in symptomatic versus asymptomatic

patients[18] the difference in median mean SUV_{max} between the groups was 0.32 (1.75 versus 1.43). In two studies using TBR max SUV_{max} as uptake parameter the difference was found to be 0.19 and 0.29.[20, 21] Thus, methods with reader difference of 0.25 prohibit differentiation between symptomatic and asymptomatic patients.

We found an ICC for background blood pool activity of 0.77. This discordant assessment of background blood pool activity introduces variation in TBR and cSUVs due to methodology rather than biology. The background blood pool activity in our study was obtained from four ROIs within the lumen of the jugular vein preferably in the same craniocaudal level as the plaque. The vena jugularis has a small diameter and it was often challenging to draw reproducible ROIs within the vein that excluded contribution from neighbouring structures. In a ^{18}F-FDG PET study of generalized vascular inflammation in which the background blood pool activity was obtained from eight ROIs in the jugular vein the ICC for TBR mean SUV_{max} of the carotid arteries was 0.94-0.96.[14] This suggests that including data from more slices or from a larger vessel segment such as the vena cava superior or atria of the heart could have reduced the inter-reader variability of measuring the blood pool activity. In this study the two readers also had trained together by co-reading several pilot studies before they established an analysis protocol.[14] This is optimal for research studies, but hard to accomplish in larger trials where the readers often are located in different departments.

There is a large amount of studies that quantifies the ^{18}F-FDG uptake in the vessel wall of patients with suspected generalized vascular inflammation (atherosclerosis not necessarily confirmed by other imaging methods). Although our findings cannot automatically be generalized, one might question the need for background correction for these patients.

Reader 2 included significantly more plaque-containing slices than reader 1. This did not reduce the ICC of the ^{18}F-FDG measurements, supporting that the plaque slices with the highest uptake values all were included in both readers plaque area and that the number of slices included in the plaque area has minimal influence on mean SUV_{max}. Our interpretation of this finding is that the plaque inflammation we can detect with ^{18}F-FDG PET is homogeneously spread out, and also present in the extreme tails of the plaque. This was also one of our main findings when we explored associations between different ^{18}F-FDG uptake parameters and plaque inflammation at histopathology.[17] Furthermore, this is in accordance with the study results from Kwee et al.[12] who found a strong correlation between TBRs of ipsilateral symptomatic plaques and contralateral asymptomatic plaques and supports the hypothesis that plaque inflammation is systemic to some extent.

A strength of our study is a relatively large patient population with a wide range of uptake values (max SUV_{max} from 1.18 to 2.66) representing low to high plaque inflammatory activity confirmed by histology.[17]

In conclusion, our study confirms the reproducibility of quantification of ^{18}F-FDG uptake in carotid artery plaques and supports the superiority of quantification methods that do not include blood pool background**.** The ICC was highest for max SUV_{max} (the single highest uptake value within the plaque) and thus, our suggestion is to further explore this parameter for atherosclerosis imaging.

Declaration of Conflicting Interests

The authors declare that there is no conflict of interest.

References

(1) NASCET Group. Long-term prognosis and effect of endarterectomy in patients with symptomatic severe carotid stenosis and contralateral carotid stenosis or occlusion: results from NASCET. North American Symptomatic Carotid Endarterectomy Trial (NASCET) Group. J Neurosurg 1995;83:778-82.

(2) European Carotid Surgery Trialists' Collaborative Group. Randomised trial of endarterectomy for recently symptomatic carotid stenosis: final results of the MRC European Carotid Surgery Trial (ECST). Lancet 1998;351:1379-87.

(3) North American Symptomatic Carotid Endarterectomy Trial Collaborators. Benefit of carotid endarterectomy in patients with symptomatic moderate or severe stenosis. N Engl J Med 1998;339:1415-25.

(4) Libby P. Inflammation in atherosclerosis. Nature 2002;420:868-74.

(5) Stoll G, Bendszus M. Inflammation and atherosclerosis: novel insights into plaque formation and destabilization. Stroke 2006;37:1923-32.

(6) Jander S, Sitzer M, Schumann R et al. Inflammation in high-grade carotid stenosis: a possible role for macrophages and T cells in plaque destabilization. Stroke 1998;29:1625-30.

(7) Rudd JH, Warburton EA, Fryer TD et al. Imaging atherosclerotic plaque inflammation with [18F]-fluorodeoxyglucose positron emission tomography. Circulation 2002;105:2708-11.

(8) Chowdhury MM, Tarkin JM, Evans NR et al. (18)F-FDG Uptake on PET/CT in Symptomatic versus Asymptomatic Carotid Disease: a Meta-Analysis. Eur J Vasc Endovasc Surg 2018;56:172-9.

(9) Bucerius J, Hyafil F, Verberne HJ et al. Position paper of the Cardiovascular Committee of the European Association of Nuclear Medicine (EANM) on PET imaging of atherosclerosis. Eur J Nucl Med Mol Imaging 2016;43:780-92.

(10) Huet P, Burg S, Le Guludec D, Hyafil F, Buvat I. Variability and uncertainty of 18F-FDG PET imaging protocols for assessing inflammation in atherosclerosis: suggestions for improvement. J Nucl Med 2015;56:552-9.

(11) Graebe M, Borgwardt L, Hojgaard L, Sillesen H, Kjaer A. When to image carotid plaque inflammation with FDG PET/CT. Nucl Med Commun 2010;31:773-9.

(12) Kwee RM, Truijman MT, Mess WH et al. Potential of integrated [18F] fluorodeoxyglucose positron-emission tomography/CT in identifying vulnerable carotid plaques. AJNR Am J Neuroradiol 2011;32:950-4.

(13) Marnane M, Merwick A, Sheehan OC et al. Carotid plaque inflammation on 18F-fluorodeoxyglucose positron emission tomography predicts early stroke recurrence. Ann Neurol 2012;71:709-18.

(14) Rudd JH, Myers KS, Bansilal S et al. Atherosclerosis inflammation imaging with 18F-FDG PET: carotid, iliac, and femoral uptake reproducibility, quantification methods, and recommendations. J Nucl Med 2008;49:871-8.

(15) Rudd JH, Myers KS, Bansilal S et al. (18)Fluorodeoxyglucose positron emission tomography imaging of atherosclerotic plaque inflammation is highly reproducible: implications for atherosclerosis therapy trials. J Am Coll Cardiol 2007;50:892-6.

(16) Grant EG, Benson CB, Moneta GL et al. Carotid artery stenosis: gray-scale and Doppler US diagnosis--Society of Radiologists in Ultrasound Consensus Conference. Radiology 2003;229:340-6.

(17) Johnsrud K, Skagen K, Seierstad T, Skjelland M, Russell D, Revheim ME. (18)F-FDG PET/CT for the quantification of inflammation in large carotid artery plaques. J Nucl Cardiol 2019;26:883-93.

(18) Skagen K, Johnsrud K, Evensen K et al. Carotid plaque inflammation assessed with (18)F-FDG PET/CT is higher in symptomatic compared with asymptomatic patients. Int J Stroke 2015;10:730-6.

(19) Boellaard R, Delgado-Bolton R, Oyen WJ et al. FDG PET/CT: EANM procedure guidelines for tumour imaging: version 2.0. Eur J Nucl Med Mol Imaging 2015;42:328-54.
(20) Muller HF, Viaccoz A, Fisch L et al. 18FDG-PET-CT: an imaging biomarker of high-risk carotid plaques. Correlation to symptoms and microembolic signals. Stroke 2014;45:3561-6.
(21) Tarkin JM, Joshi FR, Evans NR et al. Detection of Atherosclerotic Inflammation by (68)Ga-DOTATATE PET Compared to [(18)F]FDG PET Imaging. J Am Coll Cardiol 2017;69:1774-91.